8-17-2013

Multilevel Design Optimization of Automotive Structures Using Dummy- and Vehicle-Based Responses

Imtiaz Shareef Gandikota

Multilevel design optimization of automotive structures using dummy- and vehicle-based responses

By

Imtiaz Shareef Gandikota

A Thesis
Submitted to the Faculty of
Mississippi State University
in Partial Fulfillment of the Requirements
for the Degree of Master of Science
in Aerospace Engineering
in the Department of Aerospace Engineering

Mississippi State, Mississippi

August 2013

Multilevel design optimization of automotive structures using dummy- and vehicle-based responses

By

Imtiaz Shareef Gandikota

Approved:

_____	_____
Masoud Rais-Rohani Professor Aerospace Engineering (Director of Thesis)	Thomas E. Lacy Professor Aerospace Engineering (Committee Member)
_____	_____
Keiichi Motoyama Research Professor Aerospace Engineering (Committee Member)	J. Mark Janus Associate Professor Aerospace Engineering (Graduate Coordinator)
_____	
Royce O. Bowden Interim Dean of Bagley College of Engineering	

Name: Imtiaz Shareef Gandikota

Date of Degree: August 17, 2013

Institution: Mississippi State University

Major Field: Aerospace Engineering

Major Professor: Dr. Masoud Rais-Rohani

Title of Study: Multilevel design optimization of automotive structures using dummy- and vehicle-based responses

Pages in Study: 121

Candidate for Degree of Master of Science

A computationally efficient multilevel decomposition and optimization framework is developed for application to automotive structures. A full scale finite element (FE) model of a passenger car along with a dummy and occupant restraint system (ORS) is used to analyze crashworthiness and occupant safety criteria in two crash scenarios. The vehicle and ORS models are incorporated into a decomposed multilevel framework and optimized with mass and occupant injury criteria as objectives. A surrogate modeling technique is used to approximate the computationally expensive nonlinear FE responses. A multilevel target matching optimization problem is formulated to obtain a design satisfying system level performance targets. A balance is sought between crashworthiness and structural rigidity while minimizing overall mass of the vehicle. Two separate design problems involving crash and crash+vibration are considered. A major finding of this study is that, it is possible to achieve greater weight savings by including dummy-based responses in optimization problem.

DEDICATION

I would like to dedicate this work to my parents, brothers and sister.

ACKNOWLEDGEMENTS

I thank my advisor Dr. Masoud Rais-Rohani for his immense support and advice during the course of this work. This work would not have been possible without his guidance. I thank Dr. Thomas E. Lacy and Dr. Keiichi Motoyama for serving on my committee. I am grateful to Sarba Guha of LSTC for helping me with the seatbelt model, Dr. Morteza Kiani, Saber DorMohammadi and Suryatej Potula for their assistance.

I am thankful to Department of Aerospace Engineering, Center for Advanced Vehicular Systems and US Department of Energy for funding this research.

I also thank all my friends at MSU for their support.

TABLE OF CONTENTS

LIST OF TABLES

LIST OF FIGURES

CHAPTER I

INTRODUCTION

The growing demand for increased fuel efficiency of cars and light trucks has led to increased research on innovative applications of lightweight materials and advanced design methods toward vehicle weight reduction (light weighting) without compromising crashworthiness, occupant safety, and other vehicle design requirements. These efforts are also directed partly at accommodating various regulations set by the U.S. government in terms of higher fuel economy standards and lower CO_2 gas emissions.

This study considers a design approach based on structural optimization techniques and finite element (FE) simulations. Improvements in crashworthiness behavior, occupant safety and reduced structural mass are sought by considering structural and vibration design criteria governing the overall design of a car. The general design process is captured by the flowchart shown in Figure 1.1.

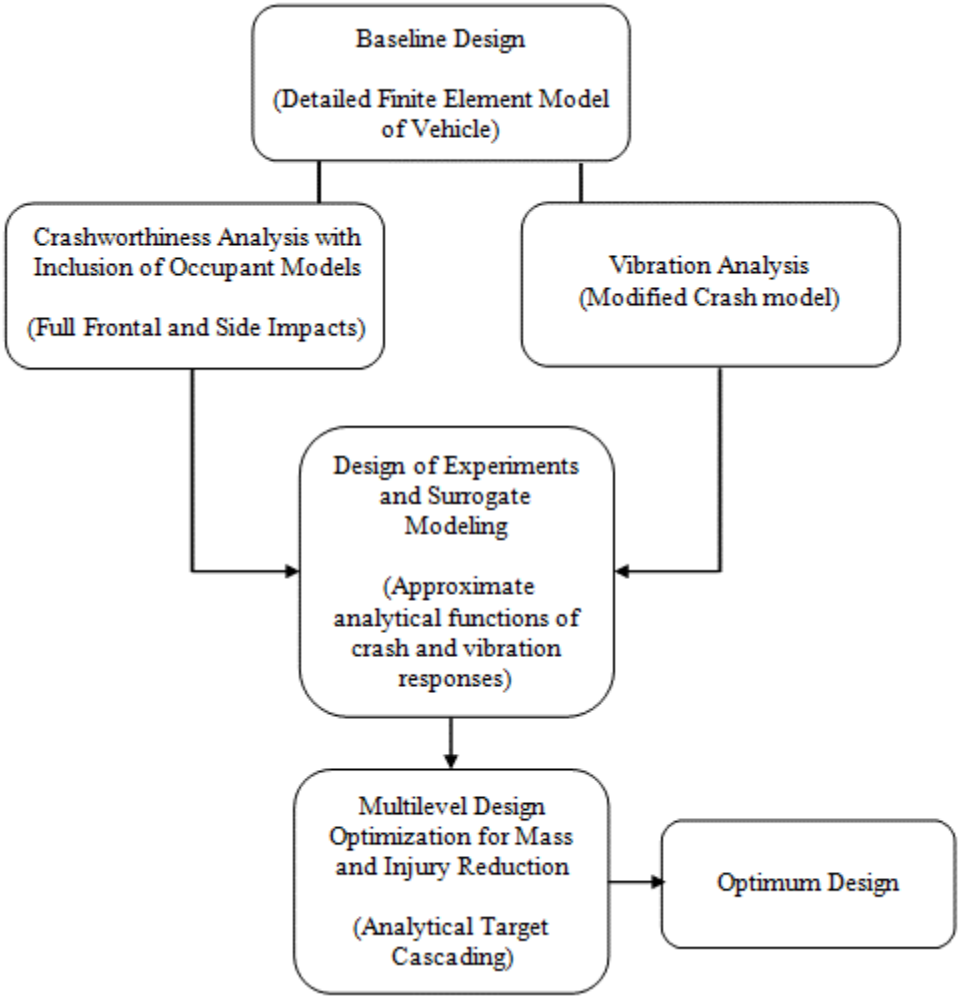

Figure 1.1 Design process considered in study.

1.1 Crashworthiness and Occupant Safety

Crashworthiness is the study of mechanical behavior of automotive structures in the advent of a crash. To have better crashworthiness performance, all the major structural components are required to participate efficiently and effectively in absorbing the crash-induced energy. The structural energy absorption directly affects the safety of vehicle occupants by substantially reducing the acceleration felt by the occupants as well as the possibility of the deformed structure coming in contact with the occupants, both of

which could cause significant injury. For example in the case of a full frontal impact, the vehicle inner and outer frontal rail components serve as the major energy absorbing parts of the car. During car crashes, the crush behavior of these components should be in axial mode to have better energy absorbing capabilities [1].

The increasing trends in both the number of car crashes and occupant fatalities led to the creation of National Highway Traffic and Safety Administration (NHTSA) by the U.S. Department of Transportation in 1970. NHTSA has proposed and formulated various regulations pertaining to occupant safety under Federal Motor Vehicle Safety Standards (FMVSS) [2]. These standards provide the metrics that must be fulfilled by the automotive industry for vehicles manufactured by and imported to the U.S. As part of satisfying these standards, the vehicles manufactured are subjected to physical crash tests; corresponding rating such as good, acceptable or poor are provided depending on the performance of vehicle in full frontal impact, side impact, offset frontal impact, rear impact and rollover tests. The FMVSS includes certain limits pertaining to various occupant responses that are critical in car crashes. The crash tests are conducted to check if the responses generated in each crash scenario are within the specified FMVSS limits. For example, the head injury criterion, head acceleration, chest acceleration and femur loads are the most critical responses affecting the occupant injury in advent of a frontal crash, whereas accelerations at pelvis, spine, and rib locations are important in side impacts.

To meet the recent stricter regulations in safety [2] along with fuel efficiency and environmental protection, structural weight reduction of automotives through design optimization is considered to be an effective approach.

1.2 Finite Element Analysis of Crashworthiness

Advanced finite element analysis (FEA) tools such as LS-DYNA [3] and ABAQUS [4] make it possible for automotive engineers to carryout virtual crash tests using computer simulations and to apply the findings to improve a vehicle design in terms of crashworthiness and other design criteria. The development of high fidelity crash simulations has allowed engineers to predict crash behavior of a vehicle and also occupant injury using FE models of vehicle and occupants. The National Crash Analysis Center (NCAC) at George Washington University has developed several FE models of cars and light trucks that have been used for both crashworthiness analysis and design.

A highly detailed FE model of a car consists of thousands of elements. For example, the FE model of 1996 Dodge Neon developed by NCAC (without interiors) consists of 270,768 elements [5]. Analyzing this model for 150-ms full frontal crash using an IBM cluster with 16 Pentium III processors would take 10 hours [6], but recent advances in computer capabilities have reduced the computation time of the same vehicle crash simulation to 3 hours with four 6-core Intel Processors with 48 GB of RAM. The computation cost associated with analyzing these large models can be further reduced by using fine meshes only at locations of large deformations and relatively coarse meshes elsewhere.

Many FEA codes such as LS-DYNA, PAMCRASH, and RADIOSS have been developed to perform highly nonlinear transient dynamic crash simulations. Toyama et al. [7] studied the frontal crash phenomenon and deformation modes of a vehicle model with 5,300 elements using PAM-CRASH. Solanki et al. [8] compared the characteristics of LS-DYNA and PAM-CRASH codes for crash analysis and concluded that both codes

show good correlation with actual crash test results. In this study, the LS-DYNA [3] FEA code is used to conduct crash simulations.

Apart from vehicle models, the use of FE modeling techniques has also helped in developing full-scale occupant dummy models and Occupant Restraint System (ORS) models such as airbags and seatbelts. Noureddine et al. [9] developed and validated an FE model of hybrid III crash test dummy with major parts such as head, neck and chest using 13,000 elements. Later, a more detailed FE model of the 50^{th} percentile hybrid III called Anthropomorphic Crash Test Dummy (ATD) was developed by Ennis et al. [10]. This model consists of 45,000 elements representing each part of the dummy in high detail.

Using preprocessing software, the vehicle, occupant and restraint system models can be combined into one consolidated model to study important crashworthiness characteristics based on both vehicle and occupant responses. The occupant restraint system models can vary depending upon the type of crash scenario. For example, the type of airbag used in frontal impacts is different from the one used in side impact analysis. Potula et al. [11] used side curtain airbag deployment to study out-of-position occupant safety in a side impact scenario.

Besides FE models, multibody dynamic models of vehicles and occupants are also used, which tend to be computationally cheap to analyze compared to large FE models. Teng et al. [12] used the concept of multibody dynamics to build an occupant model consisting of 15 segments connected through different types of joints for analysis of occupant safety characteristics in a frontal collision. MADYMO [13] software is an efficient and widely used tool for analysis of occupant models using multibody dynamics.

Sled tests of occupant models and restraint systems have also emerged as an efficient method for crash safety analysis. Viano and Arepally [14] used multiple sled tests for different combinations of occupant restraint systems such as unbelted occupant, belted occupant and the combination of belt and airbag. Different parameters pertaining to belt restraint systems were analyzed and a criterion assessing the injury risk in frontal crash was formulated. Crandall et al. [15] performed sled tests of the 1993 Ford Taurus model to analyze the frontal collision performance of force-limited belts and airbag. The study showed that a force-limited belt system along with side airbags offers better frontal restraint performance as compared to a side airbag with a standard three-point belt system.

1.3 Design Optimization for Crashworthiness and Occupant Safety

The crashworthiness characteristics of a car can be enhanced using optimization techniques that rely on different mathematical programming approaches for finding an improved design subject to the specified design constraints. The important responses obtained from a crash analysis can be treated as objectives or constraints, and different parameters pertaining to vehicle or occupant restraint system design can be treated as design variables to find an optimum design with better crash characteristics. For example, in recent years, the demands for improved fuel efficiency of automobiles have led to vehicle structure optimization with mass as objective function. Further, design optimization can be classified into three major divisions i.e., sizing optimization, shape optimization and topology optimization.

The selection of design constraints in a vehicle structure optimization problem depends on the responses that are considered to be important in a crash analysis. For

crashworthiness study without occupants, depending on the type of crash scenario, structural responses such as intrusion distances, accelerations and internal energy absorption of vehicle components are considered as substitutes for occupant responses; these vehicle-based responses are also known as energy-based responses.

Xu et al. [16] used topology optimization to improve crash behavior of the front rails of a car model using vehicle-based responses, whereas Rais-Rohani et al. [17] used a shape optimization technique to optimize the front rails considering frontal crash structural responses as design constraints.

Since design optimization is a mathematical approach, the objectives and constraints are defined as functions of certain design variables, and optimization involves the evaluation of these functions at different points in the feasible design space bounded by design constraints. If FE simulations or sled tests were to be used to evaluate the crash responses at each design point, the computation costs associated with such a process would be enormous. Thus, approximation techniques are often used in vehicle design optimization.

Surrogate modeling uses a collection of mathematical and statistical techniques to approximate the system response with an analytical function based on responses obtained through FE simulations or physical tests at a set of design (training) points. The gain in overall computation cost has led to the application of surrogate modeling techniques in crashworthiness and occupant restraint system design.

Fang et al. [18] used energy-based responses such as internal energy absorption of selected components of a vehicle model as design constraints and solved a mass minimization problem with surrogate models of responses in multiple crash scenarios as

design constraints. Intrusion distances of toeboard, dashboard for full frontal and offset frontal impacts and intrusion distance of door for side impacts were considered as substitutes for the occupant-based responses [19]. A multi-objective optimization problem was also solved by considering mass of vehicle parts and intrusion distances as objectives with internal energy absorption as constraints for both offset frontal and side impact crash scenarios [20]. Horstemeyer et al. [21] used optimization techniques to improve the baseline design of 1996 Dodge Neon and formulated a comparison between energy-based designs without occupants versus injury-based design consisting of occupants in a side impact crash analysis. Parrish et al. [22] performed multi-objective optimization using 1996 Dodge Neon vehicle model by replacing 22 steel components in the baseline design with those made of AZ31 magnesium alloy by considering energy-based responses for full frontal, offset frontal and side impact crash analysis. Liao et al. [23] suggested a two-stage approach in formulating a multi-objective crashworthiness optimization problem for frontal crash analysis. The vehicle structure was optimized first for reducing mass and intrusion distances and later, in the second stage, the occupant restraint system was optimized using MADYMO software. Hou et al. [24] performed design optimization of restraint systems including a driver-side airbag using occupant dynamic simulations to study the effect of ORS parameters on injury severity. The study involved a sensitivity analysis to determine the parameters that are most influential in occupant injury; it also indicated that the inclusion of a driver-side airbag for an optimized restraint system reduced the overall injury by 9% with further reduction in injury possible by optimizing the airbag itself.

The preceding studies involved the application of surrogate modeling and optimization techniques for improving crashworthiness behavior using FE models. Occupant safety and crashworthiness optimization can also be evaluated using sled tests, which are approximate models of occupant dummy model and vehicle interior involving mainly seat, occupant restraint system, floor panel, etc.

1.4 Multidisciplinary design optimization

Apart from structural crashworthiness and occupant safety, there are many other design requirements that have to be taken into consideration during the vehicle design process. For example, a vibration design criterion considers the potential impact of structural stiffness on handling characteristics of the vehicle. Prior studies focused on optimization of automotive structure for improving noise, vibration and harshness (NVH) characteristics have involved the consideration of both crash and vibration in the design problem. Sobieszczanski-Sobieski et al. [25] optimized a car structure for mass minimization considering both crash and NVH responses as design constraints. Duddeck [26] solved a multidisciplinary optimization problem considering NVH and offset frontal impact analysis in the design problem. Wang et al. [27] used FE simulations, topology and shape optimization techniques to improve structural rigidity of a Porsche 928 model by considering fundamental frequencies as objectives.

1.5 Thesis Overview

The thesis is organized as follows. Chapter II consists of the FE models of vehicle, occupant and restraint systems used in this study and different crash scenarios and their validation. Chapter III includes design problems along with analytical target

cascading optimization framework. Surrogate modeling is discussed in chapter IV. Chapter V presents and compares the optimization results for different design cases, with the conclusions and future work presented at the end in Chapter VI.

1.6 References Cited

[1] Ibrahim, H. K. “Design optimization of vehicle structures for crashworthiness improvement”, PhD dissertation, Concordia University, 2009.

[2] Federal Motor Vehicle Safety Standards and Regulations. US Department of Transportation, National Highway Traffic Safety Administration. Washington DC, 1998.

[3] LS-DYNA keyword manual, Livermore Software Technology Corporation.

[4] Hibbitt, Karlsson, & Sorensen. “ABAQUS/Explicit: user's manual.” Hibbitt, Karlsson and Sorenson Inc, Vol. 1, 2009.

[5] Finite Element Model Archive, National Crash Analysis Center, http://www.ncac.gwu.edu/vml/models.html, June 2011.

[6] Fang, H., K. Solanki, & M. F. Horstemeyer. “Numerical simulations of multiple vehicle crashes and multidisciplinary crashworthiness optimization.” International Journal of Crashworthiness, 10, 2, 2005, pp: 161-172.

[7] Akira, T, & K. Hatano. "Numerical analysis of vehicle frontal crash phenomena.” SAE Technical Paper, 1992.

[8] Solanki, K., D. Oglesby, C. Burton, H. Fang, & M. F. Horstemeyer. "Crashworthiness Simulations Comparing PAM-CRASH and LS-DYNA." SAE Technical Paper, 11-20, 2004.

[9] Noureddine, A., A. Eskandarian, & K. Digges. "Computer modeling and validation of a hybrid III dummy for crashworthiness simulation." Mathematical and computer modelling, 35, 7, 2002, pp: 885-893.

[10] Ennis, J. B., D. Marzougui, A. Eskandarian, & N. E. Bedewi. “Finite element modelling of anthropomorphic test devices for vehicle crashworthiness evaluation”. International Journal of Crashworthiness, *6*, 4, 2001, pp: 511-524.

[11] Potula, S. R., K. N. Solanki, D. L. Oglesby, M. A. Tschopp, & M. A. Bhatia. "Investigating occupant safety through simulating the interaction between side curtain airbag deployment and an out-of-position occupant." Accident Analysis & Prevention, 49, 2012, pp: 392-403.

[12] Teng, Tso-Liang, Fwu-An Chang, Yung-Sheng Liu, & Cheng-Ping Peng. "Analysis of dynamic response of vehicle occupant in frontal crash using multibody dynamics method." Mathematical and Computer Modelling, 48, no. 11, 2008, pp: 1724-1736.

[13] Wismans, J., & J. H. A Hermans. MADYMO 3D simulations of Hybrid III dummy sled tests. Society of Automotive Engineers, 1988.

[14] Viano, D. C., S. Arepally. "Assessing the safety performance of occupant restraint systems, SAE Technical Paper, 1990.

[15] Crandall, J. R., R. Cameron, W. D. Pikey, H. J. Miller, J. Sikorski, & M. Wilkins. "Thoracic response and injury with belt, driver side airbag, and force limited belt restraint systems." International Journal of Crashworthiness, 2, 1, 1996, pp: 119-132.

[16] Xu, Tao, Yiwen Li, Qiang Li, Liang Hao, & Wenjun Song. "Crashworthiness Design of Frontal Rail Using Strain-Energy-Density and Topology Optimization Approach." In Computational Science and Optimization (CSO), Third International Joint Conference, vol. 1, 2010, pp. 24-28.

[17] Rais-Rohani, M., K. N. Solanki, E. Acar, & C. D. Eamon. "Shape and sizing optimisation of automotive structures with deterministic and probabilistic design constraints." International Journal of Vehicle Design, *54*, 4, 2010, pp: 309-338.

[18] Fang, H., K. Solanki, & M. F. Horstemeyer. "Energy-based crashworthiness optimization for multiple vehicle impacts." ASME Conference Proceedings, 2004.

[19] Fang, H., K. N. Solanki, M. F. Horstemeyer, & M. Rais-Rohani. "Multi-impact crashworthiness optimization with full-scale finite element simulations." In Computational Mechanics, the 6th World Congress on Computational Mechanics in Conjunction APCOM, Vol. 4, 2004, pp. 5-10.

[20] Fang, H., K. Solanki, & M. F. Horstemeyer. "Numerical simulations of multiple vehicle crashes and multidisciplinary crashworthiness optimization." International Journal of Crashworthiness, 10, 2, 2005, pp: 161-172.

[21] Horstemeyer, M. F., X. C. Ren, H. Fang, E. Acar, & P. T. Wang. "A comparative study of design optimisation methodologies for side-impact crashworthiness, using injury-based versus energy-based criterion."International Journal of Crashworthiness, 14, 2, 2009, pp: 125-138.

[22] Parrish, A., M. Rais-Rohani, & A. Najafi. "Crashworthiness optimisation of vehicle structures with magnesium alloy parts." International Journal of Crashworthiness, 17, 3, 2012, pp: 259-281.

[23] Liao, X., Q. Li, X. Yang, W. Li, & W. Zhang. "A two-stage multi-objective optimisation of vehicle crashworthiness under frontal impact." International Journal of Crashworthiness, 13, 3, 2008, pp: 279-288.

[24] Hou, J. F., J. Tomas, & L. Sparke. “Optimization of driver-side airbag and restraint system by occupant dynamics simulation.” In Proceedings: Stapp Car Crash Conference, Society of Automotive Engineers SAE,Vol. 39, 1995, pp. 461-472.

[25] Sobieszczanski-Sobieski, J., S. Kodiyalam, & R. Y. Yang. “Optimization of car body under constraints of noise, vibration, and harshness (NVH), and crash.” Structural and Multidisciplinary Optimization, 22, 4, 2001, pp: 295-306.

[26] Duddeck, F. “Multidisciplinary optimization of car bodies.” Structural and Multidisciplinary Optimization, 35, 4, 2008, pp: 375-389.

[27] Wang, L., P. K. Basu, & J. P. Leiva. “Automobile body reinforcement by finite element optimization.” Finite Elements in Analysis and Design, 40, 8, 2008, pp: 879-893.

CHAPTER II

FE MODELS AND CRASH IMPACT SCENARIOS

2.1 FE Models for Crash Analysis

2.1.1 1996 Dodge Neon Vehicle Model

A publicly available 1996 Dodge Neon FE model, developed by NCAC [1], is used for crash analysis using the LS-DYNA simulation software. The Neon FE model consists of 337 parts with 270,768 elements, the majority of which are shell elements [2]. The NCAC Neon model does not include any interior components (e.g., seats, instrument panels) nor does it include an occupant model or restraint system. Most of the structure is made of steel, defined using a piecewise linear plasticity material model (MAT24) [3]. The glass in the front and rear windshield and side windows are not designed to crack or break during crash. The total mass of the crash model is 1,336 kg, which is the same as that of an actual vehicle with several mass elements distributed throughout the FE model. Figure 2.1 shows the Dodge Neon crash model obtained from NCAC.

Figure 2.1 (a) 1996 Dodge Neon Model by NCAC with (b) roof, windshields and side windows removed to reveal the lack of any interior component.

The original NCAC Neon model was further improved as part of different research projects conducted at Center for Advanced Vehicular Systems (CAVS) at Mississippi State University. The driver seat, instrument panel and other parts of the dashboard as well as the steering wheel and column, airbag, and seatbelt were integrated into the vehicle model to accommodate a more detailed crash analysis involving dummy model responses. A total of 60 parts were added to the existing 337 parts of the NCAC model in such a way that the total mass of the FE model was kept the same as that of the actual vehicle. The added mass of new parts was countered by removing the mass elements added previously at the driver side of the FE model. With the added interiors, the total number of elements in the FE model increased to 302,132. The added parts are important for crash simulations with a dummy model, as these parts have good interaction with simulated occupant in event of a crash. The modified 1996 Dodge Neon model with interiors included is shown in Figure 2.2.

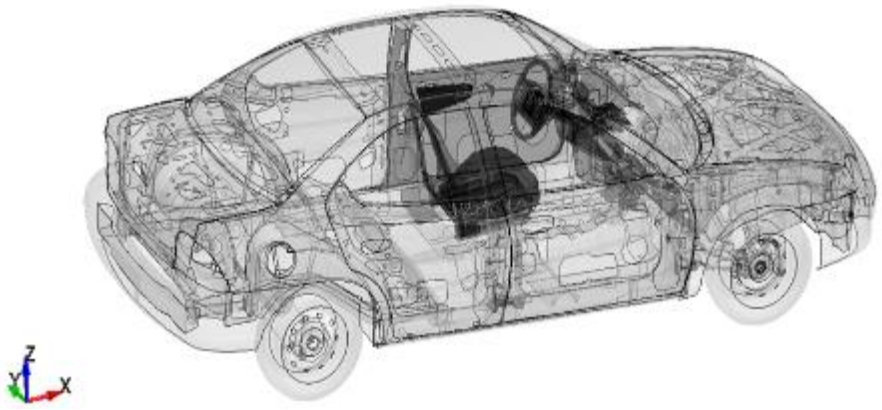

Figure 2.2 Modified Dodge Neon model with added interiors darkened for ease of viewing.

Since this study involved two crash scenarios, i.e., FFI and SI, the initial FE vehicle model without occupant was first validated by comparing the acceleration plots obtained in two different crash scenarios with the acceleration plots obtained from the actual crash tests [4, 5]. The FFI analysis involved longitudinal impact of FE vehicle model against a rigid wall at a speed of 56 km/h and SI involved a Moving Deformable Barrier (MDB) impacting the driver side of a stationary Dodge Neon FE model at a speed of 52.5 km/h at an angle of 27°. The crash test scenarios considered for model validation are shown in Figure 2.3.

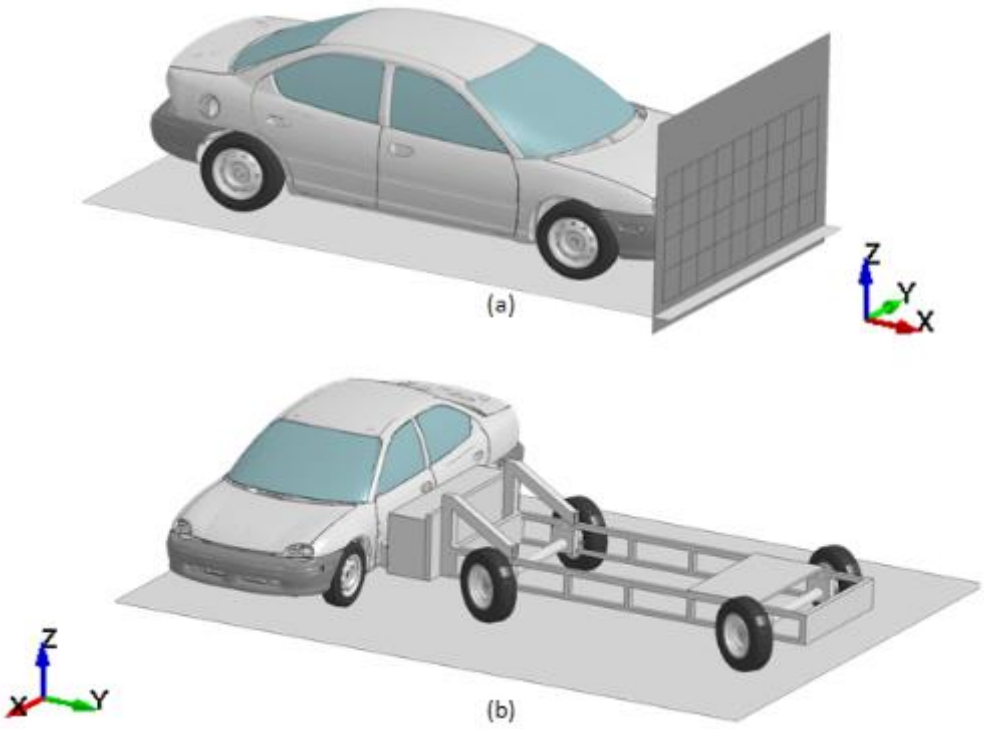

Figure 2.3 Crash scenarios without occupant and restraint system
(a) FFI against rigid wall and (b) SI by MBD.

The X-directional acceleration at left rear seat cross member for FFI and Y-directional acceleration at middle of B-pillar for SI are compared to validate the model. The locations of these points are shown in Figure 2.4. Figure 2.5 shows the comparison of acceleration data obtained from simulation with test data for both FFI and SI crash scenario.

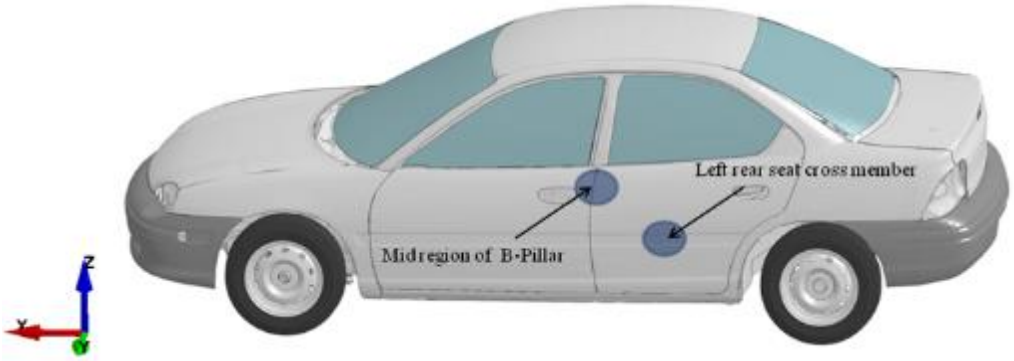

Figure 2.4 Location of left seat cross member and mid B-pillar in Dodge Neon model.

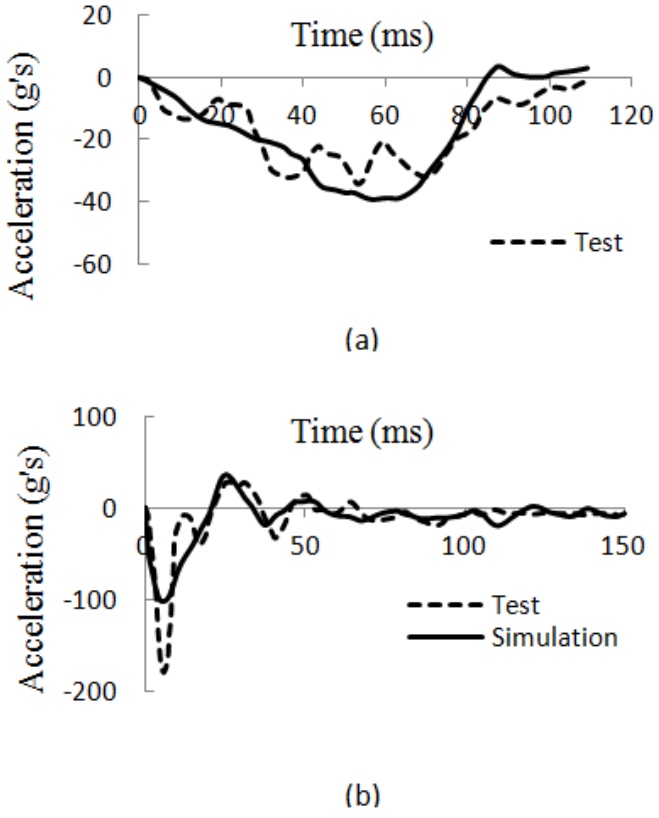

Figure 2.5 Comparison of (a) X direction acceleration of left seat cross member in FFI and (b) Y direction acceleration of B-Pillar in SI with test data [4, 5].

The overall trend and peak value of simulation data in Figure 2.5(a) matches well with the test data [5]. Although the peak values of simulation data and test data in Figure 2.5(b) are different, the overall trend of the plots is same as the experimental results [4]. The simulation model consists of a total of seven accelerometers at different locations of the vehicle model. The actual crash test had multiple virtual accelerometers defined at various locations depending on crash scenario. In the actual crash tests, the B-pillar acceleration was measured using an accelerometer placed at mid region of B-pillar. Since there was no accelerometer defined at that location in the simulation model, the average acceleration of 20 nodes was used to compare the data. The impact direction of MBD in simulation and test report are also different. In test report, the impact direction was on right end of Dodge Neon whereas in simulation it was on left end, apart from impact direction and accelerometer location the overall simulation setup matched crash test setup. The difference in peak value of the curves in Figure 2.5(b) can be due to the differences in location of accelerometers in the simulation model and the actual crash test vehicle and the impact direction. The simulation data in Figure 2.5 was filtered using a 60 Hz Butterworth filter to remove noise. A comparison of filtered and unfiltered responses appears later in this chapter as part of FFI model validation.

Once the vehicle model was validated, occupant models and occupant restraint systems were added to analyze the crash behavior and occupant safety criteria with inclusion of occupant restraint systems (i.e., seatbelt and steering wheel mounted airbag).

2.1.2 Occupant Model

To study the behavior of occupant and restraint systems during a car crash, occupant models, also known as crash test dummies or Anthropomorphic Test Devices

(ATD), are often used in laboratory crash tests. The dummy models are used to measure the approximate forces and accelerations that would be experienced by the occupants during a car crash. The dummy models for male and female occupants can vary in weight and height. The Hybrid III family of dummies includes a male, a female and three child models. The Hybrid III 50th percentile dummy model is the most commonly used model, representing a male occupant with height of 175 cm and weight of 77 kg. There are different types of dummy models available depending upon their application. For example, Hybrid III class of dummies are used for FFI analysis, whereas Side Impact Dummies (USSID) models are used for analysis involving side crash.

Livermore Software Technology Corporation (LSTC) has developed and modified various occupant models obtained from NHTSA depending on the application. These models are available free of charge to the users of LS-DYNA crash analysis software. The LSTC FE models of crash dummies are built using rigid body elements connected to each other using various types of joints.

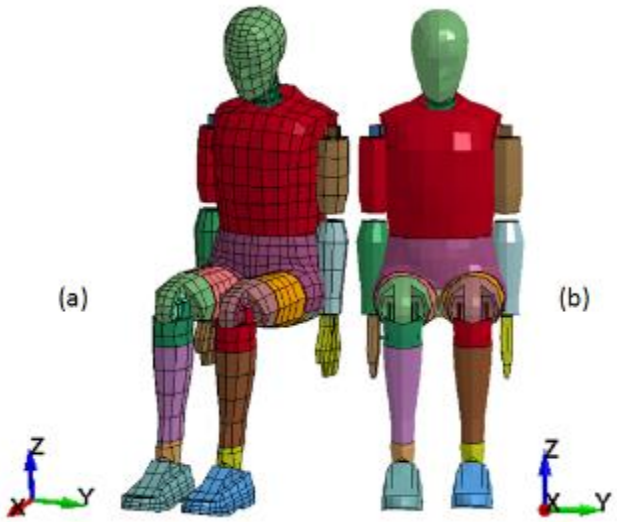

Figure 2.6 Hybrid III 50th percentile FE dummy models before placing and positioning inside a vehicle model.

(a) with mesh and (b) without mesh

The occupant (driver) used in this study is represented by a Hybrid III 50th percentile dummy model developed by LSTC [6]. The model consists of 128 parts, 4,327 elements and different types of joint mechanisms to attach various parts of the dummy model. Figure 2.6 shows the FE model of Hybrid III 50th percentile dummy model prior to its positioning in the vehicle model.

The FE dummy model includes a total of six virtual accelerometers defined at various locations to calculate important crash responses such as head acceleration, chest acceleration, pelvis acceleration, etc. These accelerometers are defined using the ELEMENT_SEATBELT_ACCELEROMETER keyword of LS-DYNA.

The dummy model was positioned into the Dodge Neon vehicle model using dummy positioning module of LS-Prepost [6]. The steps involved in positioning include the translation of dummy towards the vehicle seat, rotation of arms, legs, lumbar and other parts in such a way that the overall positioning of the dummy into the FE model of

Dodge Neon matched the actual crash test setup performed by NHTSA [5]. The positioned occupant model is shown in Figure 2.7.

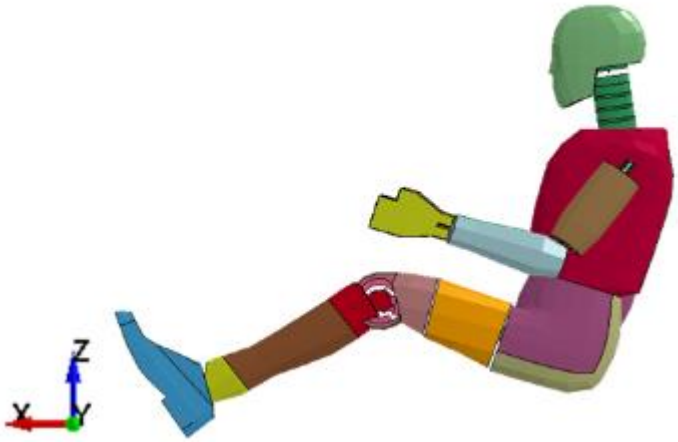

Figure 2.7 Side view of positioned dummy model.

After performing the required dummy positioning operations, the model was translated into Dodge Neon vehicle model and a number of contacts were defined between the dummy model, seat, steering wheel and instrument panel. For most of the contacts, the contact keyword AUTOMATIC_SURFACE_TO_SURFACE of LS-DYNA was used, as this contact definition is effective for crash simulations where the relative positions of the parts in contact cannot be anticipated as they undergo large deformations. The dummy model positioned into the Dodge Neon vehicle model is shown in Figure 2.8.

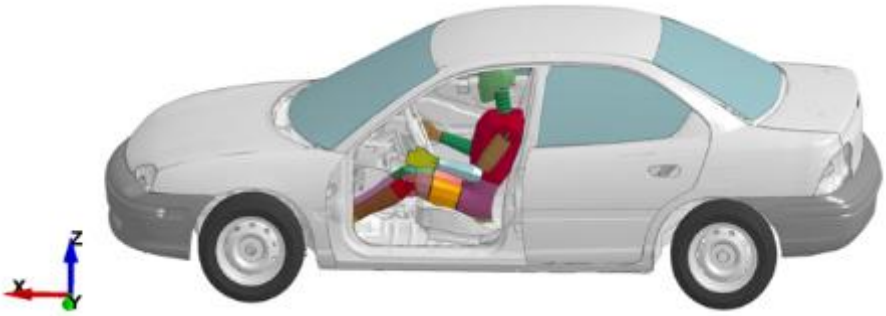

Figure 2.8 Dummy model positioned in Dodge Neon FE model with interiors (driver side door removed to ease view).

2.1.3 Seatbelt

In this study, an FE model of a seatbelt developed by LSTC was used. Instead of a more commonly used one-dimensional (1D) three-point seatbelt, a more accurate two-dimensional (2D) seatbelt was used. Even though, the modeling of a 2D seatbelt requires more effort, it offers a more realistic representation of the actual seatbelt in crash analysis.

A three-point seatbelt system consists of a shoulder belt and a lap belt attached to the vehicle at three locations. The shoulder belt runs across the chest and over the shoulder of the dummy reaching an anchor point on the B-pillar, whereas the lap belt runs over the pelvis region of the dummy. The seatbelt model consists of 1,223 elements with 327 ‘seatbelt’ elements and 896 shell elements defining the fabric part of the belt model. The ‘seatbelt’ elements are 1D elements connecting the 2D shell elements defined as fabric part of the seatbelt.

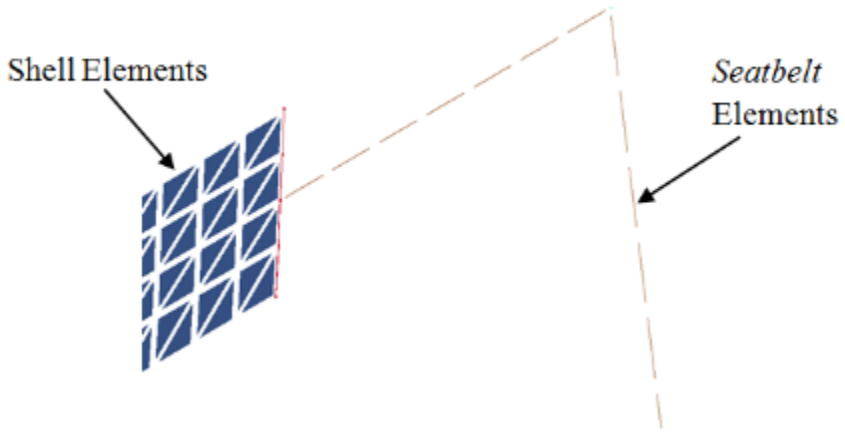

Figure 2.9 Element types in the seatbelt model

The seatbelt model used in this study consists of two slip rings located at two ends of the shoulder belt, a pyro-retractor, load limiting pretensioner, and one sensor each for retractor and pretensioner.

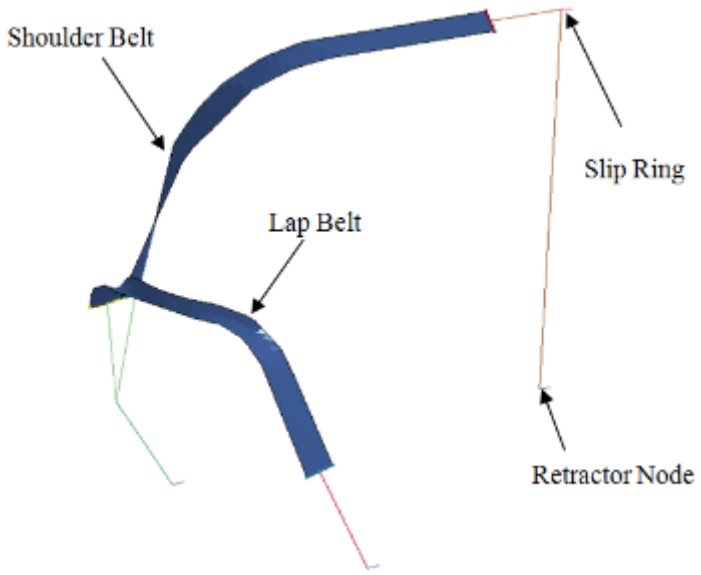

Figure 2.10 Two-dimensional seatbelt model used in this study.

A slip ring is defined as a 'ring' where the shoulder belt slips through as the belt is released or retracted. The ring is defined in the simulation software by a node in space called the slip ring node, which is static and fixed to the vehicle. This node is not part of the seatbelt elements but has the same coordinates as a node connecting the shoulder belt elements with belt elements connected to the retractor, as shown in Figure 2.11. During crash, as the belt is pulled back or released from the retractor, the belt elements pass through this slip ring node. The passing of belt elements through this node depends on whether the retractor is locked or not and also on the lengths of elements on either side of slip ring. For example, assuming the length of each element shown in Figure 2.11 to be 10mm, when element (L9067053) of shoulder belt gets pulled during crash, its length increases and the same amount of decrease in length is observed for element at other side of slipring (L9067033) in such a way that the total length of two elements is maintained same. Once the element length decreases to a specified value in slipring keyword definition, this element is passed on to other end of the slipring.

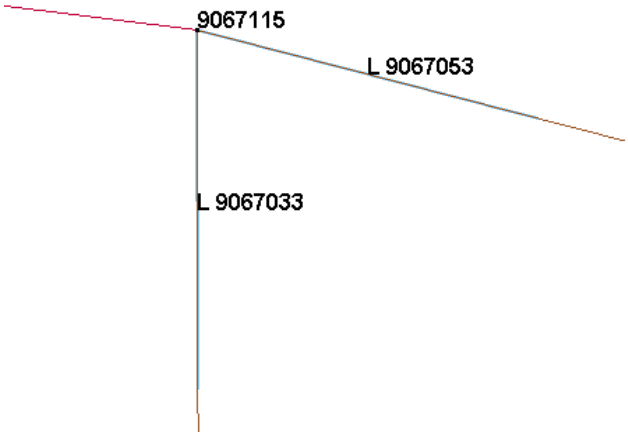

Figure 2.11 Slip-ring node and seat belt elements at slip-ring.

The function of a retractor is to control the amount of seatbelt pull-out or pull-in during crash. Similar to the slip ring, the retractor is also defined as a node in space coinciding with a node at the end of seatbelt.

A simulated sensor has been defined to trigger the locking of retractor. The sensors can be of different types, which trigger depending on different criteria such as time, acceleration or amount of belt release. The sensor used in this seatbelt model is a time-based sensor where time is specified for retractor locking. Retractor locking does not mean there is no release of belt from retractor once it has locked; rather the amount of belt release from the retractor after locking depends on the loading and unloading curves which are essentially force versus pull-out curves defined in the retractor keyword definition. The retractor also consists of some extra belt elements called 'zero-length' elements connected to each other in such a way that, once the belt is released out of the retractor, these elements exit retractor one by one depending on the amount of pull-out force.

A force limiting pretensioner was added to the belt model used in this study. A pretensioner works similar to a retractor, but it is mainly used for removing the slack present in the belt during initial stages of a crash. A force versus pull-in curve is defined in the pretensioner keyword definition and the belt pull-in is followed exactly as specified by this curve. The pretensioner also consists of a force limiting value defined in the pretensioner definition. This force is the maximum force that can be exerted on seatbelt to allow the functioning of pretensioner. During crash, whenever the belt forces exceed this limit force, the pretensioner is deactivated and retractor takes over and functions normally depending on its loading and unloading curves.

The material properties such as mass per unit length of seatbelt, force versus strain curves of the seatbelt model used in this study are consistent with data provided by LSTC, as there was no test data for seatbelt model in the actual crash test report.

The seatbelt model consists of both 2D fabric part and 1D seatbelt elements throughout the model. The 2D fabric part of the seatbelt was used at the surfaces (i.e., from shoulder over chest and lap where the belt comes in contact with the dummy model). The connections between the 2D fabric parts and the 1D seatbelt elements are made using nodal rigid body constraints. The seatbelt model was routed onto the occupant model using the seatbelt fitting application of LS-PrePost as shown in Figure 2.12. The belt model was placed with a gap of 2 mm from the surface of the dummy with the belt model consisting of four elements along the width of the belt. Various contacts between seatbelt parts and parts of the occupant model are defined after routing the seatbelt.

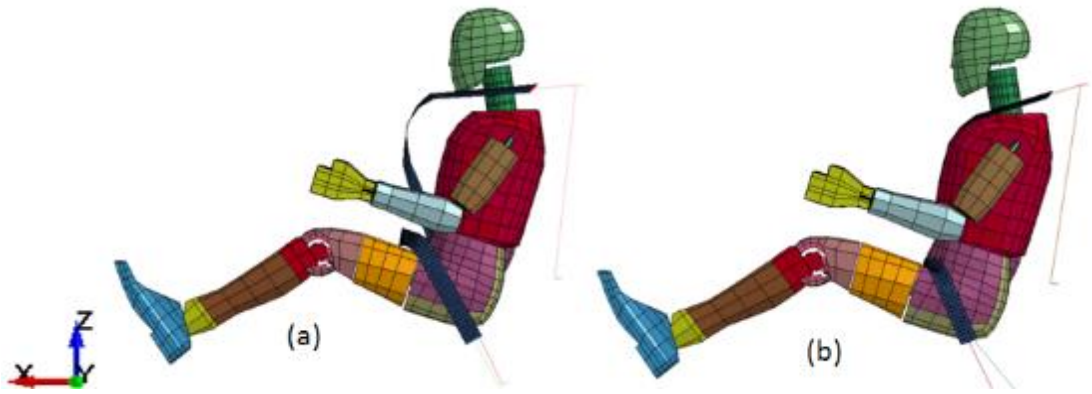

Figure 2.12 (a) Dummy model before and (b) after seat belt routing.

After routing the belt on the dummy model and defining contacts, the seatbelt model is connected to the vehicle with the help of rigid beams. Rigid beams are added to the end points of belt model and are merged with the vehicle model. This is done by defining a specific node set of the vehicle model and constraining the rigid beam parts to these node sets. Figure 2.13 shows the rigid beam defined at slipring node of seatbelt.

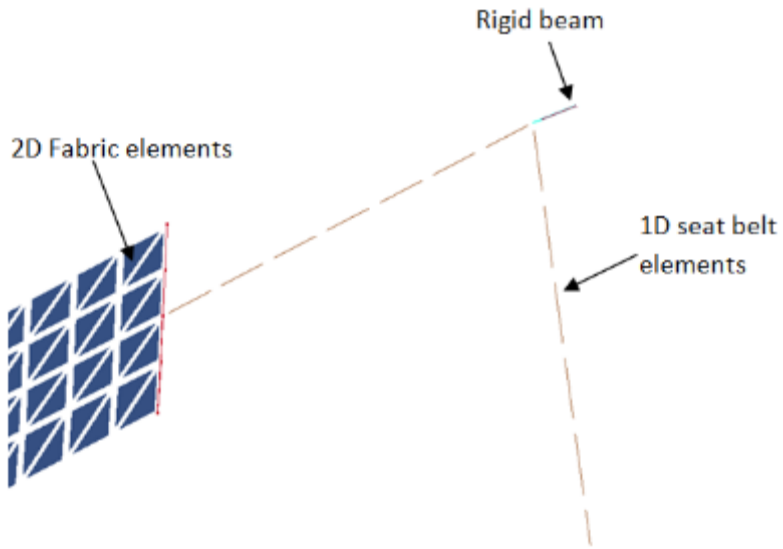

Figure 2.13 Belt elements with rigid beam defined to merge with the vehicle model.

A total of four connections are made between the seatbelt and the vehicle model. Two rigid beams located at both ends of the lap belt are connected to the vehicle floor panel whereas the other two rigid beams located at retractor and slipring are constrained to the B-Pillar.

2.1.4 Airbag Model

An FE model of the steering wheel airbag obtained from CAVS is employed as part of the occupant restraint system. The airbag is modeled using Wang-Nefske airbag definition of LS-DYNA [7]. Given the lack of experimental test data of airbag properties, data obtained from LSTC is used instead. Some of the crucial airbag properties include, for example, input mass flow rate and input gas temperature. Some of these parameters are used as design variables in the optimization problem as discussed in later sections of this thesis. Airbag venting is another important airbag property because the amount and rate of gas released from airbag affects the cushioning provided to an occupant during crash. The gas release is achieved in two ways, one is using vents/orifice and the other way is venting through porous fabric material of the airbag. The Wang-Nefske airbag formulation relies on venting through an orifice with the help of a load curve defining the vent orifice area as a function of absolute pressure [7]. The airbag model consists of two fabric parts with a total of 2,860 shell elements as shown in Figure 2.14. The airbag model was inserted into the steering wheel cavity of the Dodge Neon FE model by constraining a set of nodes at the airbag base to the middle part of steering wheel assembly as shown in Figure 2.15.

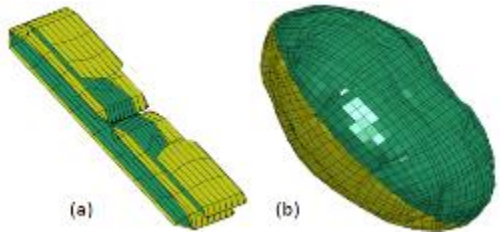

Figure 2.14 Airbag FE model
(a) before and (b) after inflation.

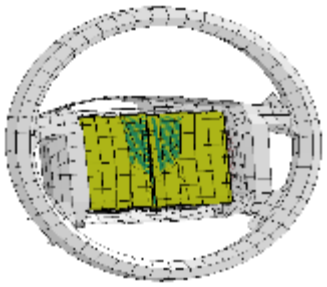

Figure 2.15 FE model of Airbag FE positioned in steering wheel assembly.

After positioning the airbag, contacts between airbag and parts of the steering wheel were defined. Apart from this, contacts between airbag and seatbelt and parts of the occupant model were also defined using automatic surface-to-surface contact definition.

The FE models of occupant, seatbelt, and airbag were positioned in Dodge Neon FE model to use as the baseline design of the overall vehicle before performing crash analysis in different impact scenarios. Multiple crash analyses were performed and various dummy response attributes such as acceleration data calculated at head, chest, spine and pelvis region were checked to ensure the accuracy of the vehicle-occupant-restraint system model. Figure 2.16 shows the Dodge Neon FE model with occupant, seat and airbag incorporated.

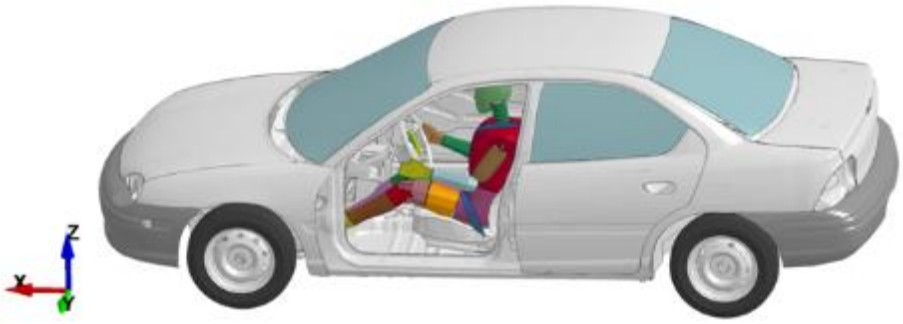

Figure 2.16 Dodge Neon FE model with occupant and occupant restraint system.

2.2 FE Model for Vibration Analysis

The FE model used for performing vibration analysis was developed as part of an earlier research effort at CAVS [8]. The vibration FE model for analysis using MSC Nastran was developed by modifying the LS-DYNA crash FE model and excluding all the moving parts such as doors, hood, etc. All the sheet metal components constituting the body-in-white were included in the model plus the windshield and the rear window glass.

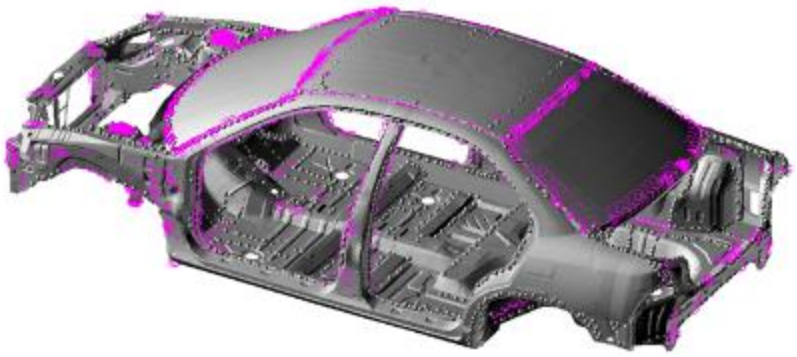

Figure 2.17 FE model of vibration analysis [8].

Several additional spot welds with a nominal diameter of 5 mm were added to the existing design using CWELD elements with elastic properties similar to welded steel parts. The constrained nodal rigid body (CNRB) elements of LS-DYNA were converted to rigid elements (RBE2) of NASTRAN. Figure 2.17 shows the vibration FE model, which consists of 701 RBE2 and 3,215 CWELD elements with 262,560 CQUAD4 and CTRIA3 shell elements.

An initial modal analysis was performed using MSC NASTRAN FE software under free-free boundary conditions. The six rigid-body modes were identified. The subsequent three flexible vibration modes, representing the responses of interest, are the first torsion mode, the first bending mode and a mixed torsion-bending mode.

2.3 Crash Scenarios

To understand and analyze the crashworthiness capabilities of vehicles and potential injury to occupants from crash, NHTSA has conducted crash tests on different vehicle models. These tests are done for different crash scenarios, and an overall safety performance rating is provided for the vehicle tested. The typical types of crash scenarios are FFI, offset frontal impact (OFI), SI, rear impact and roll over impact. Each has a defined impact setup, and NHTSA employs different dummy models to test the effect of crash on occupants by measuring certain responses at different points of the dummy model. To limit the scope of this study, only FFI and SI scenarios are considered.

2.3.1 Full Frontal Impact

2.3.1.1 FFI Simulation Setup

The FE simulation setup for FFI involves the head on collision of the vehicle model (with occupant and restraint system) traveling at a speed of 56.3 km/h (35 mph) with a rigid barrier, which consists of 36 simulated load cells. The rigid barrier model and the overall test setup are in accordance with the guidelines of New Car Assessment Program (NCAP) of FMVSS [5]. The FFI simulation is carried out for 150 ms since most occupant injuries occur within this time period. Figure 2.18 shows the FFI simulation at three different time intervals.

For FFI simulations, the FE model of the 1996 Dodge Neon vehicle including the occupant, seatbelt and airbag models presented earlier in this chapter is used. The vehicle model in FFI consists of a total of seven virtual accelerometers defined at different locations of the car. To calculate occupant related responses, the dummy model included a total of six virtual accelerometers defined at head, chest and pelvis regions of model.

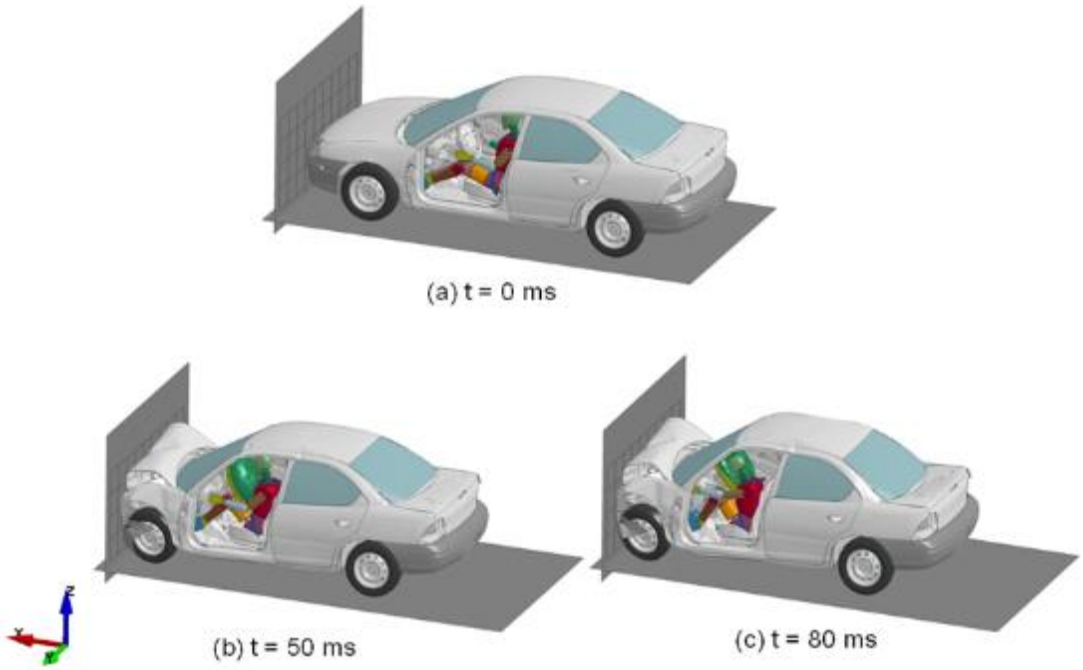

Figure 2.18 Full frontal impact simulations with dummy and restraint system models (a) t = 0 ms (b) t = 50 ms and (c) t = 80 ms (driver side door removed to ease view).

2.3.1.2 FFI Model Validation

Once the FFI simulation was performed, the overall simulation setup and interaction of various FE models used were validated by comparing acceleration plots with those obtained from actual crash test results. The resultant head and chest accelerations data measured at center location of accelerometers were used to compare the overall trends of the acceleration plots with the actual test data.

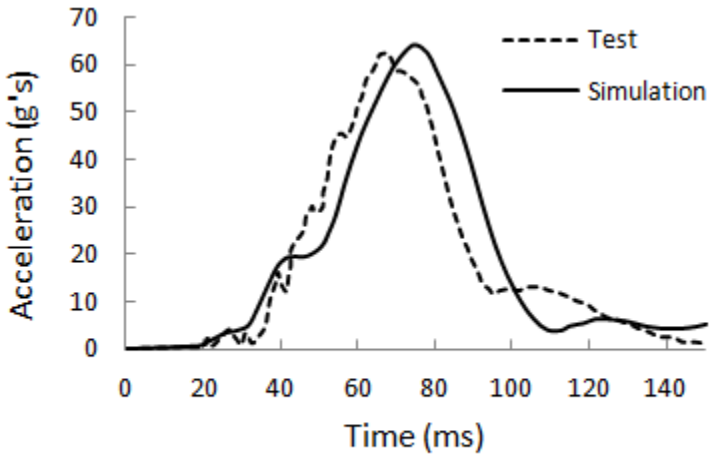

(a)

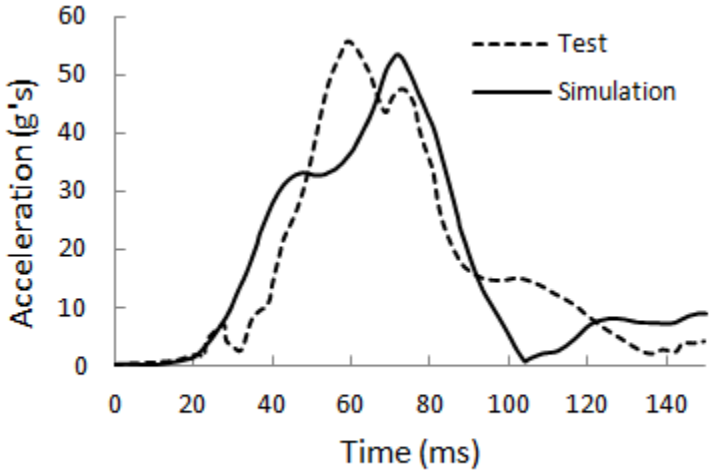

(b)

Figure 2.19 Comparisons of (a) resultant head acceleration and (b) resultant chest acceleration obtained from FE simulation with test data [5].

Figure 2.19 shows plots of resultant head and chest acceleration data obtained from FE simulations and actual crash tests. It can be seen from the plots that the general trends as well as the peak values of accelerations for simulation data matches well with the test data. The simulation data shown in the plots are resultant of X, Y, Z directional accelerations, obtained from nodes defined at center of virtual accelerometers defined in

the dummy model's head and chest regions, respectively. Since acceleration data in crash analysis are highly nonlinear and noisy, a Butterworth filter of 60 Hz was used to filter out the noise. Figure 2.20 compares the unfiltered noisy head acceleration data with filtered X, Y, and Z directional accelerations.

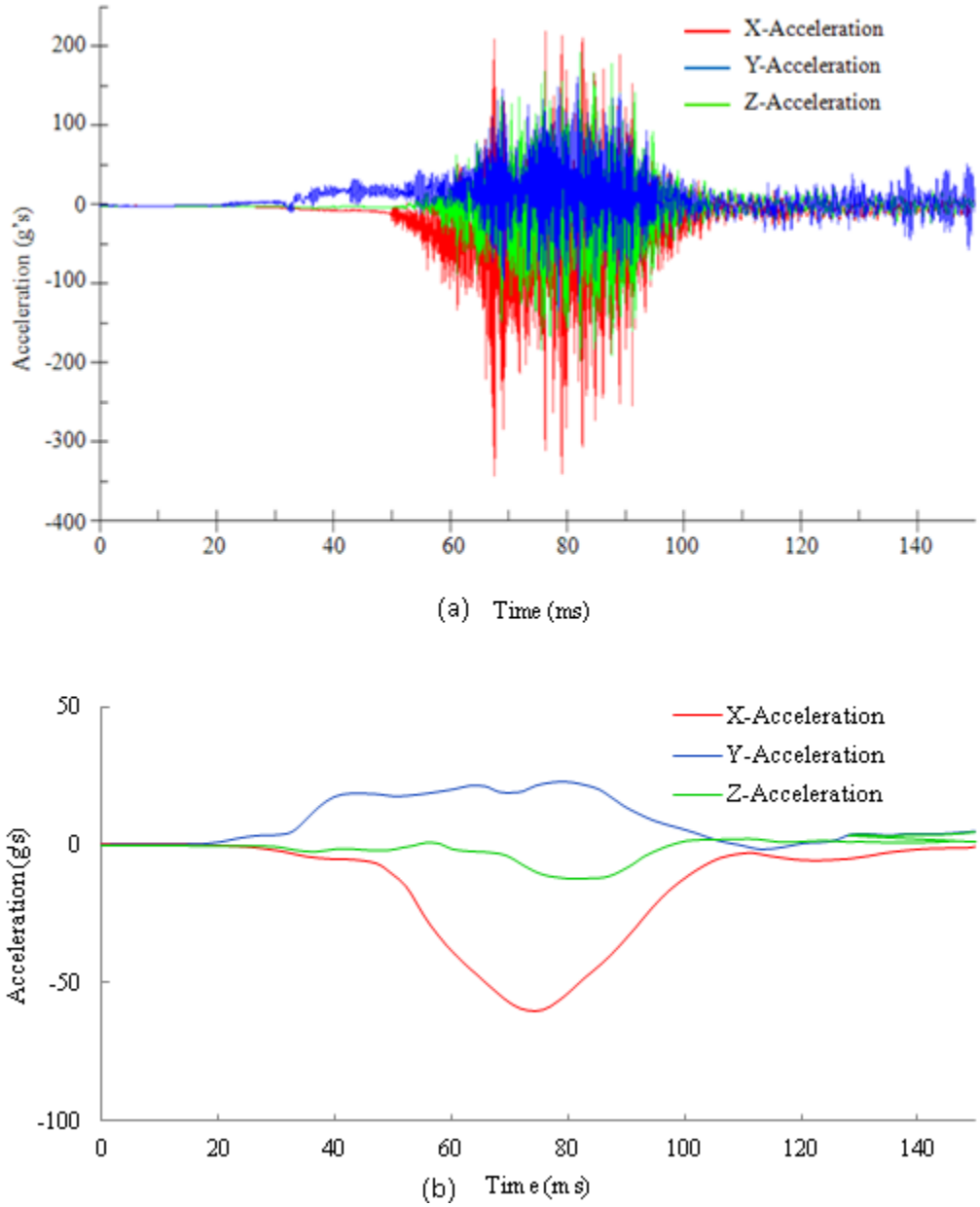

Figure 2.20 (a) Unfiltered and (b) filtered head acceleration data.

From Figure 2.20 it can be seen that the noise associated with acceleration has to be filtered so that the most critical peaks can be easily identified. These acceleration data were obtained with an output time interval of 0.01 ms. To have effective filtering, the output time interval of nodal data should be 0.01 ms or less [6].

2.3.2 Side Impact

2.3.2.1 SI Simulation Setup

The SI FE simulation consists of an MBD impacting the stationary vehicle model at an angle of 27° relative to the vehicle as shown in Figure 2.21 and at a speed of 52.5 km/h (32.6 mph). The MBD is modeled according to the guidelines of SI with a layer of honeycomb placed in front of it to simulate the impact caused by another vehicle [4]. The MDB is placed at 90° relative to the longitudinal axis of the vehicle model, but its wheels are aligned at 27° with respect to the vehicle centerline as shown in Figure 2.21.

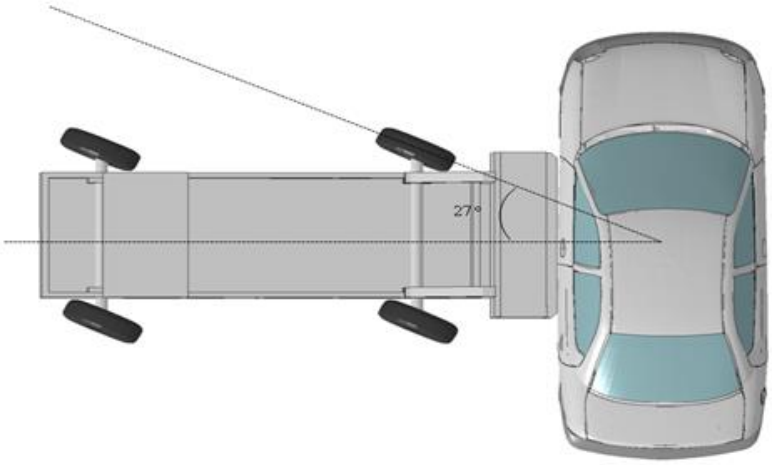

Figure 2.21 Side impact of BMD with the Dodge Neon model.

USSID models are commonly used in SI analysis whereas hybrid III dummy models are used in FFI. The seatbelt model used in FFI was used in SI as well but no airbags were used in SI analysis. The use of USSID in SI requires fresh routing of seatbelt model as the occupant models used for FFI and SI differ in geometry. However, to keep all the seatbelt properties consistent for both FFI and SI analyses, the hybrid III occupant model was used for SI analysis instead of a USSID model. The SI crash simulation is also carried out for 150 ms with Figure 2.22 showing interaction of MDB and occupant model with stationary Dodge Neon model at different time intervals.

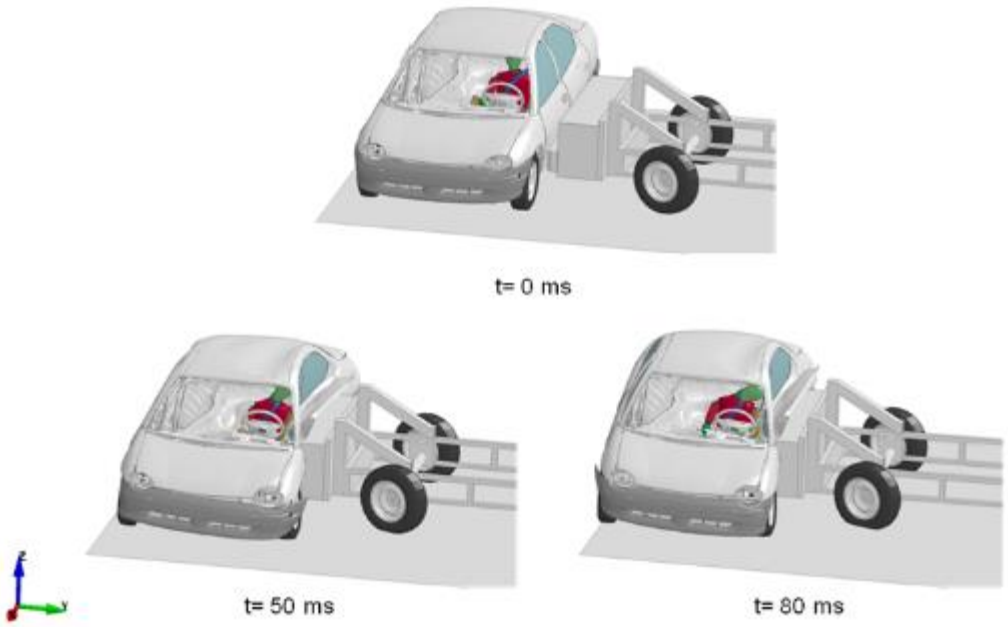

Figure 2.22 Side impact simulations with dummy and restraint system model (a) t= 0 ms, (b) t= 50 ms and (c) t= 80 ms. (windshield removed to ease view).

2.3.2.2 SI Model Validation

Earlier, the SI analysis of Dodge Neon vehicle model was validated using acceleration data obtained from the vehicle model. After incorporating dummy and

seatbelt models into the vehicle, the interaction of dummy with vehicle was validated using acceleration plots of dummy responses calculated at various locations in the dummy model. The dummy model consists of a total of six virtual accelerometers with three being at the pelvis region. To validate the overall SI simulation setup with dummy, the acceleration data calculated at pelvis and spine region towards the direction of impact were compared with the crash test data.

Pelvis acceleration was calculated at a single node located at center of the accelerometer at the center of pelvis region, but for spine acceleration, several nodes of the part defined as spine were plotted and nodal averaging was used to plot the acceleration data. Figure 2.23 shows the location of pelvis and spine regions of dummy model where acceleration data are calculated.

Figure 2.23 Acceleration response locations for SI model validation.

The comparison of Y-directional acceleration plots of simulation data with test data is shown in Figure 2.24. It can be seen that the overall trend of the simulation data

matches well with the test data. In obtaining the acceleration plots, Butterworth filter with 60 Hz frequency was used to filter out noise generated in acceleration data compared to the Channel Filter Class (CFC) filters used in crash test. The test data used in these plots are of SI test data for a 2000 Dodge Neon model compared to simulation data of a 1996 Dodge Neon model. The SI test data of 1996 Dodge Neon model was available but was not considered as the impact direction and positions of dummy models were different in this crash test.

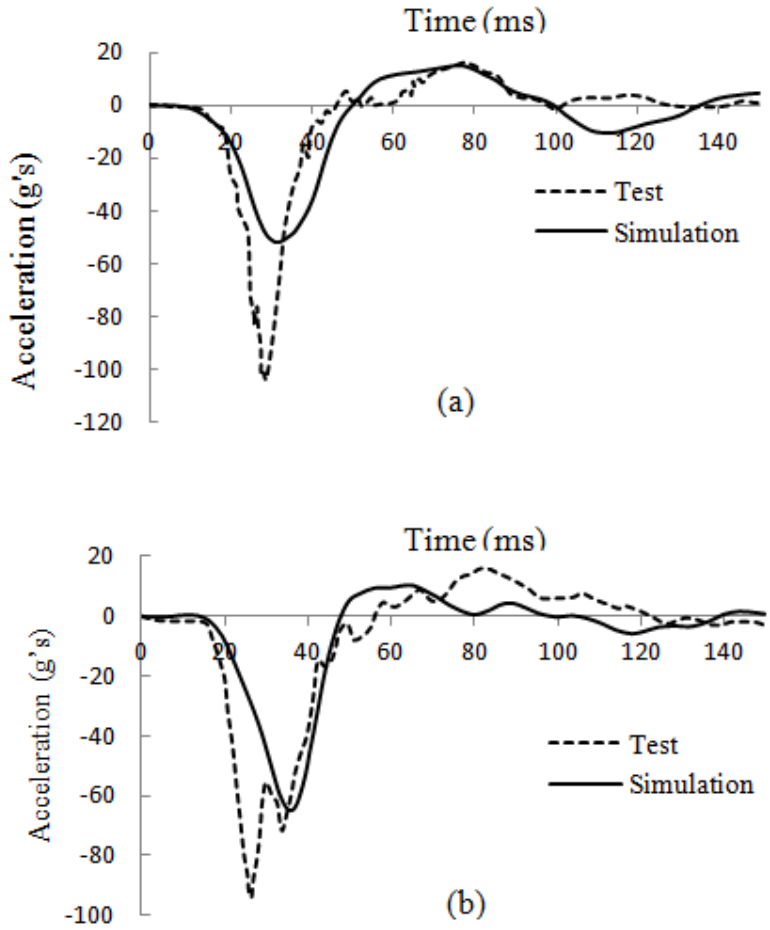

Figure 2.24 Comparison of FE simulation data

(a) Y-directional pelvis acceleration, (b) Y-directional spine acceleration with crash test data [9].

For example, in 1996 Dodge Neon SI test, the impact direction is from the right side (passenger end) of the vehicle and the vehicle consisted of dummy models in the front passenger seat and right rear seat. In SI test of 2000 Dodge Neon model, the impact of MDB is from the left side (driver end) with a dummy in the driver seat and another in the left rear seat. Therefore, this test data was used to compare with simulation data, as the overall test setup matched with the only exception being in impact velocities. The simulation impact velocity is 52.5 km/h (32.6 mph), whereas the crash test impact velocity is 61.2 km/h (38 mph). The difference in peak values of test and simulation data in Figure 2.24 can be partly due to the differences in impact velocities in simulation and crash test and also the filtering method employed.

2.4 References Cited

[1] Finite Element Model Archive, National Crash Analysis Center, http://www.ncac.gwu.edu/vml/models.html, June 2011.

[2] LS-DYNA keyword manual, Livermore Software Technology Corporation.

[3] LS-DYNA Materials Manual, Livermore Software Technology Corporation.

[4] MGA, Safety Compliance Testing for FMVSS 214 'Side Impact Protection – Passenger Cars': 1997 Dodge Neon, prepared by MGA proving Grounds, U.S. Department of Transportation, Washington, DC, 1997.

[5] New Car Assessment Program, 'Frontal Barrier Impact Test': 1996 Dodge Neon, prepared by Transportation Research Center Inc, U.S Department of Transportation, Washington, DC, 1995.

[6] Guha, S., D. Bhalsod, & J. Krebs. "LSTC Hybrid III dummies, Positioning and Post-Processing Documentation." Oct 2008.

[7] Bala, S. "Airbag Leakage Modeling in LS-DYNA." Livermore Software Technology Corporation.

[8] Kiani, M. "Modeling, Simulation and Optimization approaches for Design of Lightweight Car body Structures." PhD dissertation, Mississippi State University, 2013.

[9] MGA, Safety Compliance Testing for FMVSS 214 'Side Impact Protection – Passenger Cars': 2000 Dodge Neon, prepared by MGA Research Corporation, U.S. Department of Transportation, Washington, DC, 1999.

CHAPTER III

DESIGN PROBLEM STATEMENT

3.1 Multilevel Decomposition and Optimization

Many complex engineering systems (e.g., automobile, airplane) consist of multiple interlinked subsystems that have to be designed in such a way that various requirements are satisfied. Such a design problem can also involve a large number of design variables, constraints and objectives. Therefore, instead of designing a complex system all at once, it may be better to decompose it into various sublevels with each consisting of a number of elements that can be optimized to meet the system or subsystem level goals. Since each element of the decomposed problem will have design variables specific to it, the dimensionality associated with analyzing and optimizing each element problem can be significantly reduced.

Hierarchical decomposition is a technique where element specific design constraints and objectives are satisfied based on the inputs from lower or child elements depending on targets each element receives from its parent element. Figure 3.1 shows the basic architecture of a hierarchical decomposition. The element number ‘ij’ in the hierarchy is defined in such a way that ‘i’ represents the number of level in the decomposition and ‘j’ represents the element number in the decomposition.

To accommodate transfer of information from parent to child elements and vise-versa, a coordination strategy is required in the iterative solution process such that each

system-level objectives and constraints are each met and an optimum design is obtained. The Analytical target cascading (ATC) technique is a suitable optimization framework to accomplish this goal.

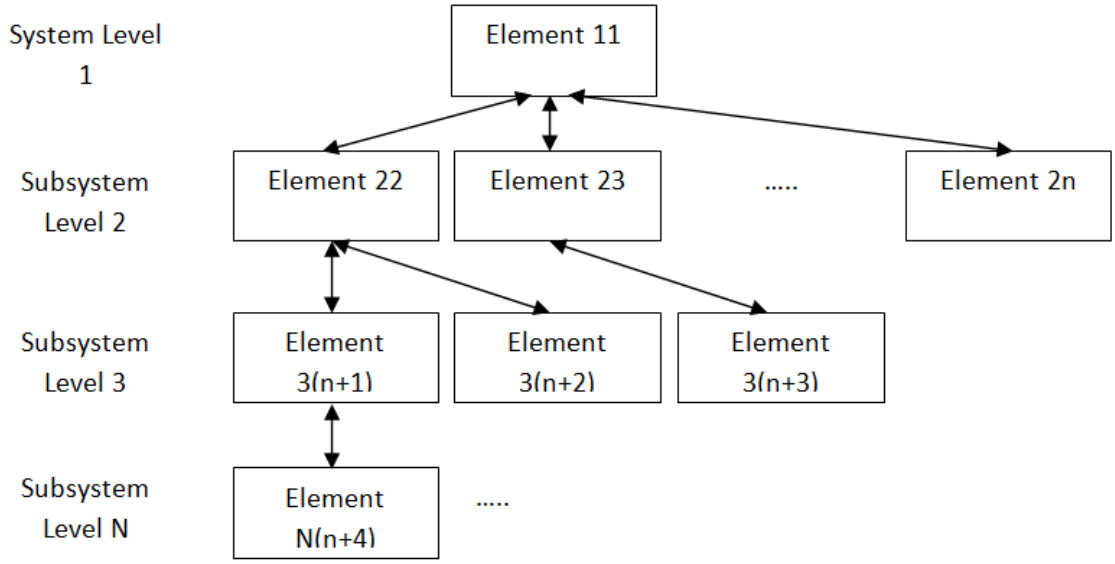

Figure 3.1 A generic hierarchically decomposed multilevel system.

3.1.1 Analytical Target Cascading

ATC is a multilevel optimization approach that is used to solve design problems, which can be decomposed into a number of elements as shown in Figure 3.1. In ATC, specific targets from upper-level elements (parents) of decomposition are cascaded down to the connecting lower-level elements (children) and, likewise, the responses from lower-level elements are sent up to higher level elements as inputs [1]. Each element of the hierarchy consists of an optimization subproblem with element-specific design variables, constraints and objectives.

A coordination strategy is implemented such that the element optimization problems satisfy the overall system-level optimality criteria. This coordination strategy allows the values of target and response variables and also the linking variables to have the same final values as the solution converges to an optimum design. The linking variables are design variables shared between elements of each level. In ATC formulation, the goal of optimization process is to reduce the difference between targets and responses apart from meeting element specific objectives and constraints.

In earlier ATC formulations, the goal of having consistent target-response and linking variables was accomplished by minimizing certain deviation tolerances subject to element specific design constraints. Kim et al. [2] used this formulation in designing chassis of a sport utility vehicle. The consistency of targets and responses is maintained by using a combination of equality and inequality constraints called consistency constraints. In recent years, quadratic penalty function formulations minimizing consistency constraints with help of suitable weight factors have been implemented.

3.1.2 Basic Approach in ATC

For a decomposed problem with N levels and M elements, the element number j in level i is denoted by subscripts ij. Different vectors of targets, responses and design variables specific to an element called as local variables are defined. The vector of target variables in each element is denoted by $\boldsymbol{t}_{ij}$, response vector by $\boldsymbol{r}_{ij}$ and the vector of local design variables by $\boldsymbol{x}_{ij}$. The decomposition based on this notation [3] is shown in Figure 3.2.

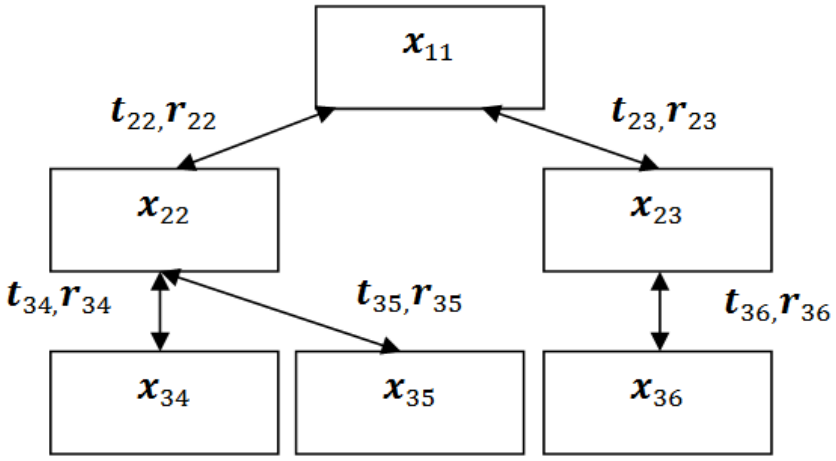

Figure 3.2 ATC notations for elemental targets, responses and local design variables.

For a decomposed problem such as that in Figure 3.2, an all-in-one (AIO) problem formulation can be written as [4]

$$\min_{\bar{x}_{11},\ldots,\ \bar{x}_{N\,M}} \quad \sum_{i=1}^{N}\sum_{j\in E_i} f_{ij}\ (\bar{x}_{ij}) \qquad (3.1)$$

$$s.t. \quad g_{ij}\left(\bar{x}_{ij}\right) \le 0$$

$$h_{ij}\left(\bar{x}_{ij}\right) = 0$$

$$\forall\, j \in E_i, i = 1, \ldots, N$$

where $\bar{x}_{ij} = [x_{ij}, t_{(i+1)k_1}, \ldots, t_{(i+1)k_{n_{ij}}}]$ is a vector of decision variables and fij, gij and hij refer to the sets of objective, inequality constraints and equality constraints, respectively. Ei is the set of elements at level i. This AIO problem becomes separable by considering additional consistency constraints given as

$$\boldsymbol{c}_{ij} = \boldsymbol{t}_{ij} - \boldsymbol{r}_{ij} = 0 \tag{3.2}$$

where tij and rij are vectors of targets and responses.

These consistency constraints are added to the existing objective function to form a relaxed AIO problem given as [4]

$$\begin{aligned} \min_{\boldsymbol{x}_{11},\ldots,\ \boldsymbol{x}_{NM}} \quad & \sum_{i=1}^{N} \sum_{j \in E_i} f_{ij}\ (\overline{\boldsymbol{x}}_{ij}) + \ \pi(\boldsymbol{c}_{ij}) \\ s.t. \quad & g_{ij}\left(\overline{\boldsymbol{x}}_{ij}\right) \leq 0 \\ & h_{ij}\left(\overline{\boldsymbol{x}}_{ij}\right) = 0 \\ & \forall\ \mathrm{j}\ \in\ \mathrm{E_i}, \mathrm{i} = 1, \ldots, \mathrm{N} \end{aligned} \tag{3.3}$$

where $\overline{\boldsymbol{x}}_{ij} = [\boldsymbol{x}_{ij}, \boldsymbol{r}_{ij}, \boldsymbol{t}_{(i+1)k_1}, \ldots, \boldsymbol{t}_{(i+1)k_{n_{ij}}}]$, $\boldsymbol{c}_{ij} = [\boldsymbol{c}_{ij}, \ldots \ldots \ldots\ \boldsymbol{c}_{NM}]$ is a vector of inconsistencies and $\pi(\boldsymbol{c}_{ij})$ represents the general relaxing function.

Equation (3.3) can be decomposed into a hierarchical system with the optimization problem in element ij given as

$$\begin{aligned} \min_{\boldsymbol{x}_{ij}} \quad & f_{ij}(\overline{\boldsymbol{x}}_{ij}) + \ \pi(c_{ij}) \\ s.t \quad & g_{ij}\left(\overline{\boldsymbol{x}}_{ij}\right) \leq 0 \\ & h_{ij}\left(\overline{\boldsymbol{x}}_{ij}\right) = 0 \end{aligned} \tag{3.4}$$

where $\overline{\boldsymbol{x}}_{ij} = [\boldsymbol{x}_{ij}, \boldsymbol{r}_{ij}, \boldsymbol{t}_{(i+1)k_1}, \ldots, \boldsymbol{t}_{(i+1)k_{n_{ij}}}]$ is the vector of local decision variables.

The ATC formulation differs in the way the relaxing function $\pi(\boldsymbol{c}_{ij})$is defined. Currently, ATC-based formulations can be classified into three types, i.e., Quadratic Penalty (QP), Ordinary Lagrangian (OL), and Augmented Lagrangian Penalty (ALP).

In this study, ALP based on exponential penalty function (EPF) is used. This approach relies on the unconstrained optimization problem formulation using method of multipliers suggested by Kort and Bertsekas [5]. The penalty function formulation is given as

$$\min_{x^k} \quad f(x) + \sum_{j=1}^{r} (\mu_j^k / a_j^k)\, \psi\,(a_j^k g_j(x)) \tag{3.5}$$

where μ_j^k and a_j^k are multiplier and penalty parameters.

To apply this formulation in an ATC framework, DorMohammadi and Rais-Rohani [4, 6] used EPF and inequality-based consistency constraints. The penalty term is given as

$$\psi(t) = e^t - 1 = 0 \tag{3.6}$$

And the consistency constraint $\boldsymbol{c}_{ij} = \boldsymbol{t}_{ij} - \boldsymbol{r}_{ij} = 0$ is modified to two inequality constraints given as

$$\boldsymbol{c}_{ij} = \boldsymbol{t}_{ij} - \boldsymbol{r}_{ij} \geq 0$$

$$\boldsymbol{c}_{ij} = \boldsymbol{t}_{ij} - \boldsymbol{r}_{ij} \leq 0 \tag{3.7}$$

Using the EPF formulation, the decomposed problem in element ij is expressed as

$$min_{x_{ij}} f_{ij}(\boldsymbol{x}_{ij}) + \left[\frac{\mu_{ij}}{a_{ij}}\left(e^{a_{ij}(\boldsymbol{t}_{ij}-\boldsymbol{r}_{ij})}-1\right)+\frac{\gamma_{ij}}{b_{ij}}(e^{b_{ij}(\boldsymbol{r}_{ij}-\boldsymbol{t}_{ij})}-1\right]$$

$$+\sum_{k\epsilon D_{ij}}\left[\frac{\mu_{(i+1)k}}{a_{(i+1)k}}\left(e^{a_{(i+1)k}(\boldsymbol{t}_{(i+1)k}-\boldsymbol{r}_{(i+1)k})}-1\right)\right.$$

$$\left.+\frac{\gamma_{(i+1)k}}{b_{(i+1)k}}(e^{b_{(i+1)k}(\boldsymbol{r}_{(i+1)k}-\boldsymbol{t}_{(i+1)k})}-1\right]$$

$$s.t. \qquad g_{ij}\left(x_{ij}\right) \leq 0 \tag{3.8}$$

$$h_{ij}\left(x_{ij}\right) = 0$$

The multipliers in Eq. (3.8) are updated using

$$\mu_{ij}^{k+1} = \mu_{ij}^{k} e^{a_{ij}^{k}(\boldsymbol{t}_{ij}^{k}-\boldsymbol{r}_{ij}^{k})}$$

$$\gamma_{ij}^{k+1} = \gamma_{ij}^{k} e^{b_{ij}^{k}(\boldsymbol{r}_{ij}^{k}-\boldsymbol{t}_{ij}^{k})} \tag{3.9}$$

Although the penalty parameters a and b can be updated with dependence on or independent of the multipliers, in this study, they are kept fixed in the iteration process.

In solving the EPF-based ATC problem, two coordination strategies to satisfy the consistency constraints and updating the multipliers have been proposed [6]. In the double loop (EPF I) approach, the ATC problem is solved in hierarchical order within an inner loop, and once the inner loop convergence criterion is met, the multipliers are updated in the outer loop. In the single loop EPF formulation (EPF II), the ATC problem is solved in hierarchical order and convergence criterion is checked and multipliers are updated at the end of the loop. In this study, EPF II formulation is used to solve the decomposed problems as the computation cost of EPF II is less [6]. A tolerance value for

consistency constraints (i.e., the difference in target and responses of each element) is selected and used as the loop convergence criterion.

3.2 Design Problem Overview

The goal of this study is to optimize the design of a vehicle structure model along with ORS such that the optimized design has less weight and improved safety. To accomplish this goal, a multilevel, multi-objective problem using ATC technique is formulated with one system-level objective being a combination of injury criteria associated with FFI and SI and the other being the mass of selected parts of vehicle model in FFI and SI. Two design cases, one with crash occupant safety constraints and another with crash+vibration design constraints are solved. The design objectives and design variables considered in both cases are the same.

A few vehicle-based and ORS-based design variables are selected depending upon their influence on critical responses measured. The crush or intrusion distance of vehicle after a crash depends on the energy absorbing capacities of the vehicle parts. To absorb the energy generated in a crash, each structural part should participate efficiently in the energy absorption process. Here, a few parts are selected based on their contribution to the overall energy absorption. As these parts influence energy absorption, they have influence on overall crush of the vehicle and, hence, influence the occupant injury responses. The parts contributing to energy absorption in FFI are different from SI with few parts influencing both crash scenarios; hence, wall thicknesses of parts specific to each crash scenario are selected as design variables.

The wall thicknesses of selected vehicle parts represent the vehicle-based design variables and parameters of seatbelt and airbag constitute ORS-based design variables.

Various occupant-related responses specific to each crash scenario are selected as design constraints in the optimization problem. A relation between part mass and wall thickness is used to determine the mass of each part at different wall thickness values. This relation is given as

$$M_{new} = t_{new}\left(\frac{M_{baseline}}{t_{baseline}}\right) \tag{3.10}$$

where M_{new} is new mass of the part, t_{new} is new wall thickness, $M_{baseline}$ is baseline mass and $t_{baseline}$ is baseline wall thickness.

3.2.1 Design Variables for FFI Analysis

The selected vehicle-based design variables (defined using shell element definition of LS-DYNA) are the wall thicknesses of the parts shown in Figure 3.3. A total of 17 parts are selected, but due to symmetry in the vehicle model, the design variables are reduced to 11.

Table 3.1 shows a list of parts selected as vehicle-based design variables for FFI, baseline wall thickness values along with the corresponding upper and lower bounds. In the optimization problem, the design variables are allowed to vary in the range of 50% to 150% (as the lower and upper bounds) relative to their respective baseline values. Figure 3.3 shows the selected parts for FFI with the symmetric parts shown in dark color.

Table 3.1 Vehicle-based design variables and associated values for FFI analysis.

Design Variables	Part Name	Part No. in LS-DYNA	Lower Bound (mm)	Baseline Thickness (mm)	Upper Bound (mm)
x_1	A-Pillar	2000310, 311	0.805	1.611	2.416
x_2	Front bumper	2000330	0.978	1.956	2.934
x_3	Firewall	2000352	0.367	0.735	1.102
x_4	Front floor panel	2000353	0.352	0.705	1.057
x_5	Outer Cabin	2000355, 356	0.414	0.829	1.243
x_6	Shotgun	2000373, 374	0.762	1.524	2.286
x_7	Inner side rail	2000389, 391	0.947	1.895	2.842
x_8	Outer Side rail	2000390, 392	0.761	1.522	2.283
x_9	Side rail extension	2000398, 399	0.947	1.895	2.842
x_{10}	Lower suspension frame	2000428	0.793	1.587	2.380
x_{11}	Upper suspension frame	2000439	1.303	2.606	3.909

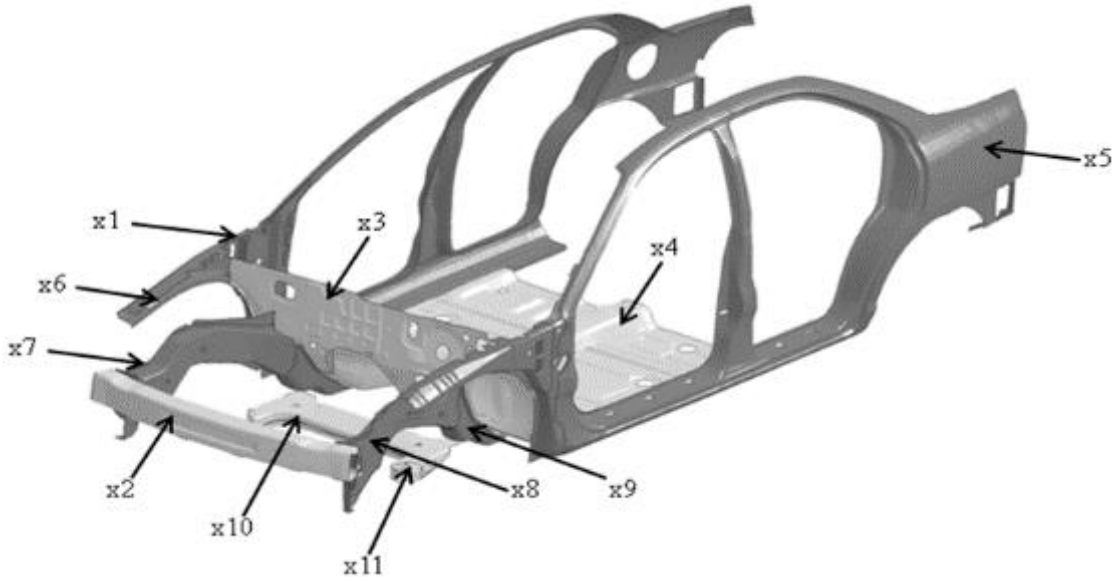

Figure 3.3 Vehicle-based design variables for FFI analysis.

Figure 3.4 shows the contribution of each part towards the internal energy absorption in an FFI analysis and Figure 3.5 shows the difference in overall energy absorption of the selected parts compared to the full vehicle. The selected parts contribute to approximately 40% of the total energy absorption of the vehicle in an FFI. The largest contribution comes from the front bumper's steel beam (x2) whereas the smallest contribution is associated with the lower suspension frame (x10).

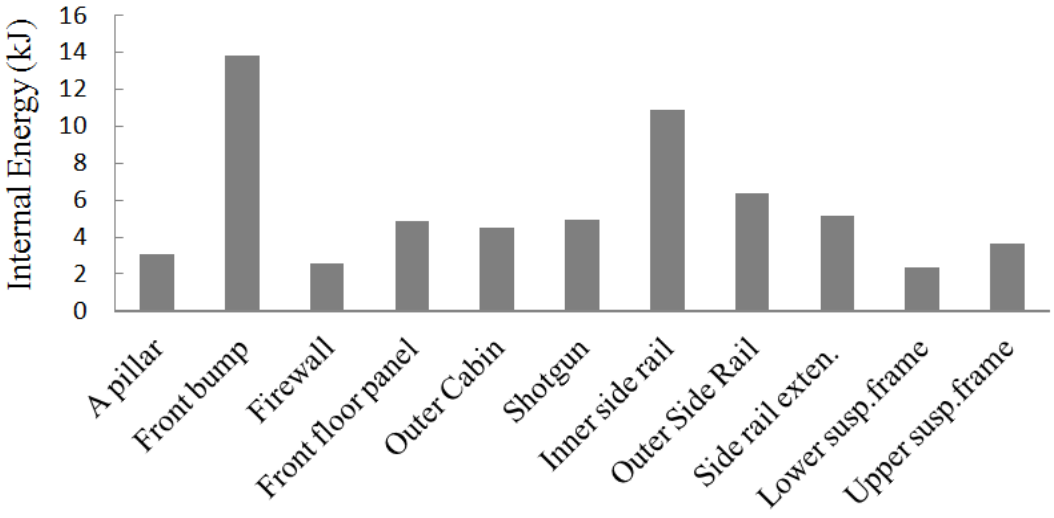

Figure 3.4 Part specific internal energy absorption of FFI analysis.

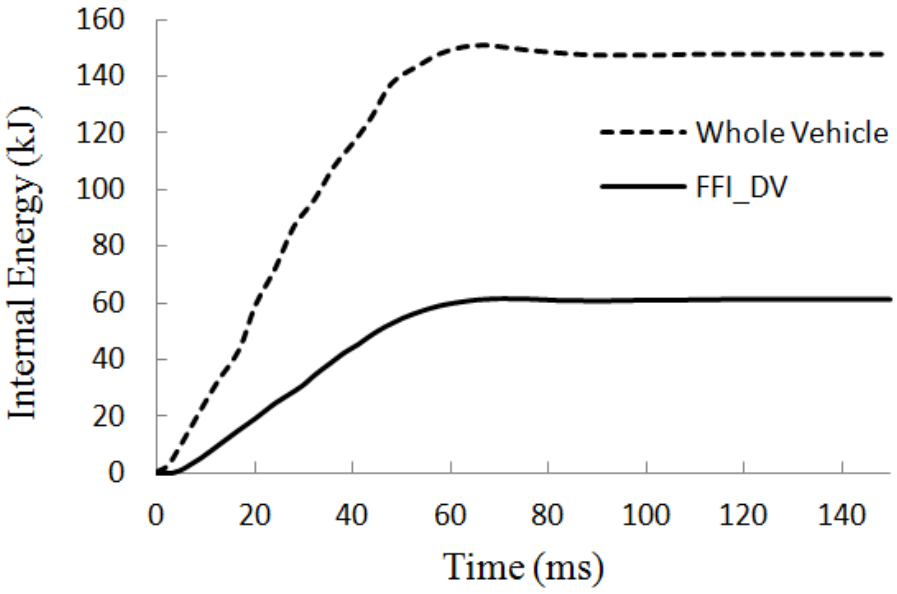

Figure 3.5 Internal energy absorption of full vehicle and selected parts in FFI analysis (FFI_DV).

Apart from vehicle-based design variables, a few variables pertaining to ORS are also used as design variables in FFI. These are pretensioner limit force of seatbelt (x12), as well as the scale factor of load curve defining mass flow rate (x13) versus time, the scale factor of vent orifice area (x14), and temperature of input gas (x15) pertaining to airbag.

In determining the ORS design variables and their respective upper and lower bounds, a design sensitivity analysis was performed initially by varying the selected parameters individually and determining their influence on the critical occupant responses. The lower and upper bounds are defined such that there are no instabilities in the crash simulations at those values of design variables. For example, a very low mass flow rate or input gas temperature would hinder the airbag inflation and could cause more

injury to the occupant as there would be insufficient volume of gas inside the airbag. On the other hand, a very high mass flow rate would make the airbag stiff and hard causing the occupant head to bounce back after impact, thus, increasing the head acceleration.

Table 3.2 ORS-based design variables and associated values for FFI analysis.

Design Variable	Name	Lower Bound	Baseline	Upper Bound
x_{12}	Seatbelt Limit Force (N)	1000	2500	5000
x_{13}	Mass flow rate (scale factor)	0.8	1	1.4
x_{14}	Vent orifice area (scale factor)	0.6	1	1.4
x_{15}	Temperature (K)	600	782	1000

3.2.2 Design Variables for SI Analysis

Similar to the design variables selected for the FFI analysis, major parts contributing towards internal energy absorption in a SI analysis are selected and the corresponding wall thickness values are treated as design variables. A total of 12 parts are selected and due to symmetry in a few parts, the design variables are reduced to 9. Within these design variables, three design variables also belong to FFI design as a few parts are important in both crash scenarios. These parts are the A-pillar, outer cabin and front floor panel. The list of vehicle-based design variables considered in SI analysis along with their respective upper bound, lower bound and baseline thickness values is shown in Table 3.3. In order to have a consistent sequence of design variables in the optimization

problem, and since FFI design variables are identified by x_1-x_{15}, the design variables specific to SI analysis are denoted as x_{16}- x_{21}, with x_1, x_4 and x_5 being common in both FFI and SI analyses. Figure 3.6 shows all the parts selected as vehicle-based design variables for SI analysis.

Table 3.3 Vehicle-based design variables in SI analysis.

Design Variable	Part Name	Part No. in LS-DYNA	Lower Bound (mm)	Baseline Thickness (mm)	Upper Bound (mm)
x_1	A-Pillar	2000310, 311	0.805	1.611	2.416
x_4	Front floor panel	2000353	0.352	0.705	1.057
x_5	Outer Cabin	2000355, 356	0.414	0.829	1.243
x_{16}	Mid B-pillar	2000328	0.353	0.706	1.059
x_{17}	Rear cabin floor	2000354	0.353	0.706	1.059
x_{18}	Cabin seat reinforcement	2000357	0.341	0.682	1.023
x_{19}	Cabin mid rail	2000358, 359	0.525	1.050	1.575
x_{20}	Rear plate	2000415	0.355	0.710	1.065
x_{21}	Roof	2000416	0.351	0.702	1.053

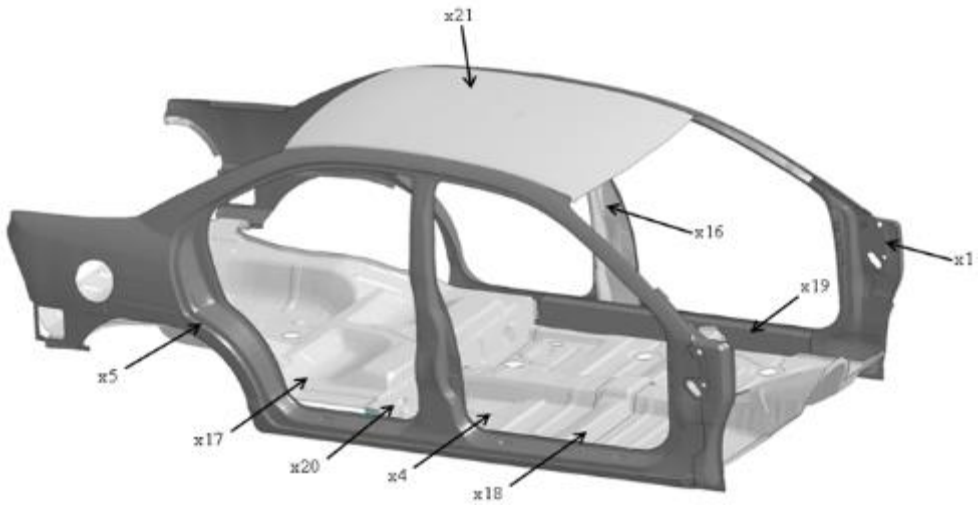

Figure 3.6 Vehicle-based design variables for SI analysis.

The contribution to internal energy absorption by each part selected in SI analysis is shown in Figure 3.7. The greatest energy absorption is associated with the outer cabin (x5) with the least contribution coming from the roof (x21).

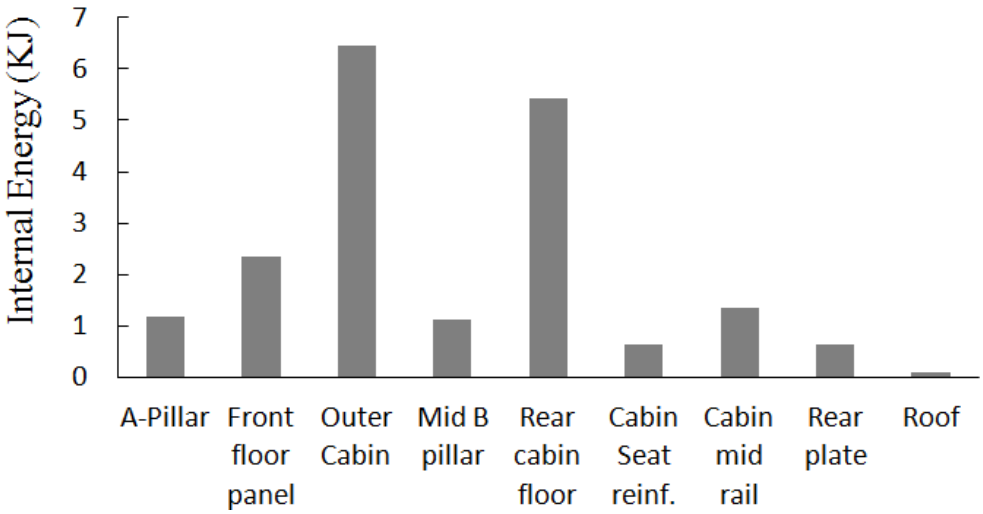

Figure 3.7 Part specific internal energy absorption in SI analysis.

Figure 3.8 shows energy absorption of the whole vehicle compared to the energy absorbed by the selected parts in SI. The overall internal energy contribution of the selected parts is approximately 38% of that for the whole vehicle.

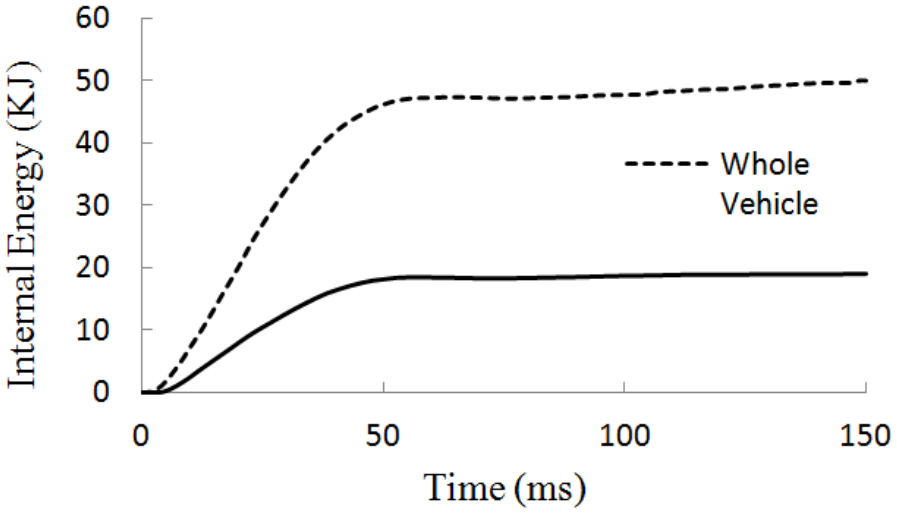

Figure 3.8 Internal energy absorption of whole vehicle and selected parts in SI analysis (SI_DV).

In SI analysis, since the same dummy model as that in FFI is used, the seatbelt design variable (x12) of FFI is also considered in SI with the same upper and lower bounds. No airbags are present in SI analysis; therefore, the seatbelt limit force is the only design variable considered in ORS of SI analysis. Therefore the total numbers of design variables considered for SI are 10 with 9 being vehicle-based and one ORS-based.

3.2.3 Design Responses

In both FFI and SI analyses, a number of occupant related design responses at various locations of the occupant model are evaluated. The internal energy absorption of parts obtained in both FFI and SI analysis is the only vehicle-based response in the design problem. There are a total of seven occupant-based responses in FFI and four in SI analyses.

The occupant-based responses in FFI analysis are Head Injury Criterion (HIC), C_{3ms} thorax criterion (C_{3ms}), Head Acceleration (HA), Chest Acceleration (CA), Chest Deflection (CD), and both Left Femur (F_L) and Right Femur (F_R) forces. A 60-Hz Butterworth filter is used for acceleration responses and femur forces to filter out noise.

HIC is a very important FFI response as it is a measure of occupant's head injury and the calculation of HIC is based on the time interval of crash during which the risk of injury is high. HIC is calculated using a time interval ranging from 15 ms to 36 ms after impact. In this study, the 36 ms time interval is used as per actual crash test [7]. The equation representing HIC calculation is given as

$$HIC = max\left[\frac{1}{(t_2-t_1)}\int_{t1}^{t2} a(t)dt\right]^{2.5}(t_2 - t_1) \tag{3.11}$$

where a(t) is the filtered resultant head acceleration varying from time t_1 = 0 ms to t_2 = 36 ms. HIC is measured directly in post processing tool of LS-DYNA (LS-PrePost) using a node at center of an virtual accelerometer defined at center of dummy model's head.

Head acceleration response is calculated at the same node as HIC and the resultant of directional accelerations is used as response. C3ms thorax criterion is the maximum of average chest acceleration calculated within 3-ms time interval of FFI analysis. Chest acceleration is calculated at a node at the center of virtual accelerometer defined at the center of the chest region. Similar to head acceleration, the resultant of chest directional accelerations is used as a response. Chest deflection is evaluated by measuring the overall deflection of spring running from sternum to spine of the dummy model. Femur forces are calculated using joints defined between the lower leg and femur bone. The compressive forces obtained in longitudinal direction of both left and right

femur bones are selected as responses. Figure 3.9 shows the locations where occupant responses are calculated. The selected FFI analysis responses are crucial for determining the overall injury to the occupant.

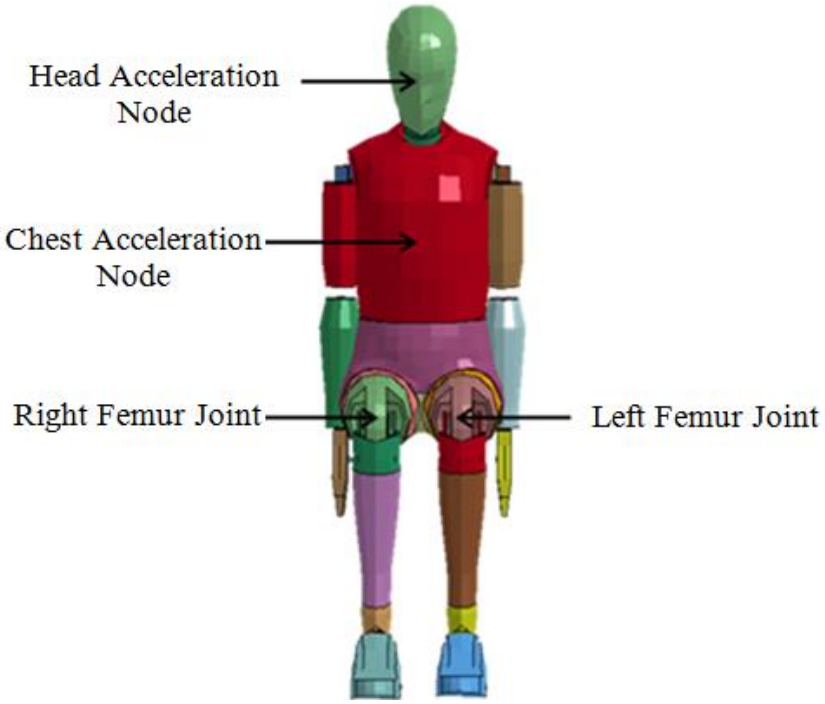

Figure 3.9 Location of FFI occupant responses.

The Weighted Injury Criterion (WIC) [8] is a good measure of occupant injury in frontal impacts. This criterion employs certain weights given to each response depending on its significance to overall occupant injury and is based on the limits provided by FMVSS 208 frontal impact injury standards. To have better occupant safety, this criterion is required to be as low as possible. The WIC is given as

$$WIC = 0.6\left(\frac{HIC}{1000}\right) + 0.35\left(\frac{C_{3ms}}{60}\right) + 0.025\left(\frac{F_L}{1000}\right) + 0.025\left(\frac{F_R}{1000}\right) \qquad (3.12)$$

where HIC, C_{3ms}, F_L, F_R responses are normalized with the corresponding FMVSS limits and the coefficient of each term represents the weight given [8] to that response in determining the overall occupant injury. This equation is used later as part of the objective function in the vehicle optimization problem. Table 3.4 shows the occupant responses obtained for the FFI simulation of the baseline vehicle + dummy model along with the associated FMVSS limits. FFI_IE in table 3.4 corresponds to internal energy absorption of parts selected as vehicle based design variables in FFI analysis.

The Weighted Injury Criterion (WIC) [8] is a good measure of occupant injury in frontal impacts. This criterion employs certain weights given to each response depending on its significance to overall occupant injury and is based on the limits provided by FMVSS 208 frontal impact injury standards. To have better occupant safety, this criterion is required to be as low as possible. The WIC is given as

$$WIC = 0.6\left(\frac{HIC}{1000}\right) + 0.35\left(\frac{C_{3ms}}{60}\right) + 0.025\left(\frac{F_L}{1000}\right) + 0.025\left(\frac{F_R}{1000}\right) \qquad (3.12)$$

where HIC, C_{3ms}, F_L, F_R responses are normalized with the corresponding FMVSS limits and the coefficient of each term represents the weight given [8] to that response in determining the overall occupant injury. This equation is used later as part of the objective function in the vehicle optimization problem. Table 3.4 shows the occupant responses obtained for the FFI simulation of the baseline vehicle + dummy model along with the associated FMVSS limits. FFI_IE in table 3.4 corresponds to internal energy absorption of parts selected as vehicle based design variables in FFI analysis.

Table 3.4 FFI Baseline responses and FMVSS limits.

FFI Response	Baseline	FMVSS Limit
HIC	711.10	1000
C_{3ms} (g's)	53.01	60
HA (g's)	64.52	-
CA (g's)	53.78	-
CD (mm)	21.68	63
L_F (N)	4692.40	10000
R_F (N)	4317.00	10000
FFI-IE (kJ)	61.70	-

Similar to FFI analysis, a few occupant responses and one vehicle-based response are selected for SI analysis. The four occupant-based responses are: Upper Rib (UR) and Lower Rib (LR) Accelerations, Spine Acceleration, and Pelvis Acceleration. Internal energy absorption is the only vehicle-based response. The upper and lower rib accelerations are calculated at 12 nodes and nodal averaging is used to find the corresponding peak values. In this study, the average peak value of upper and lower rib accelerations is used as a single rib acceleration response. Spine acceleration is calculated at a total of 35 nodes of the part defined as spine in the occupant model and nodal averaging is used to determine the response value. Similar to rib accelerations, the peak value of average acceleration of 35 nodes is selected as a response. Since a virtual accelerometer is present in the pelvis region, pelvis acceleration is calculated at center node of the accelerometer. The acceleration responses calculated at different locations of occupant in SI are Y-directional accelerations measured in the direction of side impact.

Similar to FFI analysis responses, a 60-Hz Butterworth filter is used to filter out noise from acceleration responses.

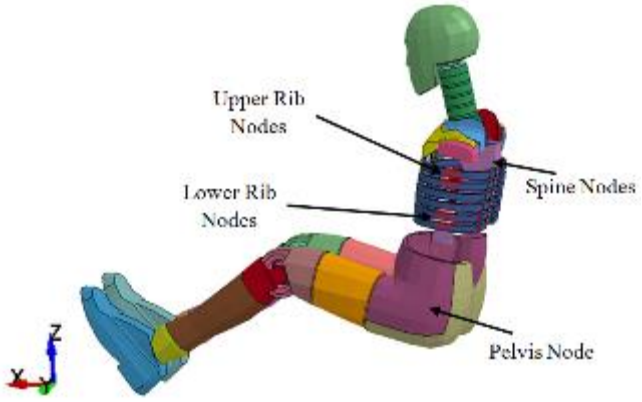

Figure 3.10 SI analysis response locations.

The Thoracic Trauma Index (TTI) is the injury criterion defined under FMVSS 214 of side impact protection [9], and it is used as part of the objective function with a goal of injury reduction. The TTI is given as

$$TTI = 0.5(Rib_{Acceleration} + Spine_{Acceleraion}) \tag{3.13}$$

Similar to FFI injury criterion, FMVSS 214 safety standard of SI has defined the maximum allowable limit for TTI to be 85 g's. Table 3.5 shows the baseline responses of SI analysis where SI_DV corresponds to internal energy absorption of vehicle based design variables of SI analysis.

Table 3.5 SI baseline responses.

SI Response	Baseline
U_R Acceleration (g's)	69.74
L_R Acceleration (g's)	58.82
Spine Acceleration (g's)	64.89
Pelvis Acceleration (g's)	51.58
SI-IE (kJ)	19.20

In the design problem with the vibration criteria included, the frequencies of first three flexible modes (Freq1-Freq3) are considered as design responses. These modes represent the first torsion, first bending and a mixed torsion-bending mode. The baseline values of these three responses are given in Table 3.6.

Table 3.6 Baseline response of vibration design.

Response (Hz)	Baseline
Freq1	35.39
Freq2	36.23
Freq3	38.37

3.3 Vehicle Design Optimization Problems

3.3.1 Crash-Based Design

The objective of this design problem is to reduce the overall occupant injury in both FFI and SI and also to obtain a lighter vehicle design without compromising occupant safety and vehicle crashworthiness. A combination of FFI and SI injury criteria are used to form a composite objective function and the variables associated with this function are treated as design targets. Since the objective function depends on both FFI and SI occupant safety requirements, a multilevel decomposition approach is used to optimize the vehicle model for occupant safety and crashworthiness in both FFI and SI.

The general optimization framework of this multilevel decomposition is shown in Figure 3.11. The element notation of decomposition shown in Figure 3.11 is in accordance with the hierarchical decomposition shown in Figure 3.1. The element 11 of the decomposition minimizes the overall injury criterion in both FFI and SI. In the second level, vehicle and occupant restraint design variables are adjusted to match the injury criteria set in level 1 and also to minimize weight of the parts specific to FFI in element 22 and SI in element 23. The total number of design variables in this case is 21 with 15 design variables in element 22 and 10 in element 23. Three design variables are common in element 22 and 23; hence, they are treated as linking variables. Table 3.7 shows all the design variables considered in the crash-based design case.

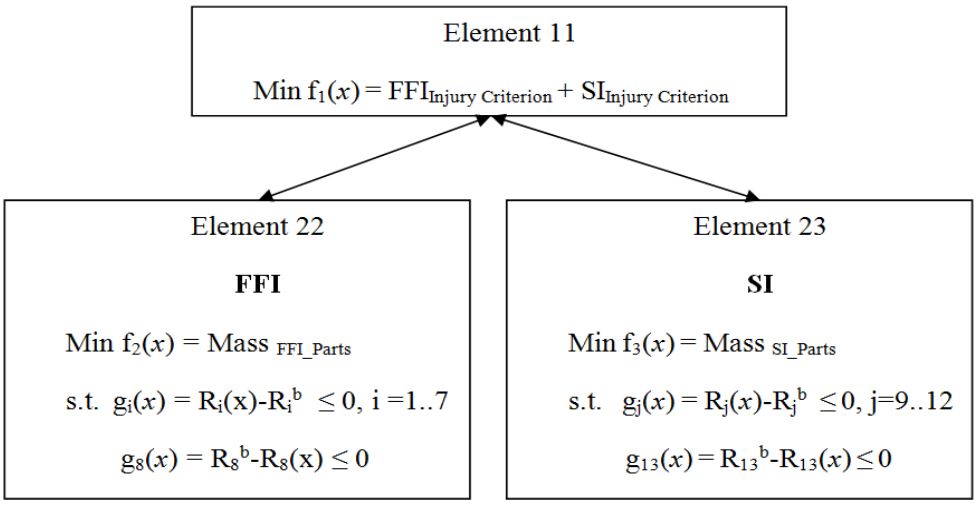

Figure 3.11 Overview of crash-based design problem.

Table 3.7 Design variables of crash-based design case.

Design Variables*	Name	Lower Bound	Baseline Thickness	Upper Bound
x_1	A-Pillar	0.805	1.611	2.416
x_2	Front bump	0.978	1.956	2.934
x_3	Firewall	0.367	0.735	1.102
x_4	Front floor panel	0.352	0.705	1.057
x_5	Outer Cabin	0.414	0.829	1.243
x_6	Shotgun	0.762	1.524	2.286
x_7	Inner side rail	0.947	1.895	2.842
x_8	Outer Side rail	0.761	1.522	2.283
x_9	Side rail extension	0.947	1.895	2.842
x_{10}	Lower suspension frame	0.793	1.587	2.380
x_{11}	Upper suspension frame	1.303	2.606	3.909
x_{12}	Seatbelt limit force (N)	1000	2500	5000
x_{13}	Mass flow rate (scale factor)	0.8	1.0	1.4
x_{14}	Vent orifice area (scale factor)	0.6	1.0	1.4
x_{15}	Airbag input temperature (K)	600	781	1000
x_{16}	Mid B-pillar	0.353	0.706	1.059
x_{17}	Rear cabin floor	0.353	0.706	1.059
x_{18}	Cabin seat reinforcement	0.341	0.682	1.023
x_{19}	Cabin mid rail	0.525	1.050	1.575
x_{20}	Rear plate	0.355	0.710	1.065
x_{21}	Roof	0.351	0.702	1.053

*Part thicknesses are in mm.

A total of eight design constraints for FFI and five for SI are considered as shown in Table 3.8. The design constraints $g_1(x)$ through $g_7(x)$ pertain to FFI occupant response, which should not exceed the corresponding baseline values and g_8 is internal energy of parts in FFI required to be no less than the baseline value. Constraints $g_9(x)$ through $g_{12}(x)$ are occupant responses from the SI analysis, which cannot exceed the respective baseline values and $g_{13}(x)$ corresponds to internal energy absorption of parts specific to SI crash analysis.

Table 3.8 Design constraints of crash-based design case.

Notation	Response	Baseline
g_1	HIC	711.10
g_2	C_{3ms} (g's)	53.01
g_3	HA (g's)	64.52
g_4	CA (g's)	53.78
g_5	CD (mm)	21.68
g_6	L_F (N)	4692.40
g_7	R_F (N)	4317.00
g_8	FFI-IE (kJ)	61.70
g_9	U_R (g's)	69.74
g_{10}	L_R (g's)	58.82
g_{11}	Spine (g's)	64.89
g_{12}	Pelvis (g's)	51.58
g_{13}	SI-IE (kJ)	19.20

The objective function used in element 11 is a combination of injury criteria in FFI and SI analyses. The Weighted Injury Criterion (WIC) is used for FFI analysis and TTI for SI analysis. The WIC and TTI consist of important crash responses that contribute to the overall occupant injury and are normalized by the corresponding FMVSS limits for FFI and SI. As the baseline occupant responses in both FFI and SI analyses are within the FMVSS limits, the WIC and TTI equations are modified by normalizing the occupant responses by the baseline response values instead of the FMVSS limits. The coefficients of occupant responses in WIC and TTI are the weights given to each response depending on its effect on the overall occupant injury criterion. Since a combination of WIC and TTI is used as the objective function, equal weights are given to WIC and TTI, and the coefficients of the injury criteria are changed accordingly. Thus, the modified objective function of element 11 is given as

$$min\, f_1(x) = 0.3\left(\frac{HIC}{711.1}\right) + 0.175\left(\frac{C_{3ms}}{53.01}\right) + 0.0125\left(\frac{L_F}{4692.4}\right) + 0.0125\left(\frac{R_F}{4317}\right) +$$

$$\frac{0.25}{2}\left(\frac{U_R}{69.74} + \frac{L_R}{58.82}\right) + 0.25\left(\frac{Spine_{Accel}}{64.89}\right) \quad (3.14)$$

The occupant responses in Equation (3.14) are treated as targets cascaded down to elements 22 and 23, where the element objective function includes mass calculation of the parts specific to each element. The targets cascaded from the top level are met by performing optimization in each element using the EPF II formulation. A more detailed decomposition of the design problem based on ATC is shown in Figure 3.12. Since exponential formulation (EPF II) is used, all the constraints are normalized by their baseline values and the design variables are normalized by their upper bounds. The element specific constraints are denoted by symbol gi and the normalized constraints are denoted by gi'. Since in the current decomposition, the decision variables related to the injury index are part of the dummy responses evaluated as constraints in the lower level, the normalized dummy responses in the upper level are denoted by G'i instead. Each elemental subproblem has been defined as 'Pij' were 'ij' follows the element notation used for decomposed problems.

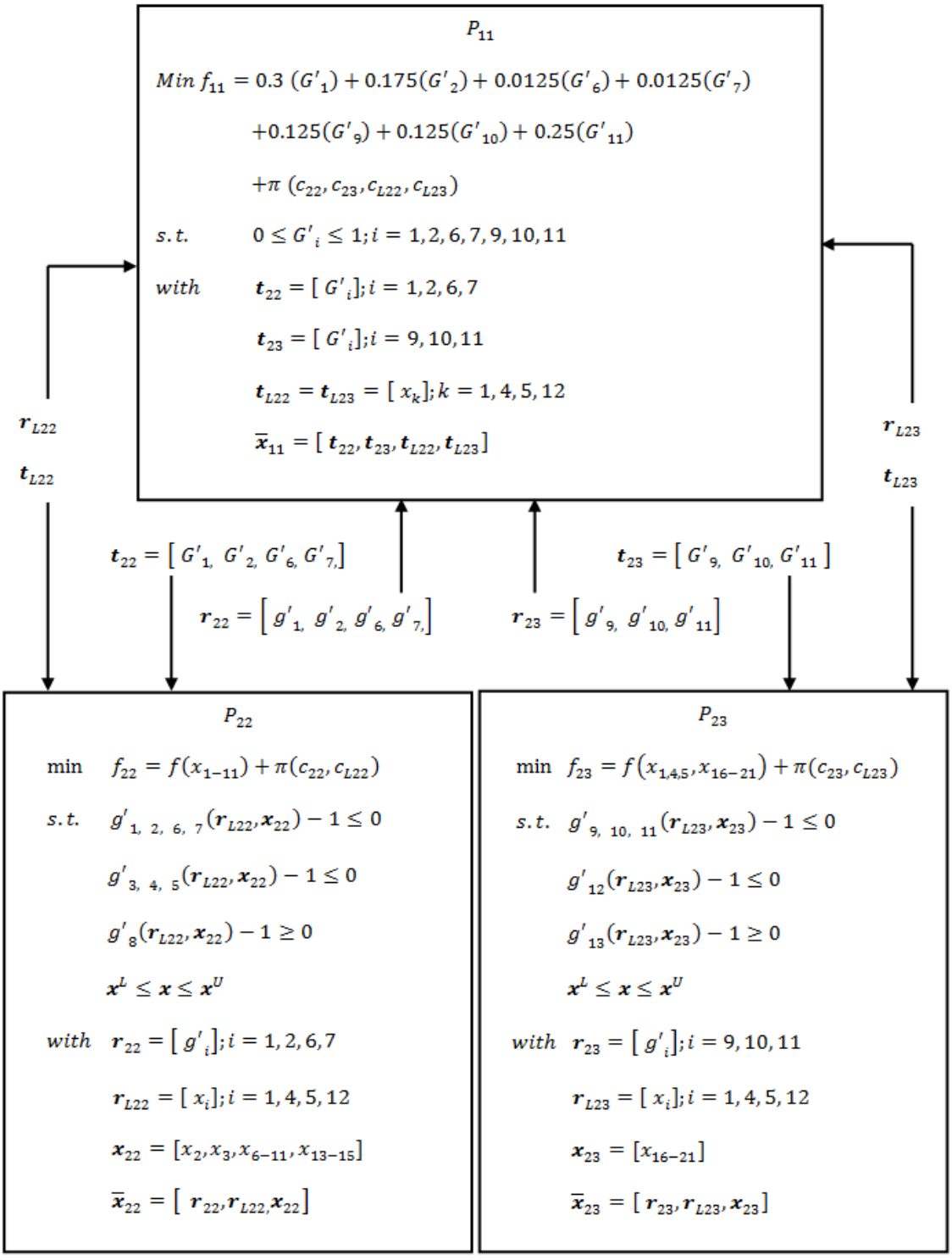

Figure 3.12 Decomposed crash-based design problem.

In the decomposition shown in Figure 3.12, the occupant responses G'_1, G'_2, G'_6, G'_7 of FFI and G'_9, G'_{10}, G'_{11} of SI along with design variables x1, x4, x5, and x12 are treated as the decision variables of element 11 and denoted by vector $\overline{\boldsymbol{x}}_{11}$. In element 11, t22 and t23 are vectors of target variables cascaded down to elements 22 and 23, respectively. The objective function of element 11 is optimized initially and the corresponding optimum values of variables are sent to the lower level as targets. G'_1, G'_2, G'_6, G'_7 are sent to element 22 and G'_9, G'_{10}, G'_{11} are sent to element 23.

tL22 and tL23 are target vectors consisting of linking variables (x1, x4, x5, and x12) shared by elements 22 and 23. In elements 22 and 23, the functions f(x1-11) and f(x1,4,5,16-21) involve mass calculation, hence, they are dependent on part thicknesses. The vectors r22 and r23 are element specific response values of the target variables, whereas rL22 and rL23 are response values of the linking variables. $\overline{\boldsymbol{x}}_{22}$ and $\overline{\boldsymbol{x}}_{23}$ are local decision variables vectors of element 22 and 23, respectively. The local decision variable vector consists of all the variables that are used in evaluation of element specific objectives and constraints. x22 and x23 are vectors of local design variables which are specific to elements 22 and 23, respectively. The relaxation function π in each element consists of consistency constraints denoted by vector c, representing the differences between targets and responses as well as the linking variables; therefore, the solution converging to an optimum design would satisfy all the element specific objectives and design constraints.

The AIO problem formulation of the decomposition shown in Figure 3.12 is given as

$$
\begin{aligned}
min\, f = \;& 0.3\,(G'_1) + 0.175(G'_2) + 0.0125(G'_6) + 0.0125(G'_7) \\
& +0.125(G'_9) + 0.125(G'_{10}) + 0.25(G'_{11}) \\
& +f\,(x_{1s2}, x_{4s2}, x_{5s2}, x_{12s2}, x_{6-11}) + f(x_{1s3}, x_{4s3}, x_{5s3}, x_{16-21}) \\
& +\pi\{(G'_1 - g'_1), (G'_2 - g'_2), (G'_6 - g'_6), (G'_7 - g'_7), (G'_9 - g'_9), (G'_{10} - g'_{10}), \\
& (G'_{11} - g'_{11}), (x_{1e1} - x_{1e2}), (x_{1e1} - x_{1e3}), (x_{4e1} - x_{4e2}), (x_{4e1} - x_{4e3}), \\
& (x_{5e1} - x_{5e2}), (x_{5e1} - x_{5e3}), (x_{12e1} - x_{12e2}), (x_{12e1} - x_{12e3})
\end{aligned}
$$

$$
\begin{aligned}
s.t. \quad & g'_{1,2,6,7}(x_{1e2}, x_2, x_3, x_{4e2-5e2}, x_{6-11}, x_{12e2}, x_{13-15}) - 1 \le 0 \\
& g'_{3,4,5}(x_{1e2}, x_2, x_3, x_{4e2-5e2}, x_{6-11}, x_{12e2}, x_{13-15}) - 1 \le 0 \\
& g'_8(x_{1e2}, x_2, x_3, x_{4e2-5e2}, x_{6-11}, x_{12e2}, x_{13-15}) - 1 \ge 0 \\
& g'_{9,10,11}(x_{1e3}, x_{4e3-5e3}, x_{12e3}, x_{16-15}) - 1 \le 0 \\
& g'_{12}(x_{1e3}, x_{4e3-5e3}, x_{12e3}, x_{16-15}) - 1 \le 0 \\
& g'_{13}(x_{1e3}, x_{4e3-5e3}, x_{12e3}, x_{16-15}) - 1 \ge 0
\end{aligned}
$$

$$
\text{with} \qquad x^L \le x \le x^U \tag{3.15}
$$

3.3.2 Crash+Vibration-Based Design

For a more realistic design, vibration requirements are also included in the design problem by considering frequency responses of the vibration model as design constraints. The general optimization framework is shown in Figure 3.13. In Figure 3.13, design constraints $g_{14\text{-}16}(x)$ are frequencies of the first three flexible modes obtained from vibration analysis of the model shown in Figure 2.17 in Chapter 2. The part wall thicknesses selected in FFI and SI analyses are considered as design variables except the front bumper, along with upper and lower suspension frames are not included in the vibration model.

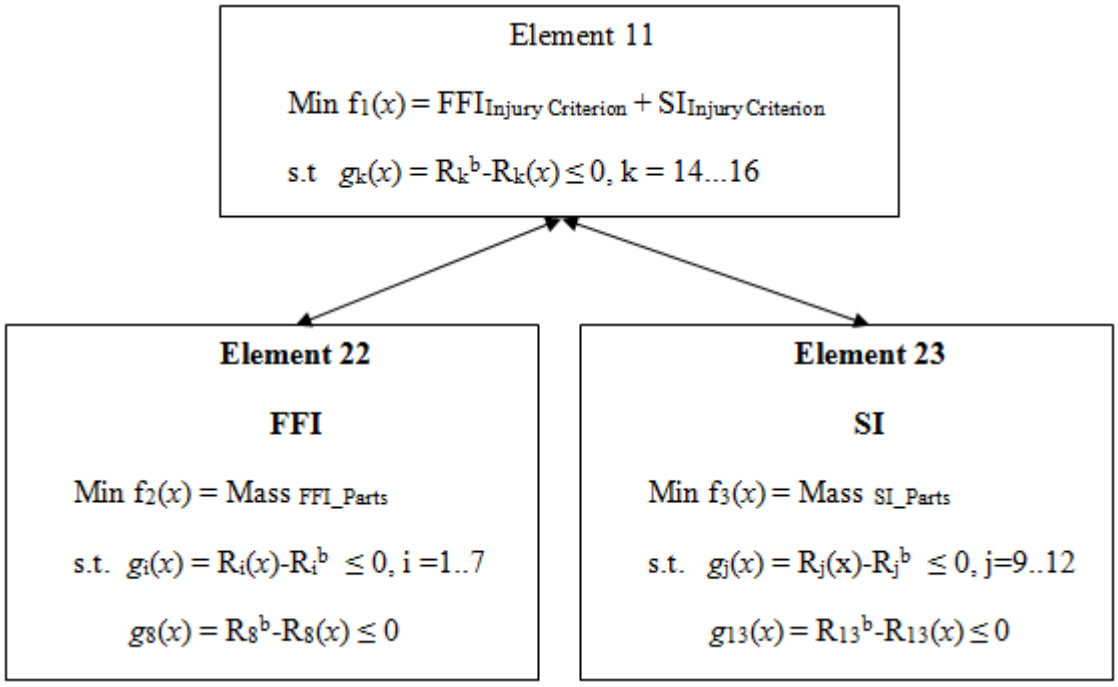

Figure 3.13 Design problem with crash and vibration design criteria.

These vibration constraints are added in the first level of the multilevel decomposition such that vehicle model is first designed for vibration characteristics and then the resulting design is cascaded down as target to fulfill the FFI and SI crash analyses requirements.

Similar to the crash-based design problem, responses associated with FFI and SI are considered as constraints in elements 22 and 23, injury criterion defined by Equation 3.14 is selected as objective function of element 11, whereas the mass of parts specific to FFI analysis and SI analysis are selected as objective functions of elements 22 and 23, respectively. Table 3.9 shows all the responses considered in this design problem together with the corresponding baseline values. All crash responses except internal energy absorption are required to be less than their respective baseline values.

Table 3.9 Design constraints of crash-vibration-based design case.

Constraint	Response	Baseline Value
g_1	HIC	711.10
g_2	C_{3ms} (g's)	53.01
g_3	HA (g's)	64.52
g_4	CA (g's)	53.78
g_5	CD (mm)	21.68
g_6	L_F (N)	4692.4
g_7	R_F (N)	4317.0
g_8	FFI-IE (kJ)	61.70
g_9	U_R (g's)	69.74
g_{10}	L_R (g's)	58.82
g_{11}	Spine (g's)	64.89
g_{12}	Pelvis (g's)	51.58
g_{13}	SI-IE (kJ)	19.20
g_{14}	Freq1 (Hz)	35.39
g_{15}	Freq2 (Hz)	36.23
g_{16}	Freq3 (Hz)	38.37

The constraints associated with the vibration characteristics (i.e., $g_{14\text{-}16}$ (x)) are required to be no less than their baseline values, as greater frequency indicates increased structural rigidity of the vehicle. A more detailed decomposition based on ATC is shown in Figure 3.14. It should be noted that the design constraints and design variables in all elements are normalized similar to the crash-based design problem.

As noted in Figure 3.14, since the vibration responses in element 11 depend on variables $G'_1, G'_2, G'_6, G'_7, G'_9, G'_{10}, G'_{11}$, and $x_{1,3\text{-}9,16\text{-}21}$, these design variables are optimized in this element, and then cascaded down to elements 22 and 23 as targets. This is evident from target and response vectors $\boldsymbol{t}_{22}$, $\boldsymbol{t}_{23}$, $\boldsymbol{r}_{22}$, and $\boldsymbol{r}_{23}$.

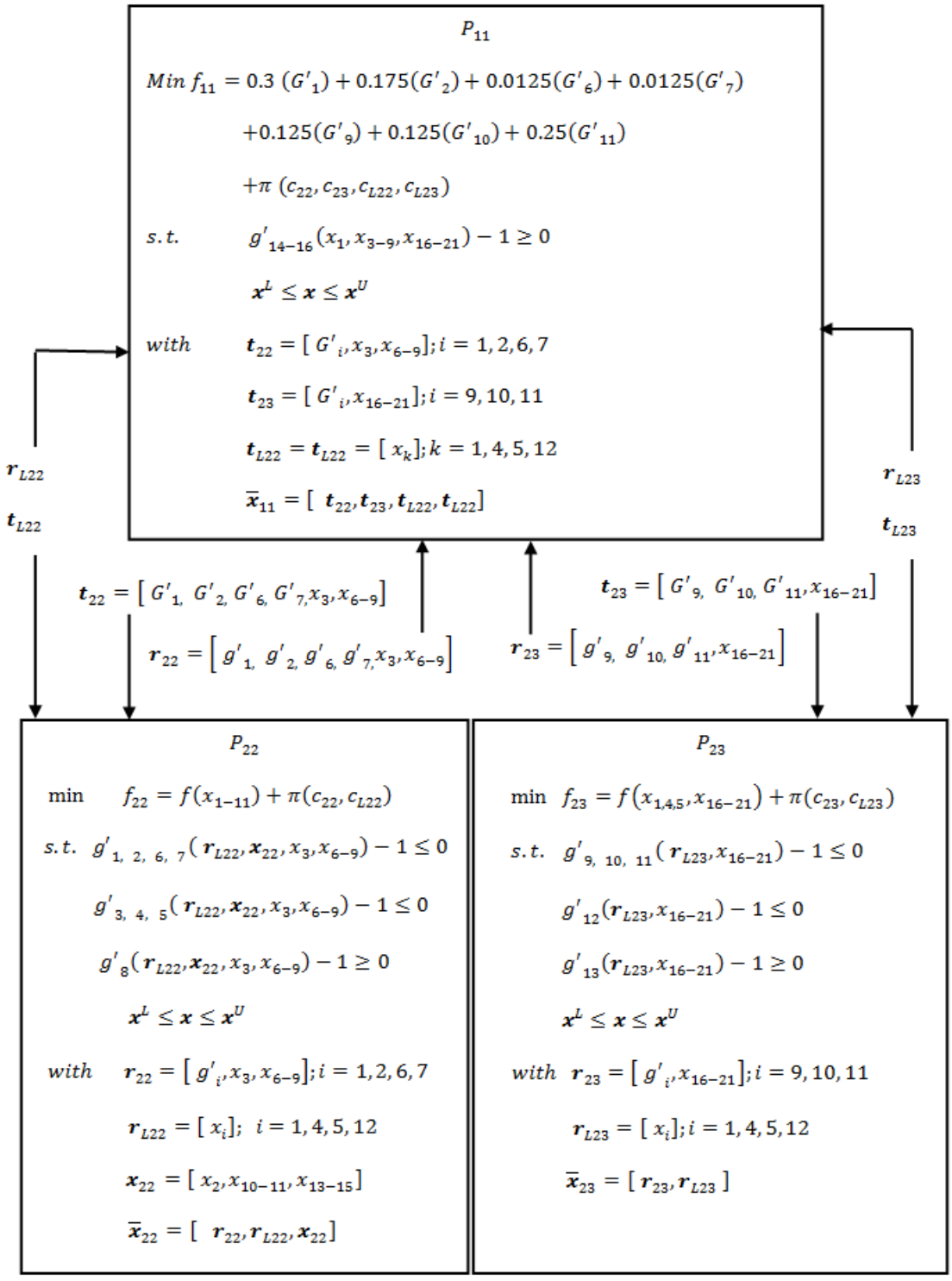

Figure 3.14 Decomposition of crash+vibration-based design case.

In the crash-based design problem, a total of seven targets (four to element 22 and three to element 23) were cascaded down, but in this case, a total of 18 targets (nine to each element of the lower level) are cascaded down. Element 22 and 23 design constraints are occupant responses in FFI and SI analyses, similar to the cash-based design case. The design variables $x_{1,4,5,12}$ are linking variables shared between elements 22 and 23. The design variables $x_{13\text{-}15}$ pertaining to airbag and x_2, x_{10}, x_{11} associated with the front bumper and suspension frames are local design variables of element 22 given as local design vector $\boldsymbol{x}$. Element 23 does not have any local variables as all the design variables of SI are either part of the target vector or linking variables.

The AAO formulation for the decomposed problem shown in Figure 3.14 is given as

$$
\begin{aligned}
min\ f = \ & 0.3\ (G'_1) + 0.175(G'_2) + 0.0125(G'_6) + 0.0125(G'_7) \\
& +0.125(G'_9) + 0.125(G'_{10}) + 0.25(G'_{11}) \\
& +f\ (x_{1s2}, x_{4s2}, x_{5s2}, x_{12s2}, x_{6s2-11s2}) + f(x_{1s3}, x_{4s3}, x_{5s3}, x_{16s3-21s3}) \\
& +\pi\{(G'_1 - g'_1), (G'_2 - g'_2), (G'_6 - g'_6), (G'_7 - g'_7), (G'_9 - g'_9), (G'_{10} - g'_{10}), \\
& (G'_{11} - g'_{11}), (x_{1e1} - x_{1e2}), (x_{1e1} - x_{1e3}), (x_{3e1} - x_{3e2}), (x_{4e1} - x_{4e2}), \\
& (x_{4e1} - x_{4e3}), (x_{5e1} - x_{5e2}), (x_{5e1} - x_{5e3}), (x_{6e1} - x_{6e2}), (x_{7e1} - x_{7e2}), \\
& (x_{8e1} - x_{8e2}), (x_{9e1} - x_{9e2}), (x_{12e1} - x_{12e2}), (x_{12e1} - x_{12e3}), (x_{16e1} - x_{16e3}) \\
& (x_{17e1} - x_{17e3}), (x_{18e1} - x_{18e3}), (x_{19e1} - x_{19e3}), (x_{20e1} - x_{20e3}), \\
& (x_{21e1} - x_{21e3})\} \\
s.t. \quad & g'_{1,2,6,7}(x_{1e2}, x_2, x_{3e2-9e2}, x_{10}, x_{11}, x_{12e2}, x_{13-15}) - 1 \leq 0 \\
& g'_{3,4,5}(x_{1e2}, x_2, x_{3e2-9e2}, x_{10}, x_{11}, x_{12e2}, x_{13-15}) - 1 \leq 0 \\
& g'_8(x_{1e2}, x_2, x_{3e2-9e2}, x_{10}, x_{11}, x_{12e2}, x_{13-15}) - 1 \geq 0
\end{aligned}
$$

$$g'_{9,10,11}(x_{1e3}, x_{4e3-5e3}, x_{12e3}, x_{16e3-15e3}) - 1 \leq 0$$

$$g'_{12}(x_{1e3}, x_{4e3-5e3}, x_{12e3}, x_{16e3-15e3}) - 1 \leq 0$$

$$g'_{13}(x_{1e3}, x_{4e3-5e3}, x_{12e3}, x_{16e3-15e3}) - 1 \geq 0$$

$$g'_{14-16}(x_{1e1}, x_{3e1-9e1}, x_{16e1-21e1}) - 1 \geq 0$$

$$\text{with} \quad \mathbf{x}^{\mathrm{L}} \leq \mathbf{x} \leq \mathbf{x}^{\mathrm{U}} \tag{3.16}$$

The solution process involving ATC for two different design problems i.e. crash-based and crash+vibration-based discussed in this chapter is shown in subsequent chapters of this thesis.

3.4 References Cited

[1] Michelena, N., H. Park, & P. Y. Papalambros. "Convergence properties of analytical target cascading." AIAA journal 41, no. 5 (2003): 897-905.

[2] Kim, H.M. “Target Cascading in Optimal System Design.” PhD Dissertation, Mechanical Engineering, University of Michigan, 2001.

[3] Tosserams, S., L. F. P. Etman, P. Y. Papalambros, & J. E. Rooda. “An augmented Lagrangian relaxation for analytical target cascading using the alternating direction method of multipliers.” Structural and Multidisciplinary Optimization, 31, 3, 2006, pp: 176-189.

[4] DorMohammadi, S., and M. Rais-Rohani. "Exponential penalty function formulation for multilevel optimization using the analytical target cascading framework." Structural and Multidisciplinary Optimization, 2013, pp: 1-14.

[5] Kort, B. W., & D. P. Bertsekas. “A new penalty function method for constrained minimization.” In Decision and Control, 1972 and 11th Symposium on Adaptive Processes. Proceedings of the 1972 IEEE Conference, IEEE, Vol. 11, pp. 162-166.

[6] DorMohammadi, S., & M. Rais-Rohani. “Analytical Target Cascading Framework using the Exponential Method of Multipliers”, AIAA, 2012.

[7] New Car Assessment Program, ‘Frontal Barrier Impact Test’: 1996 Dodge Neon, prepared by Transportation Research Center Inc, U.S Department of Transportation, Washington, DC, 1995.

[8] Viano, D. C., S. Arepally. "Assessing the safety performance of occupant restraint systems, SAE Technical Paper, 1990.

[9] Evaluation of FMVSS 214 Side Impact Protection Dynamic Performance Requirement, National Highway Traffic Safety Administration, US Department of Transportation.

CHAPTER IV

RESPONSE SURFACE APPROXIMATION

A single nonlinear transient dynamic FEA for FFI or SI simulation of the full vehicle model, with interiors and occupant as described in Chapter 2, would take 3-6 hours of CPU time using IBM cluster with four 6-core Intel X5660 processors and 48 GB of RAM. In the numerical solution of an optimization problem, the objective functions and constraints are evaluated at different design points governed by the bounds of design variables and the optimization technique used. Direct integration of crash simulations with numerical optimization is often impractical as the cost associated with running crash simulations at each design point is very high. To reduce the high computation costs of vehicle optimization problems, the desired objective and constraint functions are approximated using analytical functions called metamodel or surrogate model. These surrogate models would then be used in lieu of FEA in evaluating the candidate designs during the optimization process.

The surrogate models are built using simulation or experimental results at a specific number of design (training) points identified using a Design of Experiments (DOE) technique. The resulting DOE table consists of the design variable values and the corresponding response values at different design points. These design points are distributed over the design space defined by bounds of design variables using a sampling technique. Depending on the response of interest and its variation over the feasible design

space, a uniform or non-uniform sampling technique may be used. Taguchi orthogonal array and Latin Hypercube Sampling (LHS) are two of the commonly used sampling techniques in automotive design [1-7].

Once the training points are generated and the DOE table is built, the next step is to pick the appropriate form of the surrogate model. The selection of the surrogate model depends on the nonlinearity of the response and the number of sample points in the DOE table. There are different types of surrogate models based on the function form; for example, Polynomial Response Surface (PRS), Radial Basis Function (RBF), Gaussian Process (GP), Kriging (KR), and Optimized Ensemble of metamodels (ENS) have been used for surrogate modeling in the literature [1-7, 8, 9]. Each metamodel can be tuned to enhance its prediction accuracy by adjusting the tuning parameters, model fidelity (e.g., increasing the degree of polynomial in PRS) and/or the number of training points.

4.1 Radial Basis Function

Fang et al. [8] and others [6, 10] have shown that RBF is accurate in approximating a nonlinear crash response such as acceleration. In this study, RBF surrogate models are used to predict all crash and vibration responses.

RBF uses the Euclidian distance of a design point from all the sampling points to formulate a relation between design variables and responses in the DOE table. The RBF surrogate model is expressed as [8, 9]

$$f'(x) = \sum_{i=1}^{N} \lambda_k \ \phi \ (\| x - x_k \|) \tag{4.1}$$

where $f'(x)$ is the predicted response, N represents the number of training points, λ_k represents the coefficient associated with k^{th} term of RBF, ϕ is the type of RBF used and

$\| x - x_k \|$ represents the Euclidean distance between design point x and k^{th} training point x_k. The summation in equation (4.1) denotes that the cost associated with RBF depends on the number of training points used.

In RBF, all the design points should be normalized to the range of 0 to 1. This can be done by dividing each design variable by the corresponding maximum value in the DOE table.

There are different types of RBFs; some of the commonly used functions are as follows:

1) Thin-Plate spline: $\phi\,(r) = r^2 \ln(cr)$
2) Gaussian: $\phi\,(r) = \exp(-c\,r^2)$
3) Multiquadric: $\phi\,(r) = \sqrt{r^2 + c^2}$
4) Inverse Multiquadric: $\phi\,(r) = 1/\sqrt{r^2 + c^2}$

where *'c'* is the tuning parameter with a range of $0 \leq c \leq 1$. The choice of basis function and tuning parameter are very important in formulating an accurate RBF model as the response of interest can be very sensitive to these choices, and the best combination of ϕ and c would maximize the accuracy of the resulting response metamodel.

The coefficients (λ_i, $i = 1, N$) in equation (4.1) are obtained by minimizing the sum of squares of the deviations given as

$$R = \sum_{j=1}^{N} \left[f(x_j) - \sum_{i=1}^{N} \lambda_i \phi(\| x_j - x_i \|) \right]^2 \tag{4.2}$$

or in matrix form expressed as

$$[A]\ \{\lambda\} = [F] \tag{4.3}$$

where $[A] = \phi(\| x_j - x_i \|)$, and λ_i is determined by solving equation (4.3).

In RBF, the approximate function passes through all the training points used to formulate the surrogate model. Hence, any error statistic used to assess the accuracy of an RBF surrogate model must consider this characteristic.

4.2 Surrogate Models of Design Responses

Since crash responses are highly nonlinear, their respective surrogate models are based on a total of 100 training points defined using LHS technique, whereas the vibration response surrogate models are based on 40 LHS-based training points.

Once the surrogate models are built, the accuracy of each model is tested using ten randomly selected design points together with the baseline design. These 11 design points are referred to as the test points. The error in each surrogate model is determined by calculating the percentage difference in surrogate prediction compared to the true response obtained from FE simulations. In RBF, since the approximate function passes through each training point, the error at each test point depends on its location relative to the neighboring training point. The test points that are far away from any of the training points will have more error than points that are nearby. Therefore, the average error of all the test points is used as an overall error metric in fitting each surrogate model.

The value of the tuning parameter *c* is varied from 0 to 1 with a step size of 0.01, and the RBF metamodels are tuned by calculating average error for different combinations of basis functions and the tuning parameter. The best combination with least average error is used as the final response metamodel in the subsequent design optimization analysis. The expression for average error is given as

$$Average\ Percent\ Error = \sum_{i=1}^{N} \left| 100\ \frac{y_{i,true} - y_{i,RBF}}{y_{i,true}} \right| / N \qquad (4.4)$$

where $y_{i,true}$ is the actual response value obtained from the FE simulation at the i^{th} test point and $y_{i,RBF}$ is the approximate response value predicted by the RBF metamodel at the same point. N is the number of test points used.

Table 4.1 shows the type of RBF, tuning parameter value and the average percent error for each response surrogate model considered in this study. The surrogate model of right femur has the maximum average error of 16.7% whereas the third natural frequency response (i.e., frequency of torsion-bending mode) has the least error at 1.01%.

Table 4.1 Type of RBF, tuning parameter value and average percent error for each response surrogate model.

Response	Type of RBF (ϕ)[a]	Tuning Parameter (c)	Average Percent Error
HIC	3	0.70	8.82
C_{3ms} (g's)	3	1.00	7.04
HA (g's)	3	0.35	7.87
CA (g's)	1	0.64	7.06
CD (mm)	3	1.00	13.0
L_F (N)	4	0.29	15.1
R_F (N)	4	0.22	16.7
FFI-IE (kJ)	3	0.01	5.57
U_R (g's)	3	0.41	4.03
L_R (g's)	1	0.48	3.92
Spine (g's)	3	0.54	2.93
Pelvis (g's)	3	0.17	4.03
SI-IE (kJ)	3	1.00	0.90
Freq1 (Hz)	2	0.10	1.67
Freq2 (Hz)	2	0.01	1.06
Freq3 (Hz)	2	0.01	1.01

[a]Thin-plate spline (1), Gaussian (2), Multiquadric (3), and Inverse multiquadric (4)

The average error among all the surrogate models is 6.3%. It is evident from Table 4.1 that the surrogate models of crash responses have more error than the frequency responses, even though the number of training points used for the crash responses is 150% greater (i.e., 100 compared to 40). This difference can be due to the high nonlinearity observed in the crash responses and that each crash response represents a locally defined metric, whereas vibration frequency is a more global measure. The accuracy of crash surrogate models can be improved further by increasing the number of training points, but to limit the computation effort, the number of training points is limited to 100.

Table 4.2 shows the surrogate model percent error at the baseline design point. The average error in the baseline responses is 5% as compared to the average error of 6.3% over the entire 11 test points. It can also be noted that the surrogate error for most of the baseline responses is less than 6.3%, indicating that the baseline design point is closer to one of the training points and that a few test points are farther away, hence, increasing the overall average error.

Table 4.2 Surrogate model prediction error at the baseline design point.

Response	Exact Value	RBF Prediction	Error (%)
HIC	711.10	718.99	1.1
C_{3ms} (g's)	53.01	51.43	3.0
HA (g's)	64.52	63.72	1.3
CA (g's)	53.78	49.22	8.5
CD (mm)	21.68	19.28	11.1
L_F (N)	4692.4	5549.3	18.3
R_F (N)	4317.0	4546.1	5.3
FFI-IE (kJ)	61.70	57.48	6.8
U_R (g's)	69.74	67.46	3.3
L_R (g's)	58.82	52.13	11.4
Spine (g's)	64.89	64.71	0.3
Pelvis (g's)	51.58	48.85	5.3
SI-IE (kJ)	19.20	19.29	0.5
Freq1 (Hz)	35.39	36.21	2.3
Freq2 (Hz)	36.23	35.92	0.9
Freq3 (Hz)	38.37	38.15	0.6

4.3 References Cited

[1] Rais-Rohani, M., K. N. Solanki, E. Acar, & C. D. Eamon. "Shape and sizing optimisation of automotive structures with deterministic and probabilistic design constraints." International Journal of Vehicle Design, *54*, 4, 2010, pp: 309-338.

[2] Fang, H., K. Solanki, & M. F. Horstemeyer. "Energy-based crashworthiness optimization for multiple vehicle impacts." ASME Conference Proceedings, 2004.

[3] Fang, H., K. N. Solanki, M. F. Horstemeyer, & M. Rais-Rohani. "Multi-impact crashworthiness optimization with full-scale finite element simulations." In Computational Mechanics, the 6th World Congress on Computational Mechanics in Conjunction APCOM, Vol. 4, 2004, pp. 5-10.

[4] Fang, H., K. Solanki, & M. F. Horstemeyer. "Numerical simulations of multiple vehicle crashes and multidisciplinary crashworthiness optimization." International Journal of Crashworthiness, 10, 2, 2005, pp: 161-172.

[5] Horstemeyer, M. F., X. C. Ren, H. Fang, E. Acar, & P. T. Wang. "A comparative study of design optimisation methodologies for side-impact crashworthiness, using injury-based versus energy-based criterion."International Journal of Crashworthiness, 14, 2, 2009, pp: 125-138.

[6] Parrish, A., M. Rais-Rohani, & A. Najafi. "Crashworthiness optimisation of vehicle structures with magnesium alloy parts." International Journal of Crashworthiness, 17, 3, 2012, pp: 259-281.

[7] Liao, X., Q. Li, X. Yang, W. Li, & W. Zhang. "A two-stage multi-objective optimisation of vehicle crashworthiness under frontal impact." International Journal of Crashworthiness, 13, 3, 2008, pp: 279-288.

[8] Fang, H., M. Rais-Rohani, Z. Liu, & M. F. Horstemeyer. "A comparative study of metamodeling methods for multiobjective crashworthiness optimization." Computers & structures, 83, 25, 2012, pp: 2121-2136.

[9] Acar, E., & M. Rais-Rohani. "Ensemble of metamodels with optimized weight factors." Structural and Multidisciplinary Optimization, 37, 3, 2009, pp: 279-294.

[10] Kiani, M., I. Gandikota, A. Parrish, K. Motoyama, & M. Rais-Rohani. "Surrogate-based optimisation of automotive structure under multiple crash and vibration design criteria," International Journal of Crashworthiness, 2013. (In Press)

CHAPTER V

DESIGN OPTIMIZATION RESULTS AND DISCUSSION

The decomposed multilevel optimization framework and the two vehicle design problems presented in Chapter 4 are setup in VisualDOC [1] optimization tool with data transfer and exchange of values between different element optimization problems coordinated using the data-linking interface of VisualDOC. An equation component can be added into the VisualDOC optimizer to read constraints and objective functions, but due to the limit on the number of characters allowed in each equation, a built-in MATLAB [2] component was used to solve the large response equations obtained from surrogate modeling. Therefore, the constraint and objective functions are calculated in MATLAB component and the corresponding results are fed to the optimization component.

Sequential Quadratic Programming (SQP) [3] is used to solve each constrained optimization problem. As a gradient-based optimizer, SQP consists of a direction-finding step and a one-dimensional search step. The first step focuses on finding the best search direction at a selected design point, whereas the second part determines the optimum step size along the calculated search direction. This two-step process is repeated until a local optimum point is found.

For the search direction calculation, the original nonlinear optimization problem is transformed into a quadratic-programming subproblem with the objective function

approximated by a quadratic function and the constraints approximated by linearized functions. The resulting convex-programming problem formulation for finding the components of the search direction vector $\boldsymbol{d}$ is expressed as

$$\min \quad Q(\boldsymbol{d}, \boldsymbol{X}) = \nabla f(\boldsymbol{X}^k)^T \boldsymbol{d}^k + 0.5 \boldsymbol{d}^{k^T} B^k \boldsymbol{d}^k$$

$$\text{s.t.} \quad \beta_j g_j(\boldsymbol{X}^k) + \nabla g_j(\boldsymbol{X}^k)^T \boldsymbol{d}^k \leq 0; \qquad j = 1 \ldots N_g \tag{5.1}$$

$$\bar{\beta} h_j(\boldsymbol{X}^k) + \nabla h_j(\boldsymbol{X}^k)^T \boldsymbol{d}^k = 0; \qquad j = N_g + 1 \ldots N_g + N_h$$

where $\boldsymbol{X}^k$ represents the coordinates of the design point at k^{th} iteration step, f is the original objective function with g_j inequality constraints, h_j equality constraints, N_g and N_h are number of inequality and equality constraints, B as a positive definite approximation of the Hessian matrix of the Lagrange function, $0 \leq \beta_j \leq 1$ and $\bar{\beta} = 0.9$. The gradient vectors are denoted by the symbol $\nabla( )$, with ( ) representing the function being differentiated. Equation (5.1) may be solved by considering only the active and violated design constraints using the Lagrange multiplier method, with the Lagrange function expressed as

$$\bar{L}(\boldsymbol{d}, \lambda) = Q + \sum_{j=1}^{N_g} \lambda_j \left(\beta_j g_j + \nabla g_j^T \boldsymbol{d} + s_j^2\right) + \sum_{m=1}^{N_h} \lambda_{N_{g+m}} (\bar{\beta} h_m + \nabla h_m^T \boldsymbol{d}) \tag{5.2}$$

The step size, α is calculated by minimizing the penalty function given as

$$\phi\left(X^{(k+1)}\right) = \phi(\alpha_k) = f(\alpha_k) + \sum_{j=1}^{N_g} \mu_j^{(k)} \{max[0, g_j(\alpha_k)]\} + \sum_{m=1}^{N_h} \mu_{N_{g+m}}^{(k)} |h_m(\alpha_k)| \tag{5.3}$$

Once α is found, the design point $\boldsymbol{X}^{(k)}$ is updated as

$$X^{(k+1)} = X^{(k)} + \alpha_k d^{(k} \tag{5.4}$$

If the original nonlinear optimization problem is non-convex, the solution obtained from SQP depends on the choice of initial design point. Thus, it is common to use multiple randomly selected initial design points to increase the chances of finding a superior local optimum or possibly the global optimum design point.

5.1 Crash-Based Design Problem

The decomposition shown in chapter 3 consisted of an optimization problem at each element of the decomposition. Since the design case had three elements, three optimization problems are defined individually at each element with local objectives, design variables and constraints. The exchange of information between all the elements such as targets and responses between elements are coordinated using ATC approach by denoting the variables shared in different elements by an element number 'e_i'. The element specific sub problems are given below by equation 5.6.

$\mathbf{P}_{11}$

$$Min \quad f_{11} = 0.3\,(G'_1) + 0.175(G'_2) + 0.0125(G'_6) + 0.0125(G'_7)$$
$$+0.125(G'_9) + 0.125(G'_{10}) + 0.25(G'_{11})$$
$$+\pi\,\{(\boldsymbol{t}_{22} - \boldsymbol{r}_{22}), (\boldsymbol{t}_{L22} - \boldsymbol{r}_{L22}), (\boldsymbol{t}_{23} - \boldsymbol{r}_{23}), (\boldsymbol{t}_{L23} - \boldsymbol{r}_{L23})\}$$
$$s.t. \quad 0 \le G'_i \le 1; i = 1, 2, 6, 7, 9, 10, 11$$
$$\boldsymbol{x}^L \le \boldsymbol{x} \le \boldsymbol{x}^U \quad \text{where } \boldsymbol{x} = [x_{1,4,5,12}]$$
$$with \quad \boldsymbol{t}_{22} = [\,G'_1, G'_2, G'_6, G'_7]$$
$$\boldsymbol{t}_{23} = [\,G'_9, G'_{10}, G'_{11}]$$
$$\boldsymbol{t}_{L22} = \boldsymbol{t}_{L23} = [x_{1e1}, x_{4e1}, x_{5e1}, x_{12e1}]$$
$$\overline{\boldsymbol{x}}_{11} = \left[\boldsymbol{t}_{22},\ \boldsymbol{t}_{23}, \boldsymbol{t}_{L22,}\boldsymbol{t}_{L23,}\right]$$

$\mathbf{P}_{22}$

$$\min \quad f_{22} = f(x_{1e2}, x_{2-3}, x_{4e2-5e2}, x_{6-11}) + \pi\{(\boldsymbol{t}_{22} - \boldsymbol{r}_{22}), (\boldsymbol{t}_{L22} - \boldsymbol{r}_{L22})\}$$

$$s.t. \quad g'_{1,2,6,7}(\boldsymbol{r}_{L22}, \boldsymbol{x_{22}}) - 1 \leq 0$$

$$g'_{3,4,57}(\boldsymbol{r}_{L22}, \boldsymbol{x_{22}}) - 1 \leq 0$$

$$g'_{8}(\boldsymbol{r}_{L22}, \boldsymbol{x_{22}}) - 1 \geq 0$$

$$\boldsymbol{x}^L \leq \boldsymbol{x} \leq \boldsymbol{x}^U \text{ where } \boldsymbol{x} = [x_{1-15}]$$

$$with \quad \boldsymbol{r}_{22} = [g'_1, g'_2, g'_6, g'_7]$$

$$\boldsymbol{r}_{L22} = [x_{1e2,}x_{4e2,}x_{5e2,}x_{12e2}]$$

$$\boldsymbol{x_{22}} = [x_{2-3}, x_{6-11}, x_{13-15}]$$

$$\overline{\boldsymbol{x}}_{\boldsymbol{22}} = [\boldsymbol{r}_{22}, \boldsymbol{r}_{L22}, \boldsymbol{x_{22}}]$$

$\mathbf{P}_{23}$

$$\min \quad f_{23} = f(x_{1e3},\ x_{4e3}, x_{5e3}, x_{16-21}) + \pi\{(\boldsymbol{t}_{23} - \boldsymbol{r}_{23}), (\boldsymbol{t}_{L23} - \boldsymbol{r}_{L23})\}$$

$$s.t. \quad g'_{9,10,11}(\boldsymbol{r}_{L23}, \boldsymbol{x_{23}}) - 1 \leq 0$$

$$g'_{12}(\boldsymbol{r}_{L23}, \boldsymbol{x_{23}}) - 1 \leq 0$$

$$g'_{13}(\boldsymbol{r}_{L23}, \boldsymbol{x_{23}}) - 1 \geq 0$$

$$\boldsymbol{x}^L \leq \boldsymbol{x} \leq \boldsymbol{x}^U \quad \text{where} \quad \boldsymbol{x} = [x_{1,4,5,12}, x_{16-21}]$$

$$with \quad \boldsymbol{r}_{23} = [g'_9, g'_{10}, g'_{11}, x_{16e3-21e3}]$$

$$\boldsymbol{r}_{L23} = [x_{1e3,}x_{4e3,}x_{5e3,}x_{12e3}]$$

$$\boldsymbol{x_{23}} = [x_{16-21}]$$

$$\overline{\boldsymbol{x}}_{\boldsymbol{23}} = [\boldsymbol{r}_{23}, \boldsymbol{r}_{L23}, \boldsymbol{x_{23}}] \tag{5.6}$$

By using the above notation for design variables specific to each element, local variables and variables that are part of target and response vectors can be identified easily. Each element of the above decomposition was solved using SQP optimization

method. Table 5.1 shows the optimum values of all the design variables obtained after solving the decomposition problem.

Table 5.1 Optimum design point of crash-based design case.

Design Variables[a]	Name	Lower Bound	Baseline	Optimum	Upper Bound
x_1	A-Pillar	0.805	1.611	1.474	2.416
x_2	Front bump	0.978	1.956	1.686	2.934
x_3	Firewall	0.367	0.735	0.375	1.102
x_4	Front floor panel	0.352	0.705	0.698	1.057
x_5	Outer Cabin	0.414	0.829	0.821	1.243
x_6	Shotgun	0.762	1.524	1.909	2.286
x_7	Inner side rail	0.947	1.895	1.359	2.842
x_8	Outer Side rail	0.761	1.522	1.731	2.283
x_9	Side rail ext.	0.947	1.895	1.053	2.842
x_{10}	Lower Susp. frame	0.793	1.587	0.867	2.380
x_{11}	Upper Susp. frame	1.303	2.606	1.390	3.909
x_{12}	Belt limit force (N)	1000	2500	2700	5000
x_{13}	Mass flow rate (scale factor)	0.8	1.0	0.801	1.4
x_{14}	Vent orifice area (scale factor)	0.6	1.0	1.120	1.4
x_{15}	Airbag input temp. (K)	600	781	750	1000
x_{16}	Mid B-pillar	0.353	0.706	1.059	1.059
x_{17}	Rear cabin floor	0.353	0.706	0.438	1.059
x_{18}	Cabin seat rein.	0.341	0.682	0.414	1.023
x_{19}	Cabin mid rail	0.525	1.050	0.631	1.575
x_{20}	Rear plate	0.355	0.710	0.801	1.065
x_{21}	Roof	0.351	0.702	0.641	1.053

[a]Part thicknesses are in mm.

Since SQP is a local optimizer, the initial guess provided to all the target and design variables are crucial as the computation time in obtaining a converged solution depends on the initial guess. The Crash-based decomposition problem was solved using multiple starting points. A total of 12 random starting points were used and the best results obtained are shown in Table 5.1. The optimization process took a total of 37 loops for the EPF II ATC formulation to converge, i.e., the multipliers were updated 37 times.

The optimization process took 2.07 minutes to complete using a Dell Optiplex 960 computer with Intel core 2 duo processor having 4GB of RAM.

The optimum design shown in Table 5.1 is used to perform LS-DYNA crash simulation to determine responses at that design point. In optimization problems of this study, surrogate based FFI analysis responses and SI analysis responses had different design variables in terms of part thickness with only three part thicknesses treated as shared variables (x_1, x_4 and x_5). But in determining the simulation based responses at optimum point, the optimum thickness of all the 24 parts are substituted to get one final vehicle design satisfying FFI and SI analyses crash responses. Table 5.2 shows the responses obtained at optimum design point; the prediction of optimum responses by surrogate models, the corresponding simulation result obtained from LS-DYNA and the error associated with RBF at optimum design point are tabulated. In this study, the responses obtained through FE simulations are treated as true responses, therefore the difference in responses predicted through RBF and FE simulations is denoted as error.

In Table 5.2, a negative sign in error percentage indicate that the surrogate model has under estimated the response, whereas a positive sign indicates that the surrogate model has overestimated the response. The average error in surrogate models of all the responses is 7.18%. Chest acceleration (CA) had the least error of 1.85% whereas the left femur (LF) had the highest error of 27.8%. This difference is due to average error of 15.1% during surrogate model building stage and also since the surrogate model of LF was build using design variables specific to FFI analysis but in the above results, the optimum design variables specific to SI analysis are also used.

Table 5.2 Response of Crash-based design case at optimum point.

Response	Optimum (RBF)	Optimum (FE Simulations)	Error (%)
HIC	561.7	544.8	3.10
C_{3ms} (g's)	51.72	52.26	-1.03
H.A (g's)	63.31	61.73	2.56
C.A (g's)	51.58	52.55	-1.85
C.D (mm)	18.11	20.63	-12.22
L_F (N)	4256.95	3330.97	27.80
R_F (N)	3685.42	4091.01	-9.91
FFI-IE (kJ)	62.37	65.17	-4.30
U_R (g's)	67.34	63.77	5.60
L_R (g's)	55.53	56.73	-2.12
Spine (g's)	63.59	60.13	5.75
Pelvis (g's)	50.57	56.82	-11.00
SI-IE (kJ)	19.53	20.82	-6.20

Table 5.3 shows the simulation results of optimum design responses with respect to the baseline and the corresponding percent improvement in responses due to optimization. The baseline and optimum internal energy in both FFI and SI correspond to the energy absorption of all the 24 parts of the vehicle model considered in this design. All the responses shown in Table 5.3 have improved from their baseline values except for pelvis acceleration, with 10% increase from its baseline value. The baseline mass of all the 24 parts is 107.76 kg and the mass at optimum design point is 92.47 (i.e., a reduction of 14.19%). The surrogate-based design optimization technique has resulted in a total mass reduction of 15.29 kg. The injury index in Table 5.3 corresponds to Equation (3.14), which is the combination of FFI and SI injury criteria, this index has reduced from a

baseline value of 1.0 to 0.89 at the optimum design, indicating a total reduction (improvement) of 11% in overall occupant injury.

Table 5.3 Comparison of optimum design responses with those of the baseline design.

Response	Baseline (FE Simulations)	Optimum (FE Simulations)	Relative to Baseline (%)
HIC	711.1	544.8	-23.39
C_{3ms} (g's)	53.01	52.26	-1.41
H.A (g's)	64.52	61.73	-4.32
C.A (g's)	53.78	52.55	-2.29
C.D (mm)	21.68	20.63	-4.84
L_F (N)	4692.4	3330.97	-29.01
R_F (N)	4317	4091.01	-5.23
FFI-I.E(kJ)	62.6	65.17	4.11
U_R (g's)	69.74	63.77	-8.56
L_R (g's)	58.82	56.73	-3.55
Spine (g's)	64.89	60.13	-7.34
Pelvis (g's)	51.58	56.82	10.16
SI-IE (kJ)	20.05	20.82	3.84
Mass (kg)	107.76	92.47	-14.19
Injury Index	1.0	0.89	-11.04

5.2 Crash+Vibration-Based Design Problem

The crash+vibration design problem shown in Figure 3.14 in Chapter 3 was solved in a similar way to the crash-based design problem by defining the optimization problem in each element. Since the vibration design constraints are placed in element 11, the number of target variables from element 11 to 22 and 23 are increased. The element specific subproblems of crash+vibration design case are shown below. Similar to crash-

based design, the design variables in each element are defined by subscript *e*i, where i denotes the element number.

P$_{11}$

$$min \quad f_{11} = 0.3\,(G'_1) + 0.175(G'_2) + 0.0125(G'_6) + 0.0125(G'_7)$$
$$+0.125(G'_9) + 0.125(G'_{10}) + 0.25(G'_{11})$$
$$+\pi\,\{(\boldsymbol{t}_{22} - \boldsymbol{r}_{22}), (\boldsymbol{t}_{L22} - \boldsymbol{r}_{L22}), (\boldsymbol{t}_{23} - \boldsymbol{r}_{23}), (\boldsymbol{t}_{L23} - \boldsymbol{r}_{L23})\}$$

$$s.t. \qquad g'_{14-16} = f(x_{1e1}, x_{3e1-9e1}, x_{16e1-21e1}) - 1 \geq 0$$

$$0 \leq G'_i \leq 1; i = 1, 2, 6, 7, 9, 10, 11$$

$$\boldsymbol{x}^L \leq \boldsymbol{x} \leq \boldsymbol{x}^U \text{ where } \boldsymbol{x} = [x_{1e1,}, x_{3e1-9e1}, x_{12e1}, x_{16e1-21e1}]$$

$$with \quad \boldsymbol{t}_{22} = [\,G'_1, G'_2, G'_6, G'_7, x_{3e1}, x_{6e1-9e1}]$$
$$\boldsymbol{t}_{23} = [\,G'_9, G'_{10}, G'_{11}, x_{16e1-21e1}]$$
$$\boldsymbol{t}_{L22} = \boldsymbol{t}_{L23} = [x_{1e1}, x_{4e1}, x_{5e1}, x_{12e1}]$$
$$\overline{\boldsymbol{x}}_{11} = [\boldsymbol{t}_{22}, \boldsymbol{t}_{23}, \boldsymbol{t}_{L22}, \boldsymbol{t}_{L23}\,]$$

P$_{22}$

$$\min \quad f_{22} = f(\,x_{1e2}, x_2, x_{3e2-9e2}, x_{10}, x_{11}) + \pi\{(\boldsymbol{t}_{22} - \boldsymbol{r}_{22}), (\boldsymbol{t}_{L22} - \boldsymbol{r}_{L22})\}$$

$$s.t. \quad g'_{1,2,6,7}(\boldsymbol{r}_{L22}, \boldsymbol{x_{22}}, x_{3e2}, x_{6e2-9e2}) - 1 \leq 0$$

$$g'_{3,4,5}(\boldsymbol{r}_{L22}, \boldsymbol{x_{22}}, x_{3e2}, x_{6e2-9e2}) - 1 \leq 0$$

$$g'_8(\boldsymbol{r}_{L22}, \boldsymbol{x_{22}}, x_{3e2}, x_{6e2-9e2}) - 1 \geq 0$$

$$\boldsymbol{x}^L \leq \boldsymbol{x} \leq \boldsymbol{x}^U \text{ where } \boldsymbol{x} = [x_{1e2-15e2}]$$

$$with \quad \boldsymbol{r}_{22} = [g'_1, g'_2, g'_6, g'_7, x_{3e2}, x_{6e2-9e2}]$$
$$\boldsymbol{r}_{L22} = [x_{1e2,}x_{4e2,}x_{5e2,}x_{12e2}]$$
$$\boldsymbol{x_{22}} = [x_2,\ x_{10}, x_{11}, x_{13-15}]$$
$$\overline{\boldsymbol{x}}_{\boldsymbol{22}} = [\,\boldsymbol{r}_{22}, \boldsymbol{r}_{L22}, \boldsymbol{x_{22}}]$$

$\mathbf{P}_{23}$

$$\min \quad f_{23} = f(x_{1e3},\ x_{4e3}, x_{5e3}, x_{16e3-21e3}) + \pi\{(\boldsymbol{t}_{23} - \boldsymbol{r}_{23}), (\boldsymbol{t}_{L23} - \boldsymbol{r}_{L23})\}$$

$$s.t. \quad g'_{9,10,11}(\boldsymbol{r}_{L23}, x_{16e3-21e3}) - 1 \leq 0$$

$$g'_{12}(\boldsymbol{r}_{L23}, x_{16e3-21e3}) - 1 \leq 0$$

$$g'_{13}(\boldsymbol{r}_{L23}, x_{16e3-21e3}) - 1 \geq 0$$

$$\boldsymbol{x}^L \leq \boldsymbol{x} \leq \boldsymbol{x}^U \quad \text{where } \boldsymbol{x} = [x_{1e3,4e3,5e3,12e3}, x_{16e3-21e3}]$$

$$with \quad \boldsymbol{r}_{23} = [g'_9, g'_{10}, g'_{11}, x_{16e3-21e3}]$$

$$\boldsymbol{r}_{L23} = [x_{1e3,}x_{4e3,}x_{5e3,}x_{12e3}]$$

$$\overline{\boldsymbol{x}}_{\boldsymbol{23}} = [\,\boldsymbol{r}_{23}, \boldsymbol{r}_{L23}] \tag{5.7}$$

The subproblems of elements 22 and 23 were solved using SQP optimization technique but due to difficulties in solving element 11 through SQP, Modified Method of Feasible Direction (MMFD) [4] was used. Similar to SQP, MMFD is a gradient-based optimization method but with a stricter search in the feasible design space.

The optimum values of design variables obtained after solving the crash+vibration decomposed optimization problem are shown in Table 5.4. Similar to the crash-based design case, multiple starting points were used in solving the optimization problem. A total of six random initial points were used for all the design variables within their respective lower and upper bounds, and the results for the best solution are shown. The optimization process in coordination with EPF II formulation of ATC took 25 loops to obtain a converged solution. The optimization took approximately 2.5 minutes to complete. Using the optimum values of design variables, separate simulations for FFI, SI

and vibration analysis were performed to obtain occupant and vibration responses at the optimum design point.

Table 5.4 Optimum design point for the crash+vibration-based design problem.

*Design Variables	Name	Lower Bound	Baseline	Optimum	Upper Bound
x_1	A-Pillar	0.805	1.611	1.861	2.416
x_2	Front bump	0.978	1.956	0.998	2.934
x_3	Firewall	0.367	0.735	0.860	1.102
x_4	Front floor panel	0.352	0.705	0.508	1.057
x_5	Outer Cabin	0.414	0.829	0.877	1.243
x_6	Shotgun	0.762	1.524	1.829	2.286
x_7	Inner side rail	0.947	1.895	1.677	2.842
x_8	Outer Side rail	0.761	1.522	1.678	2.283
x_9	Side rail ext.	0.947	1.895	2.786	2.842
x_{10}	Lower Susp.frame	0.793	1.587	0.810	2.380
x_{11}	Upper Susp.frame	1.303	2.606	1.330	3.909
x_{12}	Belt limit force (N)	1000	2500	1650	5000
x_{13}	Mass flow rate (scale factor)	0.8	1.0	0.801	1.4
x_{14}	Vent orifice area (scale factor)	0.6	1.0	1.120	1.4
x_{15}	Airbag input temp. (K)	600	781	750.019	1000
x_{16}	Mid B-pillar	0.353	0.706	1.048	1.059
x_{17}	Rear cabin floor	0.353	0.706	0.561	1.059
x_{18}	Cabin seat rein.	0.341	0.682	0.522	1.023
x_{19}	Cabin mid rail	0.525	1.050	0.882	1.575
x_{20}	Rear plate	0.355	0.710	0.819	1.065
x_{21}	Roof	0.351	0.702	0.537	1.053

* Part thicknesses are in mm.

Table 5.5 shows the responses obtained at the optimum design point based on surrogate model predictions and the FE simulation results; the error associated with RBF at optimum design point is also tabulated. The average error of all the responses is 6.35% with the maximum error of 20.46% in right femur force (RF) and the minimum error of 0.01% in chest acceleration (CA) and frequency of second mode shape (Freq2). Even in this design case, similar to crash-based design, the surrogate models of FFI and SI

occupant responses are build using different vehicle part thicknesses as design variables, but in finding simulation based optimum responses, the part thicknesses of all the parts were selected so that the final vehicle model satisfies both FFI, SI and vibration design requirements.

Table 5.5 Optimum responses of crash+vibration-based design problem.

Response	Optimum (RBF)	Optimum (FE Simulations)	Error (%)
HIC	556.79	625.1	-10.93
C_{3ms} (g's)	49.88	47.88	4.18
H.A (g's)	63.92	56.09	13.97
C.A (g's)	48.25	48.24	0.01
C.D (mm)	16.89	20.96	-19.43
L_F (N)	3997.92	3781.2	5.73
R_F (N)	3544.26	4456.04	20.46
FFI-IE (kJ)	62.34	62.53	-0.3
U_R (g's)	68.35	66.11	3.38
L_R (g's)	54.94	57.41	-4.31
Spine (g's)	64.24	61.76	4.01
Pelvis (g's)	47.99	51.83	-7.41
SI-IE (kJ)	19.58	20.87	-6.14
Freq1 (Hz)	35.90	35.60	0.83
Freq2 (Hz)	36.55	36.55	0.01
Freq3 (Hz)	39.06	39.28	0.55

Table 5.6 shows the comparison of baseline responses and responses at optimum design point. The overall mass of the selected parts has reduced from 107.76 kg to 99.05 kg indicating a reduction of 8.1% (i.e., 8.71 kg mass has been reduced through

optimization). The injury index has reduced from 1.0 to 0.92 (i.e., the overall occupant injury in FFI and SI has reduced by 8%). All the crash and vibration responses have improved from their corresponding baseline values except three responses. Right femur force (RF) has a violation of 3.22%, internal energy in FFI with 0.12% and pelvis acceleration with 0.48%.

Table 5.6 Comparison of optimum design responses with those of the baseline design.

Response	Baseline (FE Simulations)	Optimum (FE Simulations)	Relative to baseline (%)
HIC	711.1	625.10	-12.1
C_{3ms} (g's)	53.01	47.88	-9.7
H.A (g's)	64.52	56.09	-13.1
C.A (g's)	53.78	48.24	-10.3
C.D (mm)	21.68	20.96	-3.3
L_F (N)	4692.4	3781.20	-19.5
R_F (N)	4317	4456.04	3.2
FFI-I.E (kJ)	62.6	62.53	-0.1
U_R (g's)	69.74	66.11	-5.2
L_R (g's)	58.82	57.41	-2.4
Spine (g's)	64.89	61.76	-4.8
Pelvis (g's)	51.58	51.83	0.5
SI-IE (kJ)	20.05	20.87	4.1
Freq1 (Hz)	35.39	35.60	0.6
Freq2 (Hz	36.23	36.55	0.9
Freq3 (Hz)	38.37	39.28	2.4
Mass (kg)	107.76	99.05	-8.1
Injury Index	1.0	0.92	-8.0

The percentage of mass and injury reduction in the crash+vibration-based design problem is less than that in the crash-based design case. This indicates that by

considering vibration requirements in the design problem, there is a tradeoff between vehicle stiffness with vehicle mass and occupant safety, but still using surrogate-based optimization techniques, a lighter vehicle design with improved occupant safety can be obtained without compromising structural rigidity of the vehicle. Table 5.7 compares the frequencies responses obtained at optimum design of both crash-based and crash+vibration-based design problems.

Table 5.7 Comparison of vibration response of crash-based and crash+vibration-based optimum designs.

Response (Hz)	Baseline	Crash-based Optimum Design	Crash+Vibration-based Optimum Design
Freq1	35.39	33.90	35.60
Freq2	36.23	34.53	36.55
Freq3	38.37	36.97	39.28

It is evident from table 5.7 that the frequency responses have decreased from their baseline values in crash-based design problem indicating reduction in structural rigidity of optimum design found based on only crashworthiness design requirements. Therefore, to maintain or improve the structural rigidity of the vehicle, vibration requirements should also be considered in the optimization process.

Figure 5.1 shows the normalized optimum values of part thicknesses considered for vibration responses (i.e. x1, x3-9, x16-21) with the corresponding optimum thicknesses obtained from crash-based design case. The optimum thickness of each part was normalized by their corresponding baseline value.

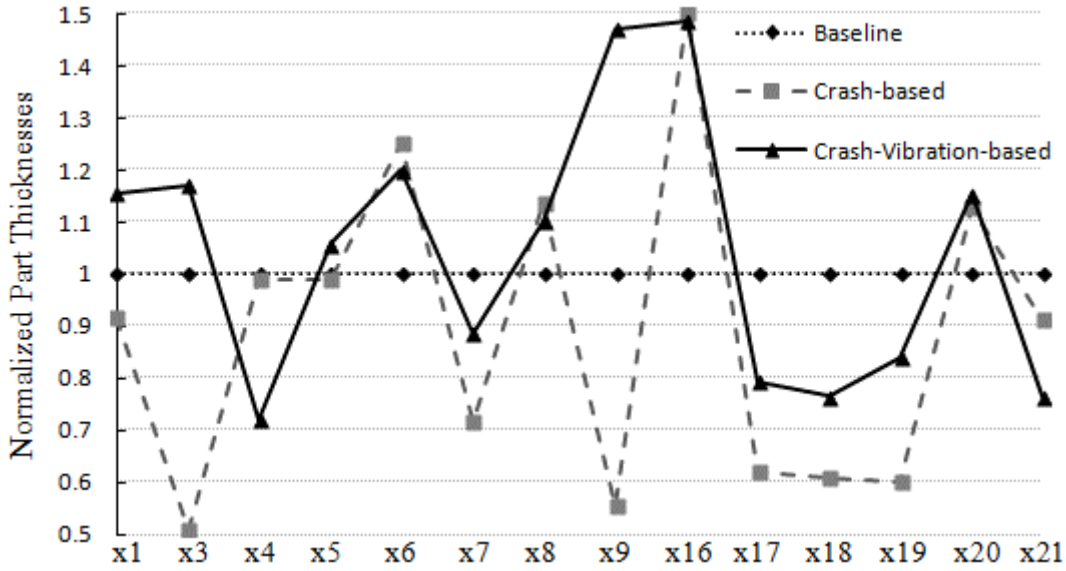

Figure 5.1 Normalized part thicknesses of baseline, optimum crash-based and optimum crash+vibration-based design case.

In Figure 5.1, it can be seen that only few part thicknesses in the two design cases are the same and most of the thicknesses of crash-based design case are less than those in the crash+vibration case. The optimizer had to adjust part thicknesses so that both crash and vibration requirements are satisfied, and hence there is a conflict in terms of mass reduction and structural rigidity.

5.3 Comparison of Vehicle-Based and Occupant-Based Responses in Crash+Vibration Optimum Design

Recent crashworthiness studies have involved mass reduction of vehicle components with vehicle-based crash responses treated as design constraints and vehicle part thicknesses as design variables [5, 6, 7]. These studies have considered crash responses such as acceleration at the upper B-pillar, intrusion distances of Toeboard and dashboard in FFI along with B-pillar acceleration and the intrusion distance of the door in

SI in lieu of actual occupant responses. Kiani et al. [7] considered vibration design requirements along with crash responses in FFI, SI and OFI by treating frequencies of the first three flexible modes as design constraints. The following discussion involves a comparison of crash+vibration design problem optimized using vehicle-based crash responses versus the design problem based on occupant-based responses as discussed in section 5.2 of this thesis.

Kiani et al. [7] considered a 1996 Dodge Neon model without interiors similar to the one shown in Figure 2.1 in Chapter 2. The thicknesses of 22 parts were selected as design variables with the number eventually reduced to 15 due to vehicle symmetry. These 15 design variables are similar to most of the vehicle-based design variables (i.e., $x_{1\text{-}9}$, x_{11}, $x_{17\text{-}21}$) considered in this study with the exception of two parts, i.e., mid B-pillar (x_{16}) and lower suspension frame (x_{10}). In crash analysis, the inclusion of interiors, occupant models and ORS is the only difference in the baseline design models of the two studies, whereas the baseline design models for vibration analysis are the same. Since in the two baseline vehicle models, 15 out of 17 vehicle-based design variables and their design bounds are similar, a comparison between optimum values of part thickness in both studies is possible.

Table 5.8 shows the optimum values of part thickness obtained in crash+vibration design using vehicle-based and occupant-based responses. Figure 5.2 shows the normalized optimum values of part thicknesses considered in both design cases. The optimum part thicknesses were normalized by their corresponding baseline values. Five of the design variables are close to each other with inner side rail (x_7) and outer side rail (x_8) being equal in both designs.

Table 5.8 Optimum part thicknesses of two designs.

Design Variable*	Part Name	Lower Bound	Baseline	Current results	Ref. [41]	Upper Bound
x_1	A-Pillar	0.806	1.611	1.861	1.471	2.417
x_2	Front bump	0.978	1.956	0.998	2.169	2.934
x_3	Firewall	0.368	0.735	0.860	0.913	1.103
x_4	Front floor panel	0.353	0.705	0.508	0.56	1.058
x_5	Outer cabin	0.415	0.829	0.877	0.897	1.244
x_6	Shotgun	0.762	1.524	1.829	1.670	2.286
x_7	Inner side rail	0.948	1.895	1.677	1.694	2.843
x_8	Outer side rail	0.761	1.522	1.678	1.654	2.283
x_9	Side rail exten.	0.948	1.895	2.786	1.952	2.843
x_{11}	Upper susp. Frame	1.303	2.606	1.330	1.923	3.909
x_{17}	Rear cabin floor	0.353	0.706	0.561	0.387	1.059
x_{18}	Cabin seat reinf.	0.341	0.682	0.522	1.009	1.023
x_{19}	Cabin mid rail	0.525	1.050	0.882	1.287	1.575
x_{20}	Rear plate	0.355	0.710	0.819	0.668	1.065
x_{21}	Roof	0.351	0.702	0.537	0.815	1.053

*All values in mm

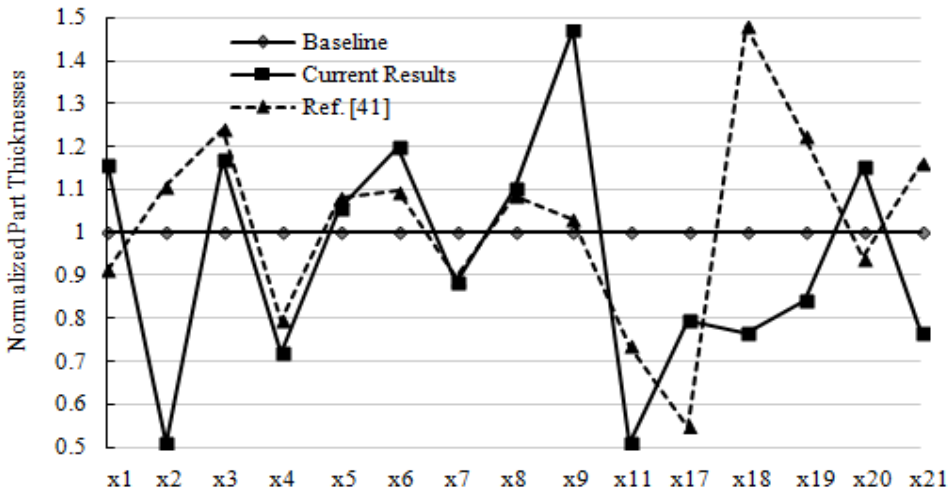

Figure 5.2 Normalized optimum part thicknesses.

From Figure 5.2 it is evident that in current results, eight design variables have decreased from their baseline values compared to six in Ref. [7], which implies that there is greater mass reduction in the current results.

Table 5.9 and Table 5.10 shows the responses considered in design involving vehicle-based responses and occupant-based responses along with baseline, optimum values and their corresponding improvements obtained from optimization. In Table 5.9, the responses are vehicle-based i.e. Toeboard and Dashboard intrusion distances calculated for FFI and OFI analysis (FFI Toe int, FFI Dash int, OFI Toe int, OFI Dash int) and intrusion of door (SI Door int) calculated for SI analysis. The B-Pillar accelerations which are calculated as substitutes for head acceleration is denoted based on impact scenario (FFI Accel, SI Accel and OFI Accel). Figure 5.3 shows the location of vehicle-based responses considered in Ref. [7].

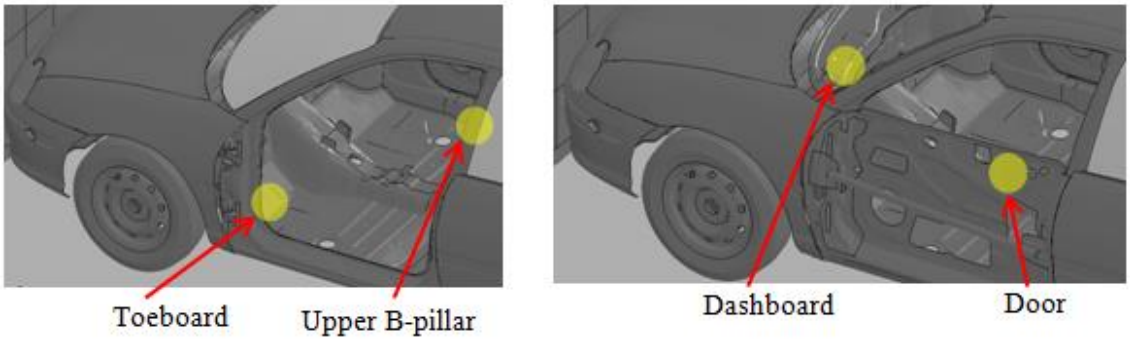

Figure 5.3 Locations of vehicle-based responses [7].

Table 5.9 Optimum values of crash and vibration responses using vehicle-based response optimization [7].

Response	Baseline	Optimum	Improvement (%)
FFI Toe int (mm)	157.07	160.29	-2.1
FFI Dash int (mm)	122.06	118.3	3.1
FFI Accel (g's)	63.51	59.12	6.9
FFI Int eng (kJ)	62.31	62.35	0.1
SI Door int (mm)	313.93	311.09	0.9
SI Accel (g's)	47.88	47.71	0.4
SI Int eng (kJ)	22.37	23.51	5.1
OFI Toe int (mm)	273.48	229.29	16.2
OFI Dash int (mm)	246.94	200.52	18.2
OFI Accel (g's)	35.02	33.91	3.2
OFI Int eng (kJ)	39.42	41.46	5.2
Average			5.3
Freq1 (Hz)	35.39	35.39	0.00
Freq2 (Hz)	36.23	36.23	0.00
Freq3 (Hz)	38.37	38.37	0.00
Average			0
Mass (kg)	105.25	101.49	3.6

In Table 5.9, the positive sign for percent improvement indicates the responses have improved relative to the corresponding baseline value. In design optimization using vehicle-based crash responses, the average improvement in crash responses is 5.3% relative to the baseline design with only 2% improvement in FFI and SI responses. The vibration responses have remained the same as the baseline with the total mass reduction

of 3.6%. Table 5.10 shows FFI and SI occupant-based crash responses along with vibration responses and their corresponding improvement from the baseline design.

Table 5.10 Optimum crash and vibration responses obtained from section 5.2.

Response	Baseline	Optimum	Improvement (%)
HIC	711.1	625.1	12.1
C3ms (g's)	53.01	47.88	9.7
HA (g's)	64.52	56.09	13.1
CA (g's)	53.78	48.24	10.3
CD (mm)	21.68	20.96	3.3
LF (N)	4692.4	3781.2	19.5
RF (N)	4317	4456.04	-3.2
FFI-IE (kJ)	62.6	62.53	-0.1
UR (g's)	69.74	66.11	5.2
LR (g's)	58.82	57.41	2.4
Spine (g's)	64.89	61.76	4.8
Pelvis (g's)	51.58	51.83	-0.5
SI-IE (kJ)	20.05	20.87	4.1
Average			6.2
Freq1 (Hz)	35.39	35.60	0.6
Freq2 (Hz)	36.23	36.55	0.9
Freq3 (Hz)	38.37	39.28	2.4
Average			1.3
Mass (kg)	107.8	99.05	8.1

In the design optimization based on occupant responses, there is 6.2% improvement in crash (FFI and SI) responses, 1.3% improvement in responses associated with vibration along with 8.1% reduction in mass.

The FFI acceleration in Table 5.9 corresponds to the resultant acceleration calculated at the upper B-pillar. This is an approximate location where the occupant head would be in an actual crash (i.e., response HA of Table 5.10). The baseline values of these two responses are approximately close to each other (only 1g difference) indicating that in FFI analysis, estimating the head acceleration response by the acceleration calculated at the upper B-pillar (in absence of a dummy model) is a good approximation. The amount of intrusion in Toeboard and Dashboard affects the occupant legs and chest. Therefore, the vehicle-based response Toeboard intrusion is considered as substitute for femur forces (L_F, R_F) and Dashboard intrusion as a substitute for chest deflection (CD). Comparing tables 5.9 and 5.10, after optimization, the FFI Toeboard intrusion in Table 5.9 worsened by 2% where as the femur forces of Table 5.10 improved by 8%. Similarly, FFI dashboard intrusion given in Table 5.9 improved by 3% and the corresponding chest deflection given in Table 5.10 , also improved by 3%. Therefore, in terms of percentage reduction obtained from optimization, most of the approximate vehicle-based responses are close to occupant-based responses.

The vehicle-based responses are good approximates of actual crash responses experienced by an occupant, but by using occupant models and ORS at an additional cost and design complexity in terms of simulation time and modeling, more accurate responses can be obtained, which helps in reducing more vehicle mass and improving structural rigidity. This is evident from the amount of mass reduced in both design cases (8.1% versus 3.6%), and also the vibration responses with occupant-based responses have increased indicating improvement in structural rigidity.

5.4 References Cited

[1] VisualDOC, A general purpose design, optimization, and process integration software. Version 7.1, Novi, MI, 2012. Available at http://www.vrand.com/visualDOC.html.

[2] MATLAB: The Language of Technical Computing, Software Package, Ver. 7.8.0347 (R2009a), The Mathworks, Inc., 2009.

[3] Rao, S. S. Engineering optimization: theory and practice, John Wiley & Sons, 2009.

[4] "VisualDoc 7.1 Theory Manual," Vanderplaats Research and Development, Inc., 2012, pp. 15.

[5] Parrish, A., M. Rais-Rohani, & A. Najafi. "Crashworthiness optimisation of vehicle structures with magnesium alloy parts." International Journal of Crashworthiness, 17, 3, 2012, pp: 259-281.

[6] Kiani, M. "Modeling, Simulation and Optimization approaches for Design of Lightweight Car body Structures." PhD dissertation, Mississippi State University, 2013.

[7] Kiani, M., I. Gandikota, A. Parrish, K. Motoyama, & M. Rais-Rohani. "Surrogate-based optimisation of automotive structure under multiple crash and vibration design criteria," International Journal of Crashworthiness, 2013. (In Press)

CHAPTER VI

CONCLUSIONS AND FUTURE WORK

This study involved the application of design optimization techniques to improve the baseline design of a 1996 Dodge Neon model in terms of mass reduction and occupant safety. The FE model of 1996 Dodge Neon with interiors was used as a baseline design and FE models of occupant and ORS were added to assess injury criteria and safety during crash. The ORS system included a seatbelt and an airbag model for FFI and only a seatbelt in SI analysis. Instead of using a one-dimensional seatbelt model, a more realistic two-dimensional seatbelt model with a pretensioner was used to remove initial slack in belt and provide better occupant safety. The baseline Dodge Neon model with ORS and occupant model was validated by comparing the resultant head and chest acceleration data of dummy obtained in FFI with the actual crash test results obtained under FMVSS 208. Pelvis and spine acceleration data were compared with the actual crash test results under FMVSS 214.

A multi-objective design optimization problem was formulated with mass and occupant injury reduction as objective. The occupant-based and vehicle-based (i.e., internal energy) responses in FFI and SI were considered as design constraints. The thickness of 24 parts of the Dodge Neon model constituted the vehicle-based design variables and four design variables were selected from ORS in which one is seatbelt parameter and three are airbag parameters.

To demonstrate the application of a decomposed multilevel optimization framework, a multilevel target matching problem was formulated with injury criteria at the top level and vehicle design and mass reduction with respect to occupant responses in FFI and SI scenarios in the lower level. The combination of Weighted Injury Criterion (WIC) of FFI analysis and Thoracic Trauma Index (TTI) of SI was used as objective function of the top level and mass calculation based on part thickness was used as the other objective. Analytical target cascading technique using EPF II formulation was used to solve the decomposed target matching problem. The decomposed problem consisted of a total of three objective functions and 13 design constraints. The responses of FFI and SI were treated as design constraints by formulating approximate analytical functions of responses using surrogate modeling technique. The vehicle mass and occupant injury were reduced without compromising the crashworthiness characteristics of the vehicle.

Vibration design requirements were added to the existing crash-based design problem by considering frequencies of first three flexible modes as design constraints. This criterion was included in the first element of decomposition along with injury criteria so that vehicle design satisfies vibration requirements first and the corresponding design is cascaded down to fulfill FFI and SI crash requirements so that the final design has better occupant safety, reduced mass and improved structural rigidity. The crash+vibration-based optimum design showed that by considering vibration requirements, the amount of mass reduced is less than the optimum design with crash alone.

Finally, a comparison of vehicle design optimization based on vehicle-based crash responses and occupant-based crash responses was shown. Optimizing the vehicle with

inclusion of occupant models and occupant restraint system, and considering both vehicle-based and ORS-based design variables, a more accurate and better design in terms of mass reduction and structural rigidity was obtained compared to the optimum design obtained from approximate vehicle-based crash responses.

This work can be extended by considering other important crash scenarios not discussed in this study such as OFI, roll over crash and rear impact analyses. The multilevel decomposition can be extended by implementing crash and vibration design with other requirements governing the vehicle design process such as fatigue design criteria to consider the durability of vehicle components. The crash analysis can be improved by considering more detailed FE models of vehicle and dummy model in terms of material properties, can be developed to simulate occupant and vehicle interaction accurately. The overall occupant safety in SI can be further improved by considering side curtain and seat mounted airbags and optimizing the corresponding parameters.

APPENDIX A

FILES USED FOR CRASH ANALYSIS

The LS-DYNA keyword below contains velocity definition and different files used in FFI crash analysis of Dodge Neon model with occupant and ORS. The translation defined for rigid wall is also given. Separate files have been used for defining FE models of vehicle, dummy, seatbelt, seatbelt properties, airbag properties, seatbelt contacts and connection with vehicle model.

```
$# LS-DYNA Keyword file created by LS-PrePost 4.0 (Beta) - 22Jul2012(13:20)
$# Created on Dec-06-2012 (01:47:57)
*KEYWORD MEMORY=76385103
*TITLE
$# title
FFI_neon_wdummy_0
*DEFINE_TRANSFORMATION
$---------------------------------------------------------------------------
$#  tranid
      1000
$# option              a1            a2        a3        a4        a5        a6        a7
TRANSL    -64.000000 160.00000     0.000     0.000     0.000     0.000     0.000
*INITIAL_VELOCITY_GENERATION
$#nsid/pid     styp     omega        vx        vy        vz     ivatn      icid
  2000011        3     0.000 15650.000     0.000     0.000         0         0
$#      xc        yc        zc        nx        ny        nz     phase    iridid
     0.000     0.000     0.000     0.000    1.0000     0.000         0         0
   7000003         1     0.000 15650.0         0.000     0.000         1         0
     0.000     0.000     0.000     0.000         1.000     0.000         0         1
   2000002         1     0.000 15650.0         0.000     0.000         1         0
     0.000     0.000     0.000     0.000         1.000     0.000         0         1
   7000003         1     0.000 15650.0         0.000     0.000         1         0
     0.000     0.000     0.000     0.000         1.000     0.000         1         1
   2000002         1     0.000 15650.0         0.000     0.000         1         0
       0.000     0.00     0.000     0.000         1.000     0.000         1         1
   7001002         3     0.000 15650.0         0.000     0.000         0         0
       0.000     0.00     0.000      0.000         1.000     0.000         0         0
   9000001          1     0.000 15650.0         0.000     0.000         0         0
        0.000     0.00     0.000     0.000          1.000     0.000          0         0
    2000003         1    52.200 15650.0          0.00     0.000         0         0
 3689.1899     0.0    300.963     0.000         1.000     0.000         0         0
   2000004          1   52.2001 5650.00         0.000     0.000         0         0
 1041.4900     0.0 304.7240     0.000         1.000     0.000         0         0
*INCLUDE_TRANSFORM
$# filename
loadcellwall.key
$#  idnoff    ideoff    idpoff    idmoff    idsoff    idfoff    iddoff
        0         0         0         0         0         0         0
$#  idroff
        0
$#  fctmas    fcttim    fctlen    fcttem   incout1    unused
```

```
    0.000     0.000     0.000     0.000         0        -1
$#  tranid
     1000
$----------------------------------
*INCLUDE
Dummy_H350.key
*INCLUDE
newbelt_lstc_2D_dodgeneonwithpret.key
*INCLUDE
best_retractor_LLCID.key
*INCLUDE
dodge_neon_seatbelt_connection.DriverSide.k
*INCLUDE
dodge_neon_SeatBeltContact.DriverSide.k
*INCLUDE
frontal_airbag_properties.key
*INCLUDE
Neon_Bint_st0.key
*END
```

SAMPLE DODGE NEON VEHICLE MODEL KEYWORDS

The following keyword file shows various database cards defined for vehicle model.

```
$# LS-DYNA Keyword file created by LS-PREPOST 3.0(Beta) - 19Jan2010(14:34)
$# Created on Mar-29-2010 (13:37:33)
*KEYWORD
*TITLE
$# title
LS-DYNA keyword deck by LS-PrePost
$------------------------------------------------------------------------------
$- This model has been developed by the FHWA/NHTSA National Crash Analysis
$- Center at The George Washington University. The FE model is based on a
$- 1996 Dodge Neon. The model has been validated to a frontal NCAP test.
$-
$- The model is continuously updated to improve its capabilities in
$- predicting responses in various impact scenarios. However, the user must
$- verify his own results. Neither NCAC, GWU, FHWA or NHTSA assume any
$- responsibility for the validity, accuracy, or applicability of any results
$- obtained from this model.
$- We ask that NCAC be acknowledged under references for any use of this
$- FE model resulting in papers and publications.
$-
$- Please feel free to contact us with any suggestions, comments, or
$- questions.
$-
$- Dhafer Marzougui <dmarzoug@ncac.gwu.edu> (703) 726-8532
$- Pradeep Mohan <pradeep@ncac.gwu.edu> (703) 726-8538
$- Vinay Nagabhushana <vinay@ncac.gwu.edu> (703) 726-8392
$- Steve Kan <cdkan@ncac.gwu.edu> (703) 726-8511
$-
$------------------------------------------------------------------------------
*DATABASE_ABSTAT
$#      dt    binary      lcur     ioopt
  0.001000         3         0         1
*DATABASE_DEFORC
$#      dt    binary      lcur     ioopt
 1.0000E-4         3         0         1
*DATABASE_GLSTAT
$#      dt    binary      lcur     ioopt
  0.001000         3         0         1
*DATABASE_JNTFORC
$#      dt    binary      lcur     ioopt
  0.001000         3         0         1
*DATABASE_MATSUM
$#      dt    binary      lcur     ioopt
  0.001000         3         0         1
*DATABASE_NODOUT
$#         dt    binary      lcur     ioopt      dthf     binhf
 1.0000E-5          3         0         1     0.000          0
*DATABASE_RCFORC
$#      dt    binary      lcur     ioopt
 2.0000E-4         3         0         1
```

```
*DATABASE_RWFORC
$#         dt    binary      lcur     ioopt
 1.0000E-4          3         0         1
*DATABASE_BINARY_D3PLOT
$#         dt      lcdt      beam     npltc    psetid
  0.010000         0         0         0         0
$#   ioopt
           0
```

APPENDIX C

SAMPLE SEATBELT KEYWORD DEFINITIONS

The sample keyword input files for seatbelt model is shown below. Important keyword definitions of the seatbelt model used in this study are shown along with contact definitions.

```
$$$$$$$$$$$$$$$$$$$$$$$$$$$$$$$$$$$$$$$$$$$$$$$$$$$$$$$$$$$$$$$$$$$$$$$$$$$$$$$$
$ SeatBeltModel
$ The subject model ("Model") has been developed by Livermore Software
$ Technology Corporation (LSTC).
$
$ The Model is distributed free of charge to licensees of LSTC's LS-DYNA
$ software who are current with their annual license fees (Annual License) or
$ maintenance fees (Paid-up License). LSTC and its distributors hereby grant
$ Model users a non-exclusive and non-transferable license to use the Model
$ for their own internal business purposes.
$
$ As a condition for the free use of the Model, user agrees that it will
$ not employ the Model or parts thereof outside the LS-DYNA environment.
$
$ Even though the Model is continuously updated and improved, each user is
$ solely responsible for its own results. LSTC assume no responsibility
$ whatsoever for the validity, accuracy, or applicability of the Model or any
$ results obtained with the Model.
$
$ LSTC endeavors to make the Model as complete, accurate, reliable, and easy
$ to use as possible. Suggestions and comments should be e-mailed to
$ support@lstc.com. Please report any errors encountered in either the
$ documentation or results immediately to LSTC.
$
$ Copyright (C) 2007-2011
$ by Livermore Software Technology Corp. (LSTC)
$ All rights reserved
$
$$$$$$$$$$$$$$$$$$$$$$$$$$$$$$$$$$$$$$$$$$$$$$$$$$$$$$$$$$$$$$$$$$$$$$$$$$$$$$$$
*ELEMENT_SEATBELT_PRETENSIONER
$
$ sbprid = Seat Belt Pretensioner ID
$ sbprty = Seat Belt Pretensioner Type = 5 for pyro pretensioner with limiting load for the pretensioner
$ sbsid  = Seat Belt Sensor ID
$
$ sbrid  = Seat Belt Retractor ID (the one being Pulled by the pretensioner)
$ time   = Time between Sensor Firing and Pretensioner acting
$ ptlcid = Load Curve for Pretensioner
$ lmtfrc = Limiting Force for Retractor (beyond which it will not pull)
$
$#  sbprid    sbprty    sbsid1
$                       (sensor)
  9067000         5   9067001         0         0         0
$
$
$#     sbrid          time       ptlcid       lmtfrc
  9067111    0.000E+00     9067002    2500.0000
```

```
$
*ELEMENT_SEATBELT_SENSOR
$ The Following Sensor is used for Pretensioner Firing.
$
$      sbsid    sbstyp
  9067001           3        0
$
$#    time
 1.300E-02
$
*ELEMENT_SEATBELT_RETRACTOR
$ sbrid   = Seat_Belt Retractor ID
$ sbrnid  = Seat_Belt Retractor Node (not on the Belt)
$ sbid    = First Belt Element ID that is just outside the retractor
$ sid1    = First Sensor ID
$ tdel    = Time Delay After Sensor Triggers
$ pull    = Amount of Pull-Out between time delay ending and retractor locking.
$             (It is a Length value).
$ llcid   = Load Curve for Loading (Force vs. Pull-Out)
$ ulcid   = Load Curve for Unloading (Force vs. Pull-Out)
$ lfed    = Fed Length
$                                      (sensor)
$#     sbrid      sbrnid        sbid         sid1      sid2      sid3      sid4
  9067111   9067117   9067000   9067000         0         0         0
$#    tdel       pull       llcid       ulcid        lfed
    0.000     0.000   9067000   9067007 10.000000
*ELEMENT_SEATBELT_SENSOR
$ See 14.37 in the LS971 Manual.
$ sbsid   = Seat Belt Sensor ID
$ sbstyp  = Seat Belt Sensor Type  -->  3=Time
$ The Following Sensor is used for Retractor Lockup.
$#   sbsid    sbstyp     sbsfl
  9067000         3        0
$#    time
  0.001000
*ELEMENT_SEATBELT_SLIPRING
$#  sbsrid     sbid1     sbid2        fc    sbrnid     ltime       fcs      onid
  9067112   9067053   9067033  0.230000   9067115     0.000     0.000         0
  9067113   9066000   9066015  0.100000   9066017     0.000     0.000         0

$$$$ Sample Keyword for seatbelt contact $$$$

*CONTACT_AUTOMATIC_NODES_TO_SURFACE
$#     cid                                                 title
$#       ssid        msid     sstyp     mstyp    sboxid    mboxid       spr       mpr
  9060000   7110002         2         2         0         0         0         0
$#         fs          fd         dc         vc        vdc     penchk        bt        dt
  0.800000  0.800000    0.000     0.000     0.000         0     0.000     0.000
$#         sfs         sfm        sst        mst       sfst       sfmt       fsf       vsf
  5.000000  5.000000    0.000     0.000  1.000000  1.00000    0.000      0.000

$$$$ Sample keyword for seatbelt connection $$$$

*CONSTRAINED_EXTRA_NODES_SET
$#        pid          nsid
```

```
  9066001   8000075
*END
```